Apicomplexan actin depolymerizing factors and capping proteins in the regulation of actin filament dynamics

Dissertation submitted to the

Department of Chemistry,

Faculty of Mathematics, Informatics and Natural Sciences of

the

University of Hamburg

For the award of the degree of

Doctor of sciences

Moon Chatterjee
From Gorakhpur, India

Hamburg

April 2015

The research work reported in this dissertation was carried out from October 2009 until November 2014 in the research laboratory of Dr. Inari Kursula at the Centre for Structural Systems Biology - Helmholtz Centre for Infection Research and University of Hamburg, Hamburg, Germany.

Reviewers of the dissertation

Asst. Prof. Inari Kursula

Prof. Dr. Andrew Torda

Examiners

Asst. Prof. Inari Kursula

Prof. Dr. Wolfgang Maison

JProf. Dr. Henning Tidow

Date of Disputation- 03-July-2015

List of Abbreviations and Symbols

A_2	second virial coeffecient
A_{280}	UV absorbance at 280 nm
A_{600}	light absorbance at 600 nm
ABP	actin binding protein
ADF	actin depolymerizing factor
ADF-H	actin depolymerizing factor homology
ADP	adenosine-di phosphate
AI	auto-induction
AMPNP	5'-adenylyl-beta,gamma-imidophosphate
Arp	actin related protein
ATP	adenosine-triphosphate
BDM	2,3-butanedione
BLAST	basic local alignment search tools
CAP	cyclase-associated protein
C_c	critical concentration
CD	circular dichroism
CP	capping protein
CytD	cytochalasin D
D_2O	deuterium oxide
DBP	vitamin D-binding protein
D-loop	DNase I binding loop
D_{max}	maximum intramolecular distance of the particle
DMPC	dimyristoylphosphatidalcholine
DNA	deoxyribonucleic acid
DNaseI	de-oxyribonuclease-1
DTT	dithiothreitol
ε-ATP	1,N6–etheno-ATP
EDC	1-ethyl-3-(3-dimethyl aminopropyl) carbodiimide
EM	electron microscope
ENTH	epsin N-terminal homology
EXPASY	expert protein analysis system
F-actin	filamentous actin
FH	formin homology
FYVE	Fab1, YOTB, Vac1 and EEA1
H-bond	hydrogen bonds
HEPES	4-(2-hydroxyethyl) piperazin-1-yl)ethanesulfonic acid
HSP	heat shock protein
HSQC	heteronuclear single quantum coherence
I(s)	scattered intensity

IMC	inner membrane complex
IPTG	isopropyl β-D-1-thioglactopyranoside
JAS	jasplakinolide
kanR	kanamycin resistance gene
K_d	binding coefficient
kDa	kilo dalton
LB	lysogeny broth
LDAO	dodecyldimethylaminoxide
MALS	multi-angle static light scattering
MLC1	myosin light chain
MM	molecular mass
MRE	mean residual ellipticity
MST	microscale thermophoresis
MWCO	molecular weight cutoff membranes
MyoA	myosin motor complex
NCBI	National Center for Biotechnology Information
NMR	nuclear magnetic resonanace
p(r)	distance distribution
Pb	*Plasmodium berghei*
Pf	*Plasmodium falciparum*
PH	pleckstrin homology
PI	phosphoinositols
PIP_2	phosphatidylinositol 4,5 bis phosphate
PPIs	phosphoinositides
R_g	radius of gyration
rpm	revolutions per min
RT	room temperature
RU	response unit
SAXS	small angle X-ray scattering
SD	sub-domain
SDS-PAGE	sodium dodecyl sulfate polyacrylamide gel electrophoresis
SEC	size exclusion chromatography
SLS	static light scattering
SPR	surface plasmon resonance
SRCD	synchrotron radiation circular dichorism
TCEP	2-carboxyethyl phosphine
T-coffee	Tree-based consistent objective for alignment evaluation
Tg	*Toxoplasma gondii*
T_m	melting temperature
TMR	tetramethyl rhodamine

TRAP   thrombospondin-related adhesive protein
Tris   tris(hydroxymethyl)amino-methane
Twf   twinfilin
v/v   volume/volume
V_p Porod volume
w/v   weight/volume
WASP   Wiskott-Aldrich syndrome protein
βME   β-mercaptoethanol

Amino acids

A	Ala	alanine		C	Cys	cysteine
D	Asp	aspartate		E	Glu	glutamate
F	Phe	phenylalanine		G	Gly	glycine
H	His	histidine		I	Ile	isoleucine
K	Lys	lysine		L	Leu	leucine
M	Met	methionine		N	Asn	asparagine
P	Pro	proline		Q	Gln	glutamine
R	Arg	arginine		S	Ser	serine
T	Thr	threonine		V	Val	valine
W	Trp	tryptophan		Y	Tyr	tyrosine

Abstract

The phylum *Apicomplexa* consists mainly of intracellular parasites. The parasite motility and invasion involves a complex and uncharacterized process called gliding motility, which is thought to be driven by the actin-myosin motor of the parasite. Though most of the actins are highly conserved, apicomplexan actins are divergent by 20% from conventional actins. Distinctively *Plasmodium,* the most harmful member of this phylum, expresses only a small sub-set of actin regulatory proteins. The current work focusses on the effect of actin depolymerizing factors (ADFs) and capping proteins (CP), the two most important regulators of actin filament dynamics.

Plasmodium expresses two actins and ADFs with stage specific expression profiles; actin2 and ADF2 are expressed in the sexual stages, while actin1 and ADF1 are expressed all through the life cycle. Conventional ADFs sever actin filaments, decrease the nucleotide exchange rate on G-actin and sequester monomers. Current results show that both *Plasmodium* ADFs bind G-actin with comparable affinities and accelerate nucleotide exchange, indicating they function analogous to conventional profilins. Analysis of SAXS data indicate that ADF2 acts as monomer sequestering protein, and ADF1 forms only a transient complex *in vitro*. Additionally, ADF1 binds to and severs filaments.

ADFs are regulated by phosphoinositols. In case of *Plasmodium* ADFs, current results confirm that ADF1 binds PIP_2 specifically. Very weak or negligible binding between ADF2 and PIP_2 was observed. Binding sites of PIP_2 and actin on ADF1 are mutually exclusive and might also involve an additional step of recognition, mediated by a loop to helix transition in the loop preceding ADF1 α-helix1.

Conventional CPs form heterodimers of α and β subunits and bind to the fast growing end of filaments, thus inhibiting addition or of loss of monomers. Here, it is snown that the α subunit of *Plasmodium* CP, in contrast to conventional CPs, forms stable homodimers *in vitro.* The homodimers were found to inhibit actin polymer elongation and had no impact on actin nucleation, indicating independent function of the two subunits in certain stages of the parasite.

Zusammenfassung

Der Stamm der *Apicomplexa* besteht hauptsächlich aus intrazellulären Parasiten. Motilität und Invasion der Parasiten beinhalten einen komplexen und bislang unvollständig verstanden Prozess, der als "gleitende Motilität" bezeichnet wird und von dem man ausgeht, dass er durch den Aktin-Myosin Motor der Parasiten angetrieben wird. Obwohl die Sequenzen der meisten Aktine hochkonserviert sind, zeigen die Aktine der *Apicomplexa* eine Divergenz gegenüber den konventionellen Aktinen von 20%. Insbesondere *Plasmodium,* der gefährlichste Vertreter dieses Phylums, exprimiert lediglich einen kleinen Teil der aktinregulierenden Proteine. Die vorliegende Arbeit untersucht den Einfluss von actin depolymerizing factors "ADFs" und capping proteins "CP" auf die Dynamik der Aktinfilamente.

Plasmodium exprimiert zwei Aktine und ADFs mit stadienspezifischen Expressionsprofilen; Aktin2 und ADF2 werden in den geschlechtlichen Stadien exprimiert, während Aktin1 und ADF1 den gesamten Lebenszyklus hindurch exprimiert werden. Konventionelle ADFs zertrennen Aktinfilamente, verringern den Nukleotidaustausch am G-Aktin und sequestrieren Monomere. Die vorliegenden Ergebnisse zeigen, dass ADFs aus *Plasmodium* sowohl G-Aktine mit vergleichbarer Affinität binden als auch den Nukleotidaustausch beschleunigen, was auf eine Funktion analog der konventionellen Profiline hinweist. Die Analyse der SAXS-Daten zeigt, dass ADF2 als monomersequestrierendes Protein fungiert und dass ADF1 *in vitro* einen transienten Komplex bildet. Zusätzlich bindet ADF1 an Filamente und abbricht diese.

ADFs werden durch Phosphoinositole reguliert werden. Die vorliegenden Ergebnisse bestätigen, dass ADF1 aus *Plasmodium* spezifisch an PIP$_2$ bindet. Für ADF2 konnte nur eine sehr schwache Bindung an PIP$_2$ beobachtet werden. Die Bindung von PIP$_2$ und Aktin an ADF1 schliesst sich gegenseitig aus und könnten einen zusätzlichen Erkennungsschritt benötigen, der durch einen Übergang der Sekundärstruktur von Loop zu Helix im Bereich der α-Helix1 vorangehenden Loops vermittelt wird.

Konventionelle CPs bilden ein Heterodimer, bestehend aus α- und β-Untereinheiten, und binden an das schnell wachsenden Ende der Filamente, wodurch Anlagerung oder Verlust von Monomeren inhibiert wird. Anhand der vorliegenden Arbeit konnte gezeigt werden, dass die *Plasmodium* CP α-Untereinheit, im Gegensatz zu herkömmlichen CPs, stabile

Homodimere *in vitro* bilden. Diese Homodimere inhibieren die Elongation der Aktinpolymere und haben keinen Einfluss auf die Aktinnukleation, was auf eine unabhängige Funktion der beiden Untereinheiten in bestimmten Stadien des Parasiten hinweist.

LIST OF FIGURES

TABLE OF CONTENTS

1   Review of the literature

1.1   *__Phylum Apicomplexa__*

The phylum *Apicomplexa* is a diverse collection of more than 5000 species, all of which are obligate, protozoan parasites, mostly intracellular (Sibley, 2011). Apicomplexan parasites invade host cells, followed by growth and cell division until host cell lysis takes place due to rapidly replicating parasites. The released parasites reinvade other host cells in order to survive (Morrissette and Sibley, 2002). Repeated cycles of host cell invasion, parasite replication, and host cell lysis account for the severe tissue damage (Hu et al., 2006).

Apicomplexan parasites share a variety of morphological traits that are typical to the phylum. These include an elongated shape, the presence of a collection of unique organelles termed as the apical complex, an essential chloroplast-like organelle called the apicoplast, and a composite structure called pellicle that encloses the parasite. The apical complex (Sibley, 2011) includes the following components:

1. Rhoptries and micronemes, which are unique secretory organelles that release products required for motility, adhesion, and invasion (Carruthers et al., 1999; Carruthers and Sibley, 1997).

2. The apical polar ring, which is present in all members of this phylum and serves as a microtubule-organizing center (Russell and Burns, 1984).

3. The conoid is a thimble-shaped structure, consisting of tubulin assembled into spiral filaments, which repeatedly protrudes and retracts from the apical end (Mital and Ward, 2008). The apical complex plays a role in interaction of the parasite with the host cell and subsequent invasion of the host cell (Nichols and Chiappino, 1987; Scholtyseck and Mehlhorn, 1970).

1.1.1   *Life cycle of apicomplexan parasites*

Apicomplexan parasites have a complex life cycle, involving differentiation into various morphological stages to invade distinct tissues and hosts. In *Plasmodium spp.*, the life cycle is characterized by three distinct processes – sporogony, merogony, and gametogony **(Figure 1)**. Most of the life cycle stages are haploid, but the parasites also have a sexual stage. Sporogony involves asexual division, resulting in sporozoites, and occurs immediately

after sexual reproduction. Sporozoites reinvade host cells and develop into forms that undergo another round of asexual reproduction called merogony. Merogony results in merozoites, invasive forms, which can undergo one to multiple rounds of asexual reproduction. As an alternative, to the asexual cycle, the parasite can differentiate into sexual forms known as micro- or macrogametes. This process is followed by a switch from one host organism (the warm-blooded mammal in the case of *Plasmodium*) to another (the cold-blooded arthropod) – or one cell type to another – and development into gametes by gametogenesis. Gametes fuse to form a zygote, which undergoes sporogony again. The zygote immediately undergoes meiosis to re-establish haploid cells (Black and Boothroyd, 2000; Sibley, 2011).
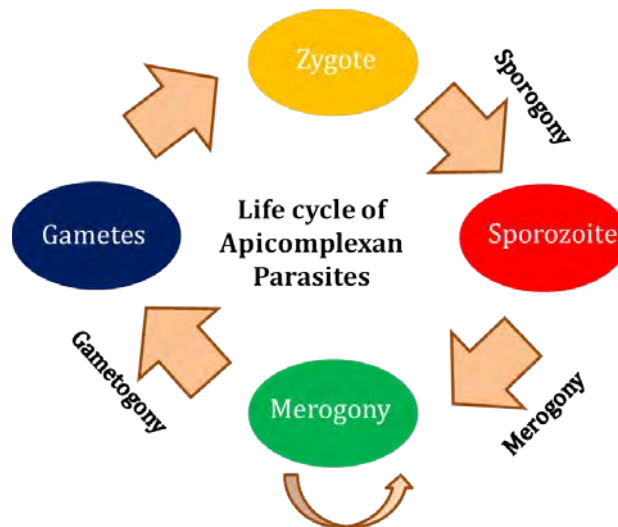
Figure 1: Schematic representation of a general life cycle within the phylum Apicomplexa.

Schematic representation of the life cycle of an apicomplexan parasite, characterized by various morphological traits, three distinct processes and involving a primary and a secondary host. In the primary host, asexual reproduction (sporogony) marks the first stage of infection, resulting in sporozoites. Sporozoites invade cells and undergo several rounds of asexual reproduction resulting in merozoites, which are invasive form. Further differentiation of merozoites into distinct male and female gametes takes place, and these undergo sexual reproduction in the secondary host to form a zygote. The zygote undergoes meiosis to re-establish haploid cells.

1.1.2 *Cytoskeleton of apicomplexan parasites*

The cytoskeleton of apicomplexan parasites is highly flexible, maintains parasite cell shape, structural integrity, and also helps to adjust the cell shape during migration and host cell invasion. Apicomplexan parasites are delimited by the pellicle, a tri-bilayer structure, comprising the plasma membrane and two tightly associated membranes formed by

endoplasmic reticulum-derived flattened vesicles named the inner membrane complex (IMC) (Kono et al., 2013). The IMC extends throughout the body of the parasite and provides support for the gliding machinery, which drives motility (Dubremetz and Torpier, 1978; Foussard et al., 1990; Meszoely et al., 1982; Vivier and Petitprez, 1969). Closely associated to the pellicle is the sub-pellicular network, which acts as the parasite skeleton and is constituted of intermediate filaments. Underneath the sub-pellicular network, at the apical tip, is the apical complex **(Figure 3)**. The basal complex is localized at the other end (Morrissette and Sibley, 2002).
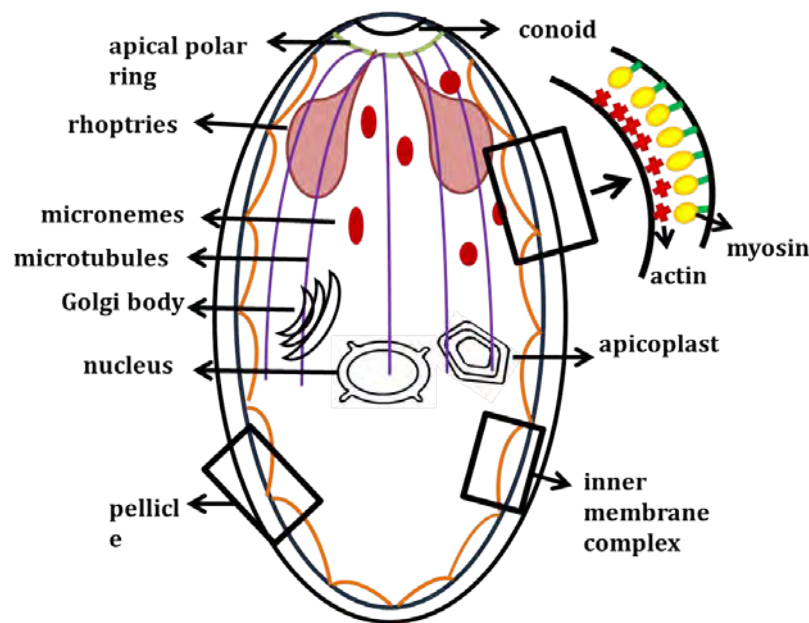
Figure 2: Schematic representation of the general structure of an apicomplexan parasite.

The apicomplexan cell enclosed by a composite tri-layered structure called the pellicle, which is composed of the plasma membrane and the IMC. The cytoskeleton is characterized by the presence of the apical complex, which includes the apical polar ring, the conoid and the rhoptries.

1.2 ***Gliding motility***

Apicomplexan parasites have complex life cycles and, hence, to be successful, it is very important that they are able to efficiently invade and migrate through host tissues. These parasites lack any specialized organelles for motility (Sibley, 2011), although the cell moves forward with an impressive speed varying from 1 of 10 μm/sec. Host cell invasion is a stepwise process that can be divided into four steps; 1) the parasite approaches the host

cell; 2) host cell recognition; 3) formation of a tight junction with the host cell; 4) host cell penetration (Baum et al., 2008b). The first and fourth steps of this process are facilitated by a unique form of motility, known as gliding motility, employed by the invasive forms of the parasite. According to the prevailing model, gliding involves the parasite cytoskeleton, a myosin A (MyoA) motor complex (Daher and Soldati-Favre, 2009), parasite actin (Dobrowolski and Sibley, 1997), and micronemal transmembrane proteins of the Thrombospondin-related adhesive protein (TRAP) family that interact with actin *via* the glycolytic enzyme aldolase (Huynh and Carruthers, 2006; Sultan et al., 1997). The sequential secretion of micronemes and rhoptries leads to formation of a tight junction between the parasite and the host cell (Meissner et al., 2013). The apical complex and the IMC actively contribute to parasite motion, which is conserved across the whole phylum.

Gliding motility has been most extensively studied in *Toxoplasma gondii,* due to its feasibility for cell biological, biochemical, and genetic studies. TRAP, a surface protein has also been implicated to be essential for invasion. The TRAP family of proteins bind to host cell heparin sulphate proteoglycans, an interaction important for invasion of hepatocytes. TRAP-deficient parasites are unable to migrate within the mosquito, implying the essentiality of TRAP for invasion (Sultan et al., 1997).

Despite the wealth of knowledge available, recent studies have questioned our understanding of gliding motility. Independent studies investigating the role of actin using actin polymerization inhibitors like cytochalasin D (CytD) reached different conclusions (Gonzalez et al., 2009). This could be explained because of various concentrations of the inhibitors used or different parasite lines. However, recent reverse genetic studies show that blocking of several components of glideosome, including actin and myosin, results in parasites still capable of infecting host cells (Andenmatten et al., 2013).

1.2.1   *Components of the gliding machinery*

Adhesive proteins, such as members of the TRAP family are discharged from the apical storage organelles, micronemes. The discharge is stimulated by contact with the host cells, and this in turn is regulated by intracellular calcium (Ca) levels in the parasite (Sibley, 2010). Following the initial contact with host cells, rhoptries are discharged, injecting their contents into the forming vacuole and also into the host cell cytosol, where they form small

4

vesicles called vacuoles. During invasion, a tight junction forms between the parasite and the host cell. This junction is called the moving junction (Hakansson et al., 2001).

According to the present model, force for gliding or invasion is generated by the concerted action of a myosin motor complex, actin filaments and the IMC (Foth et al., 2006; Heaslip et al., 2010). The myosin motor complex is comprised of a small myosin (MyoA), myosin light chain (MLC1) homologues that wrap around MyoA, and two anchoring proteins called GAP45 and GAP50 (Dobrowolski and Sibley, 1997). MyoA is only 23-24 % identical to other myosin heavy chains and has a short neck and no tail domain. The short neck domain binds MLC1, and these associate with GAP45 and GAP50 to form the myosin motor complex. The motor complex is immobilized on the IMC at one and binds the actin filament on the other end. The actin filaments communicate with ligands on the host surface through bridging proteins. The co-ordinated action of myosin along with actin filaments results in forward motion of the parasite that is sufficient for both gliding and invasion (Baum et al., 2006; Kappe et al., 1999; Opitz and Soldati, 2002)**(Figure 3)**.
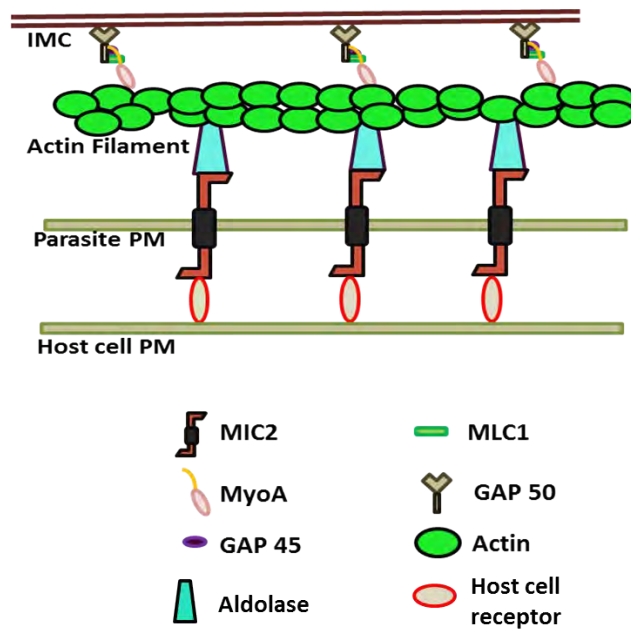
Figure 3: Schematic representation of gliding motility.

The first step involves attachment of the parasite to the host cell, which is mediated by secretion of adhesion proteins on the surface. The two cells form a connection across the parasite plasma membrane and thereby communicate between the parasite cytoskeleton and host cell receptors. The coordinated motor machinery formed by the myosin and actin filaments generates force required for the movement of the parasite.

1.3   *Conventional actins*

Actin is the major cytoskeletal protein of most cells. Monomeric actin polymerizes into filaments, up to several micrometres in length. Actin filaments within cells are organized into higher-order structures, forming bundles or three-dimensional networks with the properties of semi-solid gels. Actin filaments are abundant below the plasma membrane, where they form a network that provides mechanical support, determines cell shape, and allows movement of the cell surface, thereby allowing cells to migrate, engulf particles, and divide (Pollard and Cooper, 2009).

Many prokaryotes use actin relatives to maintain asymmetrical shapes and to move deoxyribonucleic acid (DNA) through the cytoplasm (Walsh, 2009). All eukaryotes have genes for actin. Vertebrates express three main actin isoforms, including three α isoforms of skeletal, cardiac, and smooth muscle cells as well as β and γ isoforms expressed in non-muscle and muscle cells (Herman, 1993).

1.3.1   *Sequence conservation of actin*

Actin belongs to a structural superfamily with sugar kinases, hexokinases, and heat shock protein (Hsp) 70 proteins (Bork et al., 1992; Graceffa and Dominguez, 2003). All the three families of proteins can bind and hydrolyse adenosine triphosphate (ATP). Canonical actin isoforms share more than 90 % sequence identity (Muller et al., 2005). In spite of the sequence identity being so high, the isoforms still have distinct functions. This high conservation of actin can be reasoned by the presence of multiple actin binding partners; hence, for proper function, strict sequence conservation is essential.

1.3.2   *Actin monomer structure*

The key role actin plays in various cellular processes makes it a very interesting molecule for both structural and functional studies. The most challenging part of achieving actin crystals is the fact that actin polymerizes, leaving the solution inhomogeneous and an unideal candidate for crystallization. Hence, actin has been frequently crystallized either in complex with actin binding proteins (ABP) or with small molecules or labelled to prevent polymerization. The first crystal structure of actin was determined in complex with deoxyribonuclease-1 (DNase I) (Kabsch et al., 1985) at 4.5-Å resolution and subsequently to

6

higher resolutions of 2.8 Å and 3 Å in ATP- and adenosine diphosphate (ADP)-bound forms, respectively (Kabsch et al., 1990).

The 375 amino acid polypeptide chain of actin folds into two major α/β domains, known as the inner and outer domain, based on their location in the filament, or as the small and large domain, based on their size. Each domain is subdivided into two sub-domains (SD). SD1 and 3 are structurally related and have probably evolved *via* gene duplication, while SD2 and 4 can be viewed as large insertions to SD1 and 3, respectively. The actin molecule is flat, fitting into a rectangular prism with dimensions of 55 Å x 55 Å x 35 Å (Dominguez and Holmes, 2011; Graceffa and Dominguez, 2003; Otterbein et al., 2001; Wang et al., 2010) **(Figure 4)**.

SD1 contains a five-stranded β-sheet, assembled from a β meander and a right-handed βαβ unit. The sheet is surrounded by five α-helices (residues 1-32, 70-144, 338-372). SD2 consists of a three-stranded antiparallel β-sheet, with an α-helix connecting the two strands at the edges (residues 33-69). At the top of SD2, residues 39-51, are disordered in most of the crystal structures. This loop is referred as DNase I binding loop (D-loop) as it mediates the interaction in the actin-DNase I complex. The D-loop takes up a variety of conformational states dependent *e.g.* on the nucleotide bound to actin. The nucleotide-dependent conformational change in the D-loop might underlie the difference in monomer-monomer affinity between ATP monomers and ADP monomers as seen in electron microscopic (EM) studies (Belmont et al., 1999; Khaitlina and Strzelecka-Golaszewska, 2002; Orlova et al., 2004) on filamentous (F)-actin and in biochemical studies on globular (G) and F-actin (Moraczewska et al., 1996; Moraczewska et al., 1999). SD3 consists of a five-stranded β-sheet, surrounded by three α-helices. The domain topology is identical to SD1, suggesting that actin may have evolved by gene duplication, although the sequence similarity does not predict any internal symmetry. SD4 consists a two-stranded antiparallel β-sheet and four α-helices (residues 181-269). The loop centred at Lys336 and the linker helix Gln137–Ser145 form the region of contact between SD1 and 3 and functions as a hinge between the domains. As a result, two clefts are formed; the "upper cleft" binds a nucleotide – either ATP or ADP – and a divalent cation, while the lower cleft is predominantly lined by hydrophobic residues, which bind to ABPs and participate in longitudinal contacts within

the actin filament. Communication between the two clefts forms the structural basis for the nucleotide-dependent conformational change mediated by ABPs (Graceffa and Dominguez, 2003; Wang et al., 2010).

1.3.3 *Nucleotide-binding pocket of ATP and ADP bound structures*

The adenine base of ATP or ADP fits into a pocket formed by residues Lys213, Glu214, Thr303, Met306, and Lys336. These amino acids do not form specific interactions with the base. The ribose ring is in the 2'-endo conformation. The 2' and 3'-hydroxyl groups of the ribose participate in hydrogen bonds (H-bond) with one of the oxygen atoms of the carboxylate groups of Glu214 and Asp157, respectively. The phosphate groups in ATP- and ADP-bound structures are involved in a large number of interactions. The O1-atoms of the α and β-phosphates in both ATP- and ADP-bound structures form H-bonds with the main chain amide group of Gly302 and Ser14 Gly15, Leu16, respectively. The γ-phosphate in the ATP-bound structure is involved in H-bonds with the amide group of Asp157, Gly158, and Val159. Most of these interacting residues belong to the β–hairpin loops from SD1 and 3 (Graceffa and Dominguez, 2003; Kabsch et al., 1985; Kabsch et al., 1990; Otterbein et al., 2001) **(Figure 4)**.
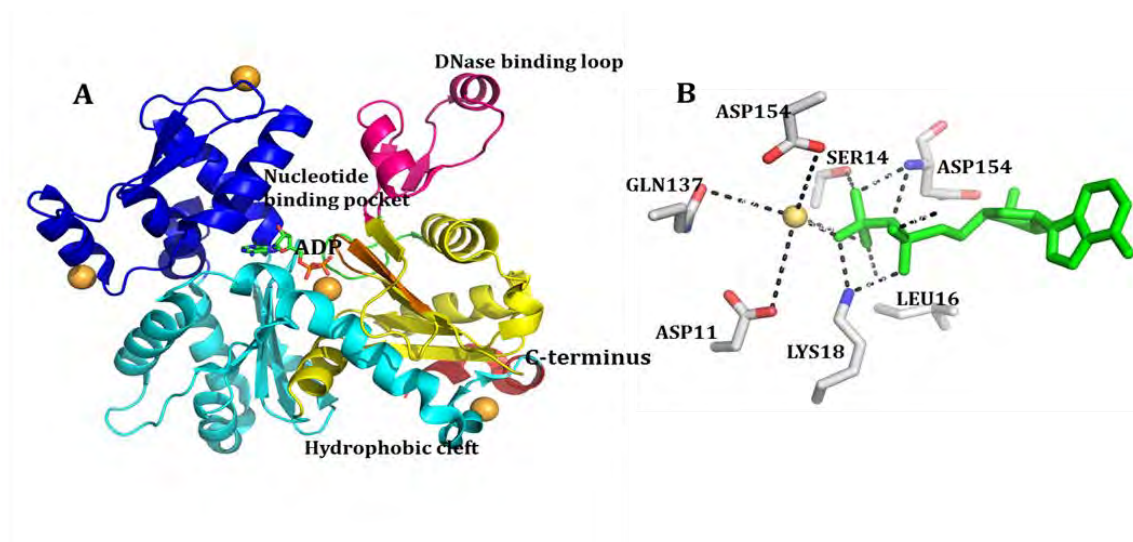
Figure 4: Structure of G-actin.

 (A) Structure of un-complexed actin in the ADP state [PDB ID 1J6Z]. The different sub-domains are represented in following colours: yellow – SD1, pink – SD2, cyan – SD3, blue – SD4. The C-terminus α-helix is shown in red, and the sensor loop is represented in green (Otterbein et al., 2001) **(B)** Enlarged view of the nucleotide-binding pocket showing residues involved in specific interactions with the nucleotide.

1.3.4   *Nucleotide-dependent conformational states of actin*

Actin undergoes two major nucleotide-dependent conformational changes; one upon the release of the γ-phosphate and the second upon the release of ADP. Structures with a bound nucleotide, either ADP or ATP, are in a closed conformation, while the nucleotide-free structure represents an open conformation. The network of H-bonds between the nucleotide and the actin backbone helps to hold the two major domains together. Two β-hairpin loops – one from each of the two major domains – account for the majority of interactions with the nucleotide and the divalent cation. Some of these interactions are lost upon γ-phosphate release, while most of the interactions, which keep the two domains together, are lost upon ADP release. Consequently, ATP-actin is more stable than ADP-actin.

1.3.5   *Kinetics of actin self-assembly and hydrolysis of ATP*

G-actin under physiological conditions assembles into double-stranded helical filaments, *i.e.* polymers, in which any subunit i interacts with subunits i+2 and i-2, in addition to the adjacent subunits i+1 and i-1 (Oda and Maeda, 2010). The filaments are assembled in a head-to-tail fashion, which gives them molecular polarity, one end being the fast growing end (called the barbed end) and the other being the slow growing end (called the pointed end). *In vitro,* without any regulatory proteins, polymerization depends on temperature, pH, and ionic strength of the solution and the concentration of actin.

One molecule of actin binds one ATP, and the transition from G to F-actin activates its ATPase activity in a process that involves formation of transient F-actin bound to ADP and P_i, followed by the release of P_i into the solution, leading to F-ADP-actin. The release of P_i is the rate-limiting step. The ADP-actin monomers are depolymerized from the pointed end. ATP is not resynthesized when F-actin depolymerizes, but the ADP molecule bound to the G-actin that dissociates from the ends of the filaments is exchanged for ATP in solution, and, thus, G-ATP-actin is regenerated. Actin continuously cycles through polymerization and depolymerisation, these states in a process called treadmilling, resulting in continuous hydrolysis of ATP (Carlier et al., 1997; Pollard et al., 2001) **(Figure 5)**.
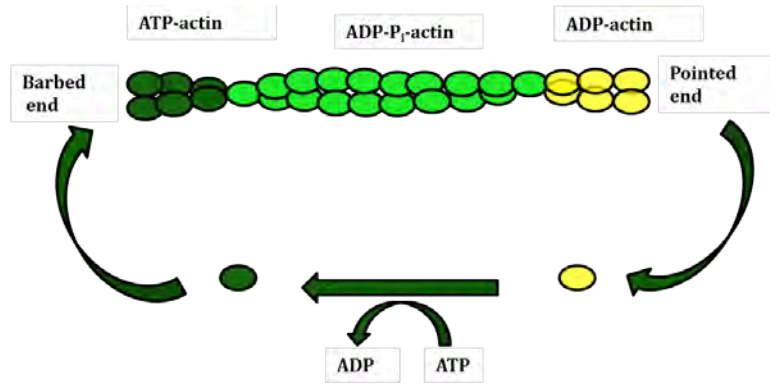
Figure 5: Actin treadmilling.

G-ATP-actin polymerizes into F-actin. During this process, ATP is hydrolyzed into ADP. ADP-actin dissociates from the filament more readily than ATP-actin. When the actin polymer is at steady-state, these kinetic differences result in a process known as treadmilling. During treadmilling, the filament maintains its constant length in a dynamic equilibrium. There is a directional growth of the filament from barbed to pointed end. The subunit flux through the polymer and the polymerization rate at the barbed end equals the rate of depolymerization at the pointed end.

The tightly-bound ATP is hydrolysed upon polymerization of G-actin to F-actin, while the reverse is not true. Hence, actin polymerization cannot be considered as a reversible process. The time course of ATP hydrolysis closely parallels the formation of F-actin under most conditions of polymerization. During very rapid polymerization, the rate of addition of ATP-actin subunits to the filament ends initially exceeds the rate of ATP hydrolysis, resulting in an increase of ATP-actin at the growing filament end; while the less distal subunits are ADP-P_i-actin and the deep core of the filament contain ADP-actin. As polymerization proceeds, the monomer concentration falls, and thus, the rate of elongation decreases, until it becomes less than the rate of ATP hydrolysis on the F-actin. The growing filament is thus not homogenous, and the degree of heterogeneity varies with the rate of growth, *i.e.*, with the concentration of G-actin: at the (so-called) steady state, the relative number of terminal ATP-actin and sub-terminal ADP-P_i-actin is minimum. When the polymerization reaches this so-called steady state, ATP hydrolysis continues at a slower, constant rate until all available ATP has been hydrolysed.
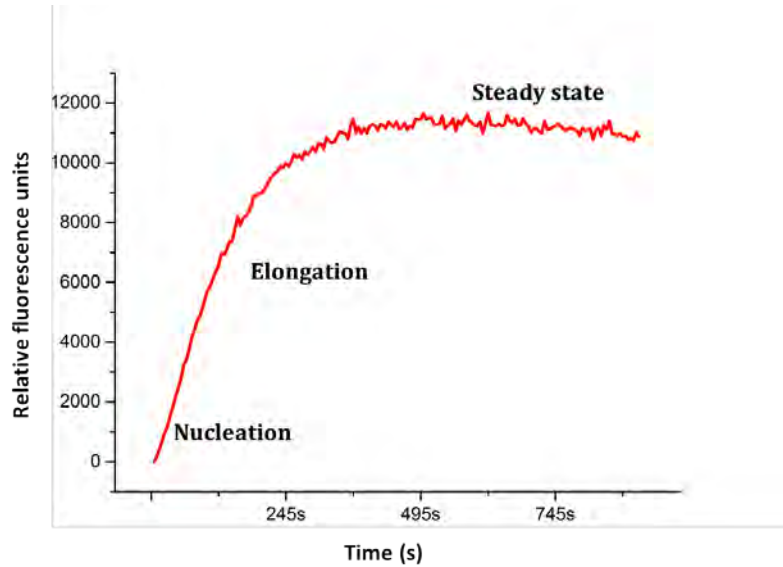
Figure 6: Time course of actin polymerization.

The initial phase of polymerization is characterized by a lag phase, were actin forms transient nuclei, followed by elongation of the nuclei into filaments. Finally, a steady state is reached where the rate of addition of monomers and loss of monomers from the two ends are the same and hence no further elongation of filaments takes place.

In addition, ATP hydrolysis plays a key role in the regulation of actin filament dynamics. G-actin is not an effective ATPase, but upon incorporation into the filament, conformational changes in the monomer lead to more efficient ATP hydrolysis. ATP hydrolysis is fast with a half time of ~2 s. The properties of ATP-actin and ADP-P_i-actin are identical, but the subsequent slow dissociation of the terminal γ-phosphate ($t_{1/2}$ ~350 s) that generates ADP-actin leads to structural rearrangements that favour the disassembly of actin filaments. Especially at the barbed end, ATP-actin dissociates less frequently than ADP-actin, as reflected by the corresponding rate constants (Blanchoin and Pollard, 2002; Pollard, 1986) **(Figure 7)**. This difference of kinetic properties at the different ends, at steady state under physiological conditions, result in average polymerizing of one end and depolymerizing of the other end, *i.e.,* treadmilling of filaments. The rate of hydrolysis of ATP depends on divalent cation bound to the high affinity site. In physiological conditions, magnesium (Mg^{+2}) is the preferred cation over Ca^{+2}, Mg^{+2} –ATP is hydrolysed six times faster than Ca^{+2} –ATP.

The actin-ATP-Ca^{+2} molecule undergoes a moderately fast (k=0.05 sec^{-1}), rate-limiting 1st order activation reaction, where it exchanges its Ca^{+2} to Mg^{+2}. The activated monomers form

11

nuclei and elongate into filaments more rapidly than inactivated molecules. The overall polymerization reaction is limited by the slow, thermodynamically unfavourable nucleation phase. The filament nuclei are transient intermediates that exist only for a few milliseconds at very low concentrations, primarily because of two reasons: (i) they are unstable and (ii) they are rapidly consumed by the subsequent rapid elongation reaction. When the concentration of actin monomers exceeds the critical concentration (C_c) for polymerization, elongation of dimer or trimer nuclei occurs at both ends. However, the elongation rate at the pointed end is 5 -10 times lower than the elongation rate at the barbed end. The dissociation rate constants are similar at both ends, resulting in a higher C_c at the pointed end. Elongation stops when the concentration of monomers decreases to the C_c, which is the monomer concentration, at which the rate of loss of monomers from filament ends equals the rate of addition of monomers (Andrianantoandro and Pollard, 2006; Tobacman and Korn, 1983)(**Figure 7)**.
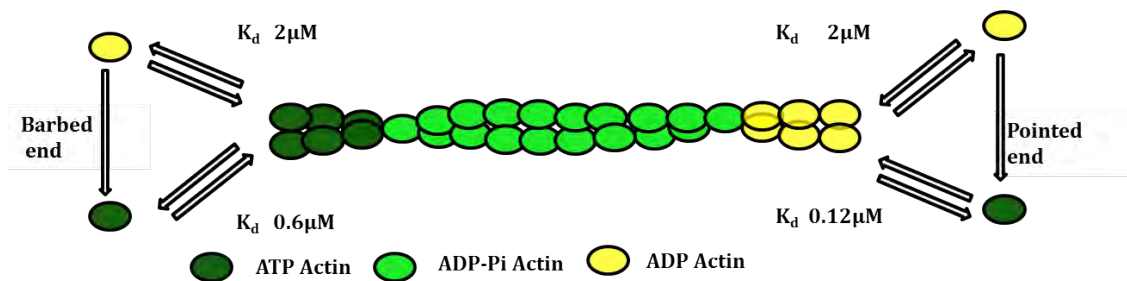
Figure 7: Dissociation equilibrium constant K_d at pointed and barbed ends.

K_d for ADP-actin at both barbed as well as pointed ends are same, however K_d is higher for ATP actin at barbed end than pointed end, thus resulting in elongation at the barbed end.

1.3.6 *Phosphate release*

Crystals of ATP-actin could be obtained in similar conditions as ADP-actin, however nucleotide hydrolysis occurs during the time of crystal growth, probably due to the high salt concentration in the crystallization condition. Hence, a non-hydrolysable ATP analogue-AMPNP actin crystals were grown to mimic the ATP-actin state (Graceffa and Dominguez, 2003; Otterbein et al., 2001). Comparison of the crystal structures of un-complexed ADP-actin (labelled with tetramethyl rhodamine (TMR)) and of non-hydrolysable ATP–actin provides valuable insight into the events involved in the release of P_i. The release of P_i involves the following structural changes; (i) rotation of Ser14, (ii) a change in the

conformation of the sensor loop, and (iii) rotation of SD2 and the D-loop. In the ATP-actin structure, the presence of the γ-phosphate forces the side chain of Ser14 to rotate, which is different from the ADP-actin structure, where it is directed towards the β-phosphate. Ser14 in the ATP structure is hydrogen bonded to an oxygen atom of the γ-phosphate and to the carbonyl oxygen of Gly74 from the loop containing the methylated His73. The orientation of Ser14 results in two different conformations of the sensor loop containing the methylated His73. In the ADP-actin structure, this loop moves towards the β-hairpin loop containing Ser14 because of steric hindrance. The sensor loop, Pro70 to Asn78, constitutes an insert between actin SD2 and 1 and functions as a switch, linking changes in the nucleotide binding site to structural transitions in SD2. The absence of stacking interactions between the His73 and Glu72 side chains in the ATP-actin structure makes the loop less stable than in the ADP-actin structure. In the ATP-actin structure, changes in the sensor loop are accompanied by a 4° rotation in SD2. The D-loop of SD2 in the ATP-actin structure is fully disordered and is undetermined in contrast to the ADP-actin structure, where it forms a stable α-helix (Graceffa and Dominguez, 2003) **(Figure 8)**.
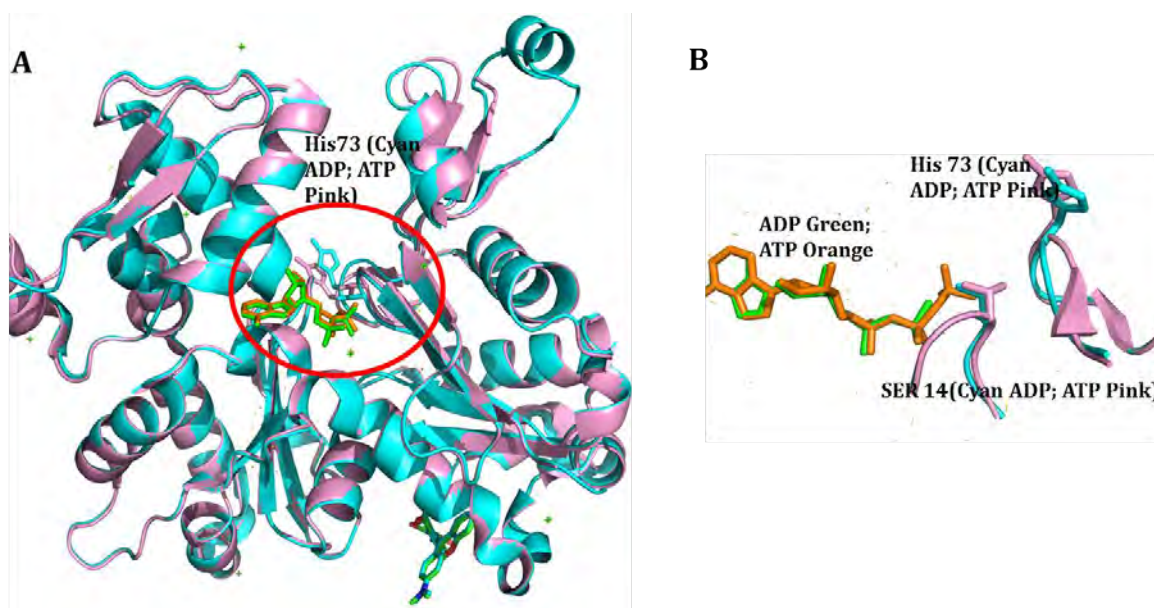
Figure 8: Superimposition of crystal structures of actin in ATP- and ADP-bound forms.

(A) ATP-actin (PDB ID 1NWK; Otterbein et al., 2002) is shown in pink and ADP-actin (PDB ID 1J6Z; Graceffa & Dominguez, 2003) in cyan. The black circle highlights the difference in orientation of the sensor loop containing residues interacting with the γ-phosphate of ATP. **(B)** Enlarged view of the region circled in black in panel A.

1.3.7   *Filamentous actin structure*

The structure of F-actin was first determined using X-ray fibre diffraction (Holmes et al., 1990). More recently, several high-resolution structures of F-actin have been determined and modelled using cryo-EM (Galkin et al., 2010; Murakami et al., 2010; Oda et al., 2009; Oda and Maeda, 2010).

1.3.7.1 Inter- and intra-strand contacts in F-actin

The intra-strand contacts, *i.e* contacts between individual actin protomers within the same strands in the filament, involve extensive contacts between SD2 and SD4 of the lower promoter and SD3 of the promoter above it **(Figure 9)**. Residues 283-294 of i+2 are enclosed by residues 61-65, 200-208 and 241-247 of subunit i. The D-loop extends towards the hydrophobic groove of subunit i+2 between sub-domains 1 and 3. Val43 and Met44 of subunit i make contacts with residues Leu346 and Phe375 of subunit i+2.

The inter-strand lateral contacts with the opposite strand of the filament are formed by two projections. One is between the C terminus of subunit i and the N terminus of subunit i+1 in the opposite strand. The other one is formed by the hydrophobic plug of i+1, which contacts four regions of i+2 including the D-loop **(Figure 8)**.

1.3.7.2 Structural changes involved in the G- to F-actin transition

The actin monomer goes through a conformational change upon insertion into the filament. The structural rearrangements involve a flattening of the actin molecule. The G-actin crystal structure and the F-actin model subunit conformations are related by a 20° rotation of the two major domains (1 and 3). Residues 141-142 and 336-337 act as hinge for the rotation. Also the D-loop in the F actin model is extended, which enables it to fit to the surface of the upper subunit along the strand **(Figure 9).**

1.4   ***Actin-binding proteins***

For the regulation of the structure and dynamics of the actin cytoskeleton, many ABPs have evolved. The process has involved duplication and mutations of DNA sequences encoding a small number of protein motifs that interact with G-actin and F-actin in a specific manner (Lappalainen et al., 1998). Most eukaryotic cells use >100 accessory proteins to maintain the pool of actin monomers, initiate polymerization, control the length of actin filaments,

regulate filament turnover, and crosslink filaments into bundles or networks (Pollard and Cooper, 2009). Though ABPs are extremely diverse, both structurally and functionally, they mostly share a common binding cleft. This binding cleft is lined by the residues Tyr143, Ala144, Gly146, Thr148, Gly168, Ile431, Ile345, Leu346, Leu349, Thr351, and Met355. The conformation of this cleft is such that it preferentially binds an α-helix of the binding partner. This helix is characterized by exposed and conserved hydrophobic side chains. As the cleft is at the hinge region between the two actin domains, binding in this region can be an effective way to sense the nucleotide dependent conformational states of actin. Crystal structures of some ABPs [gelsolin, vitamin D-binding protein (DBP) and Wiskott-Aldrich syndrome protein (WASP)- homology domain- 2 (WH2)-related proteins] and toxins (kabiramide C and jaspisamide A) with actin suggest the hydrophobic cleft between SD1 and 3 as the hot spot for binding. (Otterbein et al., 2002; Schutt et al., 1993; Yarmola et al., 2001) **(Figure 10)**.
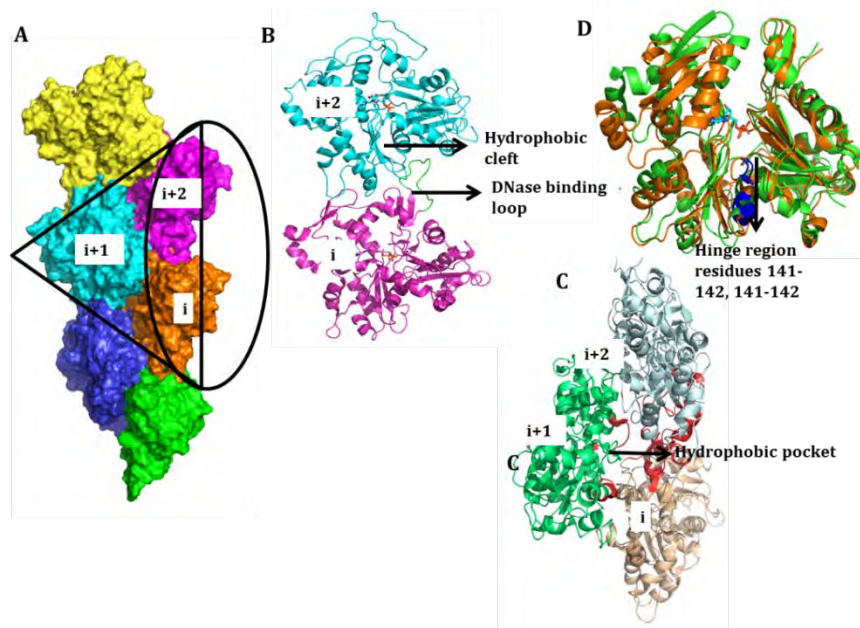
Figure 9: Structure of F-actin.

(A) Shown is the surface of a two-stranded actin helix (PDB ID 2ZWH; (Oda et al., 2009). The individual actin protomers are shown in different colours. **(B)** The lower protomer interacts with the hydrophobic cleft of the upper promoter in an extended conformation as highlighted in green color. **(C)** Inter-strand contacts 1) between the C terminus of subunit i and N terminus of subunit i+1 in the opposite strand 2) the hydrophobic plug of i+1, which contacts four regions of i+2 including the D-loop. **(D)** Superimposition of the G-actin crystal structure (PDB ID 1NWK (Graceffa and Dominguez, 2003) to a protomer of F-actin shows a rotation of 20˚ of SD3 and 4 about an axis passing through SD1 and 2, as identified by DYNDOM (Hayward and Berendsen, 1998).
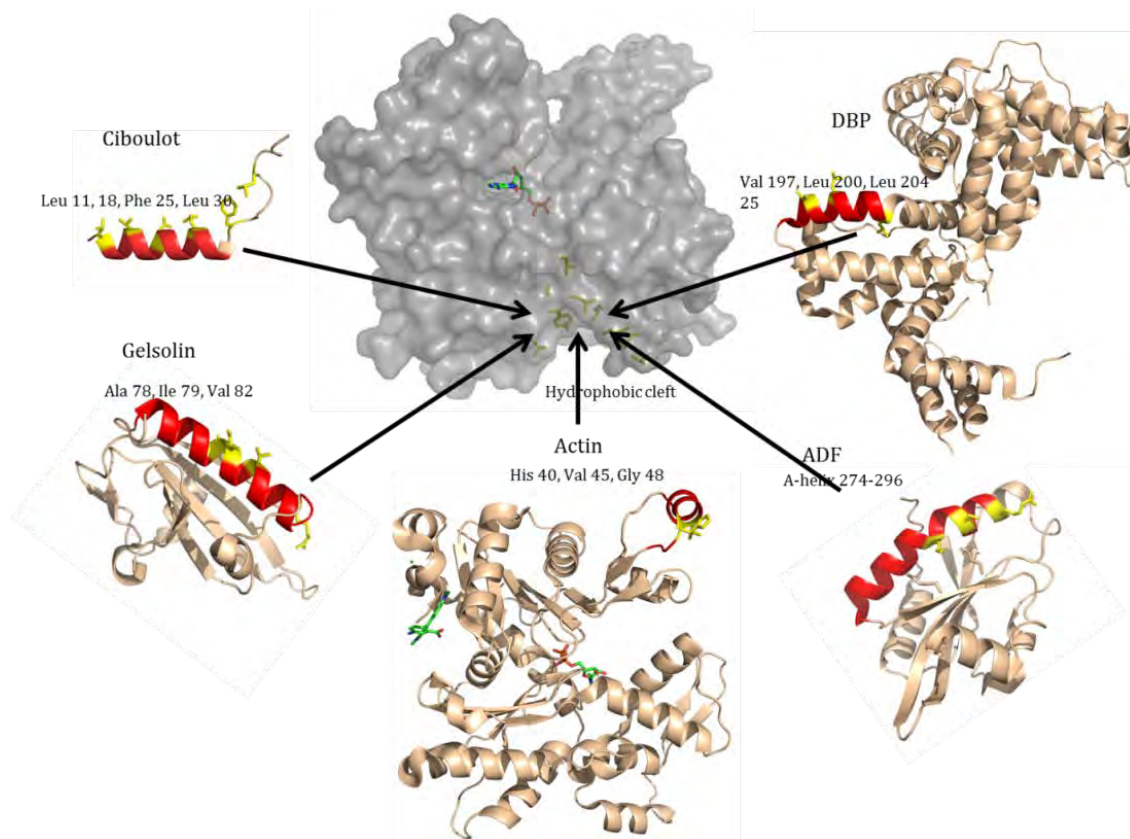
Figure 10: Hot spot of actin.

ABPs target the hydrophobic cleft of actin, which is denoted as a "hot spot". Shown in red are the actin-binding sites of various ABPs. Vitamin D binding protein [PDB ID 1LOT] (Head et al., 2002), human cofilin-1 (4BEX) (Klejnot et al., 2013), an actin monomer [PDB ID 1J6Z] (Otterbein et al., 2001), gelsolin [PDB ID 3FFN] (Hertzog et al., 2004), and ciboulot [PDB ID 1SKQ] (Vitagliano et al., 2004) bind to the hydrophobic cleft of actin via an α-helix.

1.4.1 *Monomer binding proteins*

Rapid growth of actin filaments requires tight regulation of actin monomers, which is achieved by a group of actin monomer binding proteins. A large number of monomer binding proteins have been identified – mammalian cells have more than 25 of them. These proteins bind to ADP-actin upon release from pointed ends of actin filaments (e.g. twinfilin, cofilin), facilitate nucleotide exchange from ADP to ATP (*e.g.* profilin, CAP), and deliver the monomers to barbed end for new rounds of polymerization [e.g. twinifilin, CAP, profilin, WASP and verprolin (Perelroizen et al., 1995; Winder and Ayscough, 2005). In motile cells, release of a large pool of polymerizable actin would enhance filament extension; this is achieved by monomer sequestering proteins like thymosin. Thymosin acts by clamping ATP-actin from top to bottom and releases the ATP-actin monomers on

receiving appropriate signals, resulting in a massive increase of the polymerizable actin pool (dos Remedios et al., 2003; Hertzog et al., 2004; Irobi et al., 2004).

1.4.2 *Actin nucleating proteins*

Nucleation is the first step of actin filament formation, which is indicated by a lag period. *In vivo,* actin nucleators like actin related protein (Arp) 2/3, bind to the actin nucleus and stabilize it to enable growth of filaments. Although Arp2/3 nucleates actin *in vitro,* it is likely that *in vivo* the function of Arp2/3 is facilitated by other ABPs, most importantly WASP and WAVE proteins. Additionally, the Arp2/3 complex can nucleate actin filaments from the sides of existing filaments, resulting in branched networks (Paavilainen et al., 2004). Formins are also known to facilitate the assembly of actin filaments by promoting nucleation and elongation, while remaining associated with the barbed ends. A characteristic feature of formins is the homodimeric formin homology (FH) 2 domain, which interacts with the barbed end of actin filaments. Studies have shown that the FH2 domain accommodates processive addition of monomers to the barbed end (Xu et al., 2004) (Kovar et al., 2006). In yeast, long actin cables are generated by the action of formins, while short branching networks by the Arp2/3 complex.

1.4.3 *Actin filament growth, stability, and disassembly regulators*

Once nucleated, actin filaments are able to grow rapidly by addition of monomers. Filament growth is regulated by several ways. The length of the filaments is controlled by capping proteins. Barbed end cappers, like capping protein (CP), gelsolin, and tensin, bind to the barbed end of actin filaments in a 1:1 stoichiometry to prevent addition and loss of subunits at this end (Cooper and Sept, 2008). For CPs, from experiments with conventional actin, it can be concluded that capping the barbed end decreases the overall polymerization rate, increases the critical concentration for actin polymerization to that of the pointed end and, thus, reduces the length of actin filaments (Cooper et al., 1984; Xu et al., 1999). Pointed end cappers, like tropomodulin, reduce the loss of monomers from the pointed end, thereby leading to rapid filament elongation (Yamashiro et al., 2012).

Actin depolymerizing factors (ADF) are the best characterized proteins that drive depolymerization. ADFs preferentially bind ADP-bound forms of both G- and F-actin. ADFs at steady state bind to the ADP-G-actin pool, while the ATP-G-actin pool is free for

polymerization. ADFs bound to G-actin inhibit nucleotide exchange strongly, so that only the unbound ADP-G actin undergoes nucleotide exchange to regenerate the ATP-G-actin pool for polymerization. Additionally, ADFs enhance the rate of filament treadmilling until a steady state is reached when polymerization onto the barbed end becomes equal to the dissociation of ADF-ADP-actin from the pointed end (Andrianantoandro and Pollard, 2006; Carlier et al., 1997; Pavlov et al., 2007; Schüler et al., 2005b). The other unique property of ADFs is the induction of a large structural change in the actin filament, accompanying its lateral association, which seems responsible for ADF-induced filament severing. ADFs will be discussed in more detail in chapter 1.7.
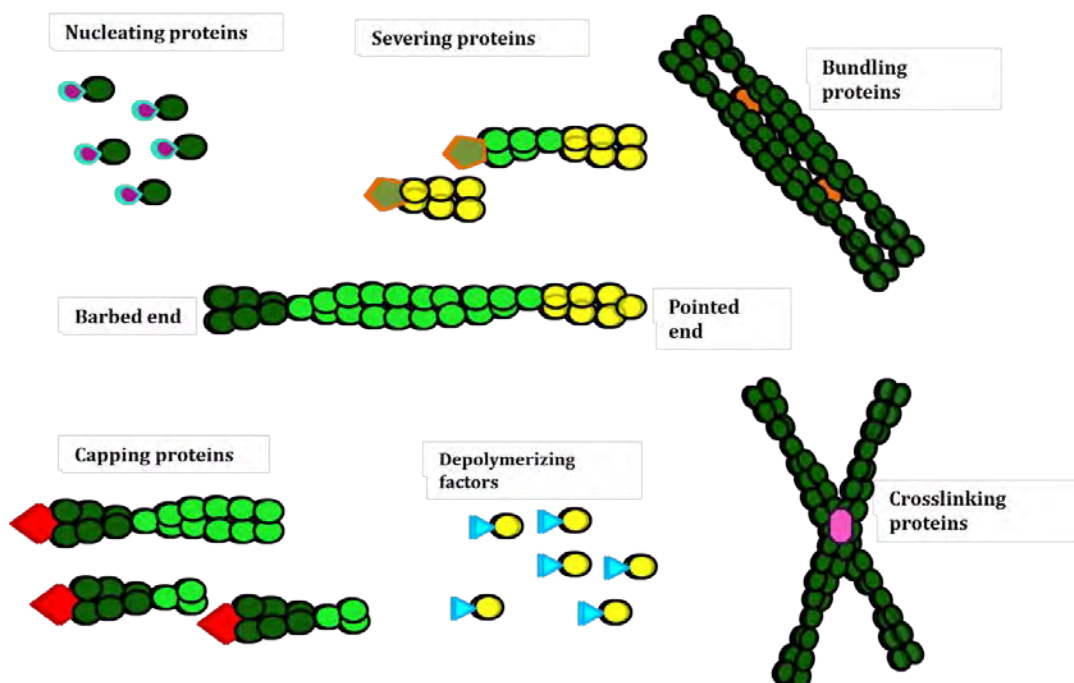
Figure 11: Schematic representation of different actin regulators.

Monomer sequestering proteins like profilin bind to ATP-actin and, hence, increase the pool of polymerizable actin. Capping proteins cap the barbed end of actin filaments and prevent the addition or loss of monomers from the barbed (+) end. Actin depolymerizing proteins accelerate the rate of dissociation from the pointed (-) end. Crosslinking proteins form the three dimensional arrangement of actin filaments. Bundling proteins form arranged bundles of actin filaments. Severing proteins bind to the filaments and introduce a twist, resulting in severed filaments.

1.4.4 *Crosslinking proteins*

Bundling and crosslinking of actin filaments are essential for various cellular processes. Spectrin (Marchesi and Steers, 1968), filamin (Razinia et al., 2012), and coronins promote network formation of actin filaments in higher eukaryotes (Cai et al., 2007; Goode et al.,

1999; Humphries et al., 2002). Coronin is necessary for rearrangements of the actin cytoskeleton and also important for cytokinesis and locomotion.

1.4.5   *Actin bundling proteins*

Bundling proteins bind actin filaments using two discrete binding sites and arrange actin into linear arrays, either parallel or antiparallel. Bundling proteins, such as fimbrins, have two actin binding sites in close proximity resulting in tight actin bundles as found in microvilli (Volkmann et al., 2001). In contrast, proteins like α-actinin bundle actin into loosely ordered structures, as the actin binding sites as far away and separated from each other by helical spacer regions (Burridge and Feramisco, 1981).

1.5   ___Apicomplexan actins___

An actomyosin motor is thought to be the power generator for gliding motility, enabling the parasite to cross nonpermissive biological barriers and driving the entry into and exit from host cells. The contribution of actin and myosin in motility was suggested in the 1970s and 1980s. It became later clear from inhibitor studies that drugs interfering with actin dynamics [cytochalasin D (CytD), jasplakinolide (JAS), and latrunculin B] or myosin ATPase function [2,3-butanedion (BDM)] inhibit parasite gliding and invasion (Dobrowolski et al., 1997; Hegge et al., 2010). Generation of a *Toxoplasma* mutant line resistant to CytD demonstrated that the invasion process relies essentially on the parasite actomyosin cytoskeleton and not on host actin. Though gliding motility of *Toxoplasma* can be blocked by treatment with CytD, attachment was unaltered (Ryning and Remington, 1978). Surprisingly, recent reverse genetics studies have demonstrated that removal of core components of gliding motility is possible without blocking host cell penetration, suggesting an additional invasion mechanism that facilitates host cell invasion in knock out mutants (Meissner et al., 2013). Despite the clear contribution of an actomyosin motor in parasite motility, parasite actin filaments have never been seen *in vivo*. Recent studies have shown that actin either produced from heterologous systems or extracted directly from parasite shows unique biochemical properties by forming very short filaments (about 100 nm in length) that are less stable than conventional actin (Sahoo et al., 2006; Vahokoski et al., 2014). This would explain the failure of direct visualization by EM techniques. Though a large fraction of apicomplexan actin is found in monomeric form, filaments can be stabilized

by treatment with JAS, which induces acrosome-like structures at the apical pole of *Toxoplasma* (Hegge et al., 2010; Mehta and Sibley, 2011).

Although actins are highly conserved, with less than 10% divergence from yeast to mammals, phylogenetic analysis reveals that there are key differences between apicomplexan actins and other actins. *Plasmodium* has two actins, while *Toxoplasma* has only one actin. Both the *Plasmodium* actins at the sequence level are less than 80 % identical with both the canonical actins as well as each other (Dobrowolski and Sibley, 1997; Vahokoski et al., 2014). This difference at the sequence level might explain the different biochemical properties of parasite actins. *Plasmodium falciparum* actin 1 (*Pf*ACT1) can be detected throughout the whole life cycle, while *P. falciparum* actin 2 (*Pf*ACT2) is only expressed during the sexual stages, most highly in gametocytes (Skillman et al., 2011; Wesseling et al., 1988; Wesseling et al., 1989).

According to previous observations, *Pf*ACT1 polymerizes only inefficiently. In an *in vitro* study with recombinant *Pf*ACT1, filament formation was only detected in the presence of both gelsolin (a filament capping protein that can promote nucleation) and phalloidin (a polymer stabilizing peptide). It is conceivable that parasite-specific regulatory proteins fulfill similar tasks. Even under the influence of stabilizing agents, the *Pf*ACT1 and *Toxoplasma gondii* actin (*Tg*ACT) polymers are much shorter in comparison to bovine non-muscle actin (Sahoo et al., 2006; Schüler et al., 2005b). Hence *Pf*ACT1 forms only very short filaments *in vivo* as well, which appears to be an inherent property of apicomplexan actins.

Much of the sequence differences between apicomplexan and other eukaryotic actins are located in regions involved in monomer-monomer contacts within the actin filament (Vahokoski et al., 2014). Furthermore, structural considerations suggest that apicomplexan F-actin might prefer the ADP-bound open state and become more unstable after ATP hydrolysis than conventional actin. These characteristics may explain the lower affinity between parasite actin molecules and the different polymerization properties observed (Schmitz et al., 2010). Therefore, experiments with recombinant apicomplexan actins predict that the low polymerizability, instability and short polymer length most probably are intrinsic properties of these molecules and not simply an effect of regulatory proteins (Schmitz et al., 2005; Schüler et al., 2005b; Vahokoski et al., 2014). The repertoire of ABPs in apicomplexan parasites appears unexpectedly small compared to other eukaryotes (Keeley

and Soldati, 2004). This might imply that the apicomplexan ABPs are specialized to perform novel functions to compensate the missing ABPs.

1.6 *Minimal repertoire of apicomplexan actin binding proteins*

1.6.1 *Monomer binding proteins*

Three classes of proteins specialized to bind monomeric actin are present in apicomplexan parasites: profilin, ADFs and Srv2/cyclase-associated protein (CAP). In *P. falciparum* and *T. gondii*, profilin has been studied and has been found to sequester G-actin, promote nucleotide exchange from ADP to ATP like conventional profilins, and mediate polymerization in the presence of nucleators, such as formins. Reverse genetic experiments performed of *P. berghei* confirmed that profilin is expressed in all stages of life cycle. *P. falciparum* profilin interacts with proline rich peptides, which are present in various regulatory proteins, including formins (Kursula et al., 2008).

Cofilins affect the filament dynamics by sequestering monomers, severing filaments and pointed end depolymerisation. *P. falciparum* expresses two different cofilins; ADF1 and ADF2, and *T. gondii* expresses one cofilin.

Apicomplexan parasites have a single CAP, which is short and contains only an actin binding domain. Apicomplexan CAPs lack the N-terminal adenyl cyclase binding region, central proline-rich motifs and a WH2 domain, which are present in conventional CAPs. *Plasmodium* CAP is important during sexual stages, in particular in oocyst development. Apicomplexan CAPs are thought to sequester actin monomers (Dodatko et al., 2004; Hliscs et al., 2010; Mattila et al., 2004). The *C. parvum* CAP structure has been determined and has a β-barrel structure, which dimerizes by domain swapping (Dodatko et al., 2004). Surprisingly, apicomplexan parasites lack the actin monomer binding protein β-thymosin.

1.6.2 *Actin nucleators*

Apicomplexan parasites lack an Arp2/3 complex and its regulators, such as WASP/WAVE, which are the most important nucleators across eukaryotes. Along with Arp2/3, apicomplexan parasites also lack any obvious orthologue to Spire. In the absence of these regulators, the most obvious nucleators are formins (Baum et al., 2008a; Daher and Soldati-Favre, 2009; Prakash et al., 1990). Apicomplexans have two formins, 1 and 2, containing conserved FH2 and rudimentary FH1 domains. Also a third formin and a nuclear formin-like

protein have been identified in both *Plasmodium* and *Toxoplasma*, respectively (Daher et al., 2010; Prakash et al., 1990). Formin 1 and 2 both are expressed throughout the stages of the *Plasmodium* life cycle, though expression of formin 1 is higher before erythrocyte invasion, while formin 2 is expressed in higher amounts at the mid trophozoite stage (Baum et al., 2008b). *Plasmodium* formin 1 has two pairs of two proline residues (Baum et al., 2008b) and formin 2 has two potential profilin-binding sites, though they are not canonical penta-proline repeats common in eukaryotic formins. Formin 1 has been shown to nucleate actin monomers (Ignatev et al., 2012).

1.6.3 *Filament capping proteins*

Gelsolin, the most important filament capping protein in higher eukaryotes, is absent in *Apicomplexa*. Hence, the CP α and β subunits appear to be the only filament end capping proteins in apicomplexan parasites. CP binds to filament barbed ends and regulates their growth. Both the subunits are expressed in *Plasmodium*. Tropomodulin, the pointed end capper, is also absent in apicomplexan parasites (Baum et al., 2006).

1.6.4 *Crosslinking and bundling protein*

Coronin is the only bundling protein present in the phylum *Apicomplexa*. *T.gondii* coronin has been shown to localize in the posterior end of the parasite and affects invasion but not motility (Salamun et al., 2014). Coronin in *Babesia spp.* and in *Plasmodium spp.* has been shown to bind actin and specifically F-actin, respectively (Figueroa et al., 2004; Tardieux et al., 1998).

1.7 *Conventional actin depolymerizing factors*

ADF was first identified and purified in 1980 from embryonic chicken brain and named for its ability to depolymerize low concentrations of filamentous actin from bovine brain extract (Bamburg et al., 1980). Four years later, cofilin-1 was isolated from porcine brain and named for its ability to sediment with actin. Further characterization showed that both proteins show similar effects on filamentous actin. Since then, many related proteins have been discovered, including invertebrate depactin from *Asterias amurensis* (Maekawa et al., 1984), destrin from mammals, cofilin-1 isoform found in nonmuscle tissue, cofilin-2 isoform first identified in muscle and called m-cofilin, ADF from *Acanthamoeba* (Abe et al., 1990),

22

coactosin from *Dictyostelium* (Dancker et al., 1975), twinstar from *Drosophila melanogaster*, UNC60A and UNC60B from *Caenorhabditis elegans*. All these proteins share a considerable (30-40%) sequence identity. Mammals have multiple ADFs, and their expression patterns vary depending on developmental stages and cell types.

ADFs are essential for cell motility and appear to set the direction of motility (Ghosh et al., 2004). Every eukaryotic cell expressing actin expresses also one or multiple ADFs (Bamburg and Bernstein, 2008), and ADFs localize to subcellular regions where the activity of actin is maximal (dos Remedios et al., 2003). ADFs interact with both G-actin and F-actin with dissociation constants in the micromolar range. ADFs have a higher affinity for ADP-actin than for ATP-actin; they decrease nucleotide exchange from ADP actin monomers and promote P_i release from ADP-P_i subunits of the filament. ADFs affect actin filament dynamics in a concentration-dependent manner. At lower concentrations, when only a few molecules of ADF are bound to an actin filament, the number of torsionally strained interfaces between twisted and non-twisted filament regions may be maximal and might result in filament breakage, which is termed as severing. Enhanced severing results in more filament ends, resulting in enhanced filament assembly (Bobkov et al., 2006; Ichetovkin et al., 2002; Orlova et al., 2004; Pavlov et al., 2007). At higher concentrations, when the filament is decorated with ADFs, severing is no longer observed; ADFs then enhance the dissociation of monomers from the pointed end, resulting in faster depolymerisation of ADP-actin. Subsequently, dissociation of ADF from ADP-actin takes place, following which ADP is exchanged to ATP, resulting in a larger association flux of ATP-G-actin at the barbed ends. Additionally, in the presence of profilin, the rate of pointed end disassembly is even faster, resulting in a higher flux (Carlier et al., 1997). Finally, at even higher concentrations (in the micromolar range) of ADFs, monomer binding and nucleation are enhanced, and assembly of filamentous actin is promoted **(Figure 12)**. However the mechanism, by which ADFs promote filament assembly, is a matter of debate. It has been thought that ADFs promote assembly of filaments by increasing the rate of elongation at the barbed end. In another view, ADFs are argued to stabilize actin nuclei, intermediates of actin assembly, by lowering the rate of dissociation of the nuclei (Carlier et al., 1997).
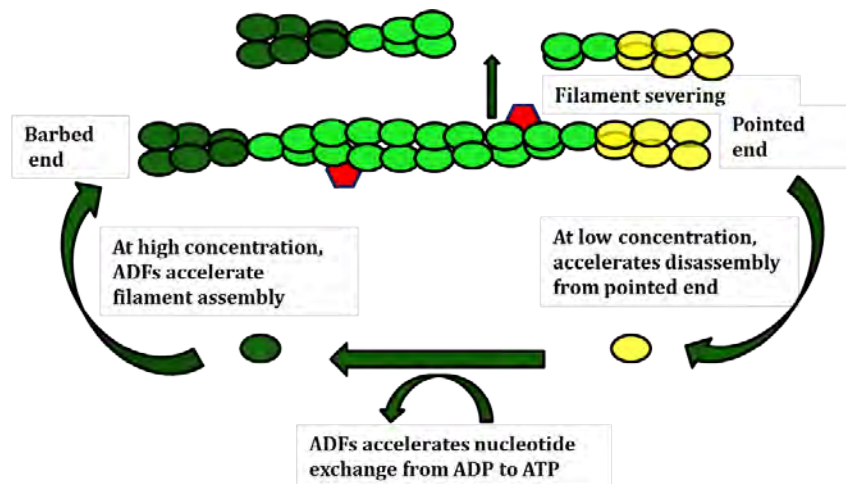
Figure 12: Role of ADF during the actin polymerization cycle.

The action of ADF is dependent on the ADF:actin ratio. At low concentrations, ADF induces treadmilling of actin from the pointed end and severing of actin. At high concentrations, ADFs accelerate the elongation of filaments from the barbed end.

1.7.1 *Structure of the ADF homology domain*

ADFs have an ADF-homology (ADF-H) domain as the basic structural motif. The basic feature of this domain is a central hydrophobic core, built up of a central β sheet containing 4 or 5 β strands, flanked by a pair of α helices **(Figure 13)**. The most notable X-ray Crystal structures of ADFs are from *Acanthamoeba castellanii* (Leonard et al., 1997), *Arabidopsis thaliana* (Bowman et al., 2000)*,* yeast cofilin (Fedorov et al., 1997) and *Plasmodium falciparum* ADF1 (*Pf*ADF1)and *Plasmodium berghei* ADF2 (*Pb*ADF2) (Singh et al., 2011; Wong et al., 2011) as well as solution structures of human cofilin (Klejnot et al., 2013), *Toxoplasma gondii* ADF (*Tg*ADF) (Yadav et al., 2011) and mouse coactosin (Hellman et al., 2004) have been determined (Pope et al., 2004).

1.7.2 *Actin-ADF interactions*

Further insight into understanding actin regulation by ADFs was gained from crystal structure and EM studies of G and F-actin in complex with ADFs. To date, the only crystal structure available of an ADF-H domain bound to G-actin is that of the C-terminal domain of twinfilin (Twf-C) in complex with rabbit muscle actin (Paavilainen et al., 2008). Interaction of ADFs with actin can be divided into two regions: the upper site binding to G-actin, named as the G-site, and the lower region binding to F-actin, called the F-site (Galkin et al., 2011).

24
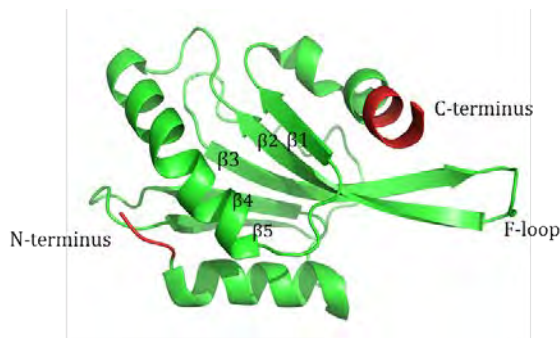
Figure 13: Structure of the ADF-H domain.

The structure of yeast cofilin [PDB ID 1QPV] (Fedorov et al., 1997), showing the basic structural motif of an ADF-H domain, consisting of a core of 5 β strands flanked by α helices. The N and C termini are shown in red, and the F-actin binding F-loop is is labelled (Fedorov et al., 1997).

1.7.2.1 G-actin binding site of ADFs

In the crystal structure of Twf-C bound to actin, Twf-C binds to the hydrophobic cleft of actin through an interface that buries an area of ~1200 Å. Three major interaction sites can be categorized into: (1) Two N-terminal residues which are part of a flexible extension (Fedorov et al., 1997) of the ADF-H domain in the absence the of actin but become ordered in the presence of actin, (2) the long α helix 3, and (3) the region before the C-terminus of the Twf-C domain **(Figure 14)**. Among these regions, the most obvious contacts are made between residues Q176, R276, R269, S273, K276, K294, E296 of Twf-C with F375, S348, A144, Y143, E167, and T148 of actin (Paavilainen et al., 2008). In addition, several residues are involved in hydrophobic contacts across the interface. Mutagenesis and biochemical studies have also revealed that these residues are important for interaction with G-actin. Deletion of the five N-terminal residues and mutations of R96, K98, D34, E36, and K38 to alanine are lethal, and hence, are particularly important for the interaction between yeast cofilin and G-actin. Binding of ADF also causes conformational changes in the D-loop and the C-terminus of actin (Lappalainen et al., 1997).
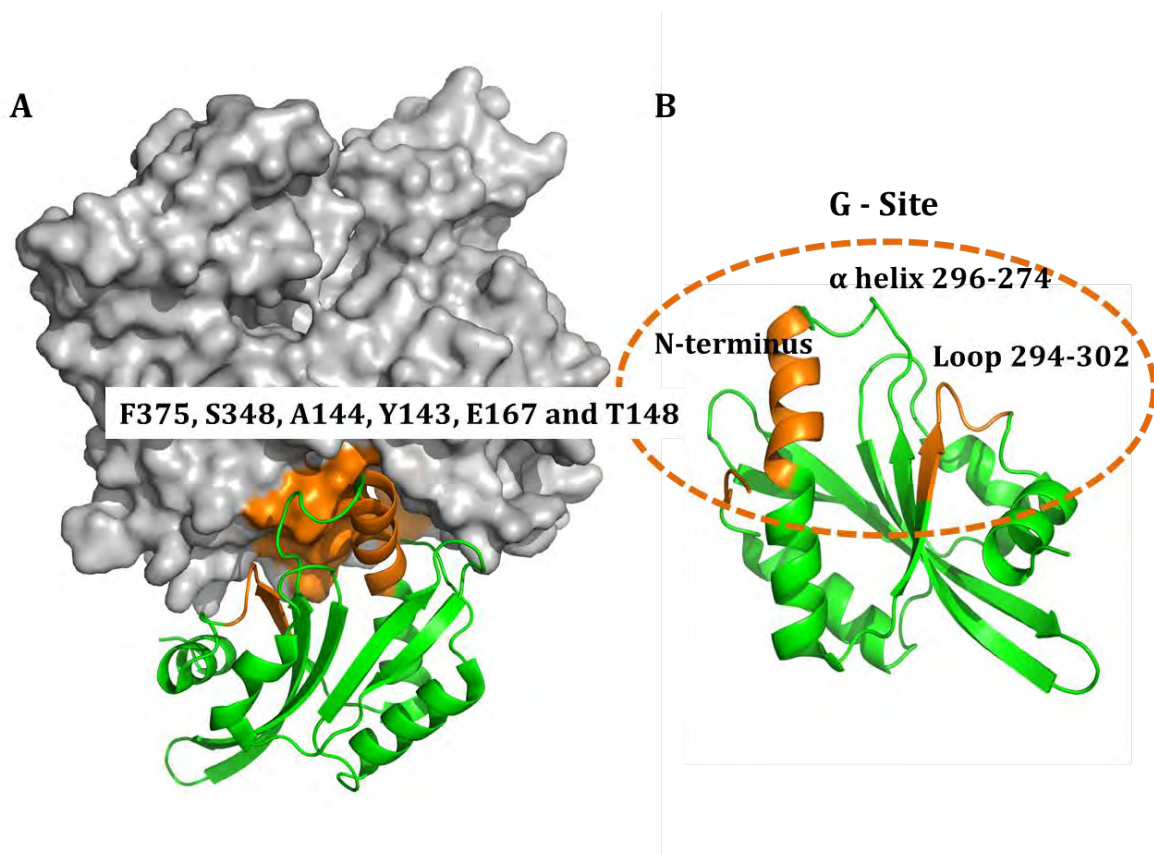
Figure 14: Structure of actin bound to Twf-C.

(A) Monomeric actin bound to Twf-C domain. Marked in orange is the ADF G-site that interacts with the hydrophobic cleft of actin shown between subdomains 2 and 4 [PDB ID 3DAW] (Trukhanov, 1991). **(B)** The regions on Twf-C interacting with actin are shown in orange, as in panel A.

1.7.2.2 F-actin binding site of ADFs

It is essential to understand the interaction ADFs and F-actin in order to understand how ADF influences actin dynamics. A cryo-EM structure of actin filaments decorated with human cofilin-2 has been determined at 9-Å resolution (Galkin et al., 2011). According to cryo-EM studies on F-actin decorated with human cofilin-2, cofilin has two sites of contact with the filament. The first site is between a small loop of cofilin (residues 154-158**) (Figure 15)** with actin residues 242 and 243 in SD4, which are crucial for maintaining the integrity of the filament. Mutations of yeast cofilin residues corresponding to A150, E151 and G154 of human cofilin-2 also lead to a reduced affinity to F-actin. The second site involves cofilin residues 94-98 that form extensive contacts with residues 21-28 and 90-96 in SD1 of actin **(Figure 15)**. Mutations of yeast cofilin residues corresponding to K96 and

D98 in human cofilin-2 also showed weak binding to F-actin and depolymerizing activity (Lappalainen et al., 1997; Moriyama et al., 1990). ADFs change the twist in actin filaments by changing the rotation per subunit by about 5° (Galkin et al., 2011), while maintaining a constant rise per subunit, which results in a reduction of the filament crossover distance without changing the overall length of the filament.
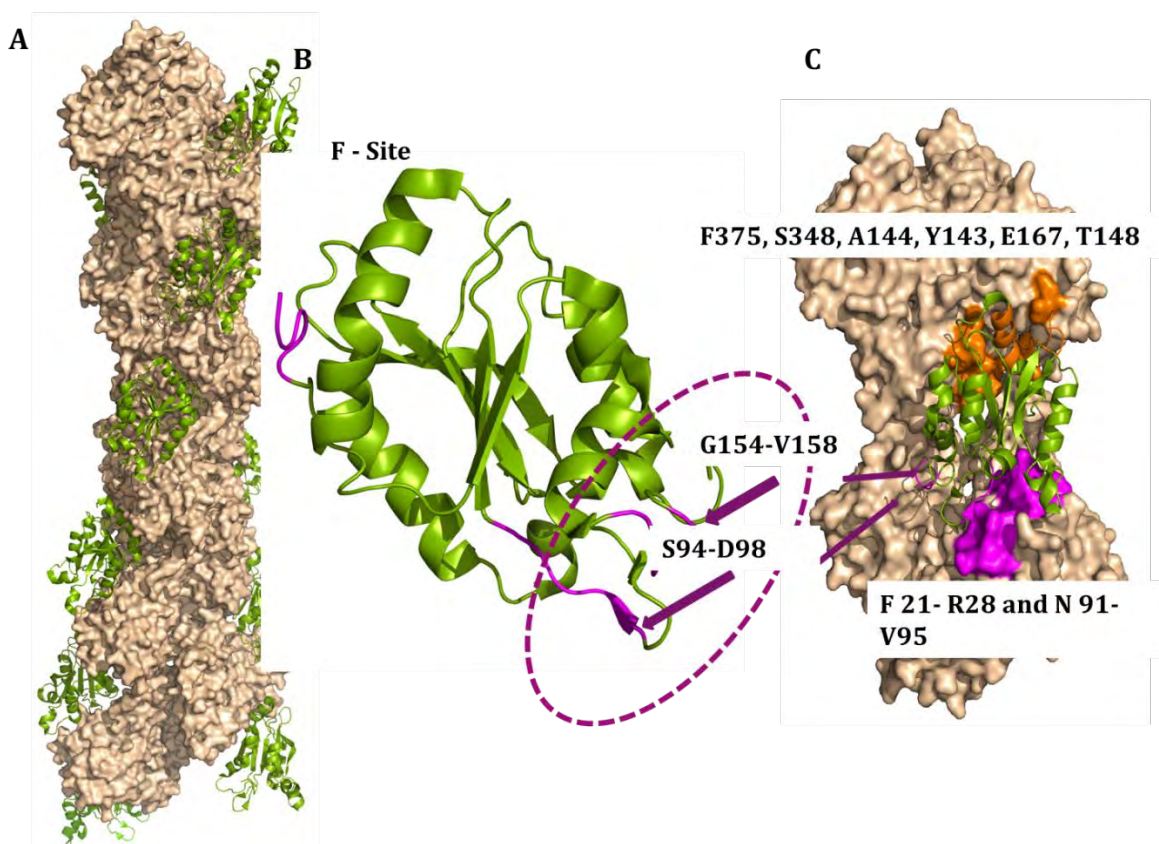
Figure 15: Structure of ADF bound to F-actin.

(A) The surface of the cryo-EM structure of F-actin is shown in grey bound to the ADF-H domain of cofilin in represented green [PDB ID 3JOS] (Galkin et al., 2011). **(B)** Shown in green is the X-ray crystal structure of cofilin and the residues highlighted in magenta are involved in F-actin binding. **(C)** Enlarged view of cofilin binding site on F-actin (Galkin et al., 2011).

1.8   *Apicomplexan actin depolymerizing factors*

Most members of the phylum *Apicomplexa,* including *Toxoplasma* and *Cryptosporidium,* have one ADF, while *Plasmodium spp.* have two. Apicomplexan ADFs are among the smallest members in the family. *Plasmodium* ADF1 is expressed in all life cycle stages, while *Plasmodium* ADF2 is expressed only in the sexual stages of the parasite life cycle within the

mosquito host. ADF1 lacks the conserved F-actin binding motif and binds to G-actin, while ADF2 resembles canonical ADFs at the sequence level and binds both G-actin as well as F-actin. Both *Plasmodium* ADFs promote nucleotide exchange from ADP to ATP in the actin monomer, unlike the conventional ADFs (Schüler and Matuschewski, 2006). *Pf*ADF1 shows 29% sequence identity with *A. castellanii* actophorin, and *Pb*ADF2 shows 38% sequence identity *Arabidopsis thaliana*. *Tg*ADF shows 39% identity to actophorin (Allen et al., 1997).

1.8.1 *Structure of Plasmodium actin depolymerizing factors*

Crystal structures of *Pf*ADF1 and *Pb*ADF2 have been determined (Singh et al., 2011; Wong et al., 2011). Both proteins closely resemble the classical ADF family members. The core consists of a six-stranded β-sheet flanked by two helices **(Figure 16).**
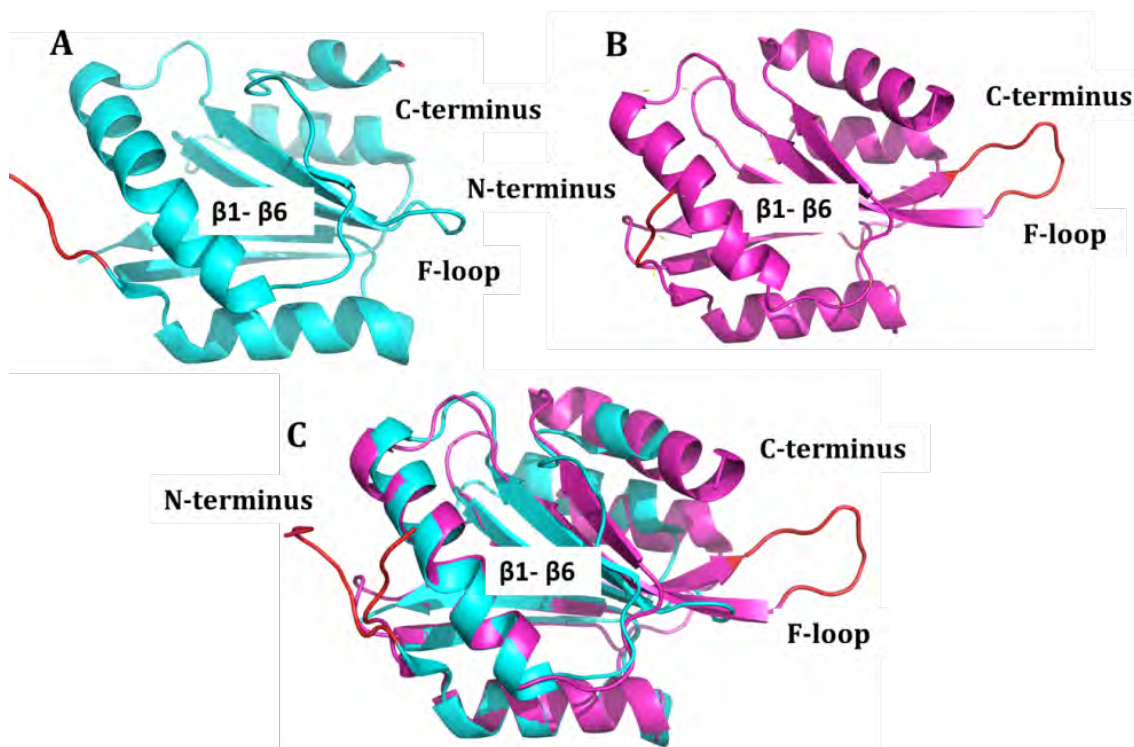
Figure 16: Crystal structures of PfADF1, PbADF2 and yeast cofilin.

(A) The X-ray crystal structure of *Pf*ADF1 is shown in cyan [PDB ID 2XF1] (Singh et al., 2011). **(B)** The X-ray crystal structure of *Pb*ADF2 is shown in magenta [PDB ID 2XFA] (Singh et al., 2011; Wong et al., 2011). **(C)** Superimposition of *Pf*ADF1 in cyan [PDB ID 2XF1] (Singh et al., 2011) and *Pb*ADF2 in magenta [PDB ID 2XFA](Singh et al., 2011). In figures 16 C, D, E is marked F-loop is marked, the N-terminus and C-terminus are marked in red. Note that the F-loop and C terminus shorter in *Pf*ADF1 (Fedorov et al., 1997; Singh et al., 2011).

However, there are some significant differences in the *Plasmodium* ADFs compared to each other and to the canonical ADFs. In particular, these differences concentrate to the G-actin and F-actin binding sites. The largest differences in the apicomplexan ADFs lie in the C-terminal half of the protein. The C-terminal β-hairpin loop connecting the β sheet 5 to the C terminus is missing in ADF1, while is conserved in ADF2. The C terminus of ADF2 is longer, while it is truncated in ADF1. α-helix 3, which is highly conserved and is involved in G-actin binding, has some small differences, the hydrophobic patch of residues surrounding the N terminus α-helix 3   which are involved in actin binding in are not conserved, these differences may be significant in case of apicomplexan ADFs. Also the C-terminal α-helix 4 has a kink in other ADFs, which is missing in *Plasmodium* ADFs **(Figure 16)**.

1.9   ***Phosphoinositide regulation of the cytoskeleton***

Phosphoinositides (PPIs), collectively refer to phosphorylated derivatives of phosphoinositols (PI) and have pivotal role as precursors to important secondary messengers and in signalling pathways. Cytoskeletal proteins were the first to be shown to be regulated by PPIs. The first reports came in 1985 the about interaction between actin skeleton of erythrocyte membrane and PPIs (Anderson and Marchesi, 1985). Next, it was shown that phosphatidylinositol 4,5 bisphosphate (PIP$_2$) dissociated the profilin-actin complex *in vitro* to promote actin polymerization, which was followed by reports of the gelsolin-actin complex also dissociating in the presence of PIP$_2$ (Yin and Janmey, 2003). These findings showed that PIP$_2$ affects actin polymerization possibly by recruiting ABPs to membranes and, hence, altering their effects. Most of the cytoskeleton studies have focused on PIP$_2$ as the other PIs are present at much lower concentrations in cells.

Many PI binding motifs have been recognized recently through sequence searches for well-conserved lipid-binding modules, such as the pleckstrin homology (PH), FYVE (named after four cysteine rich proteins: Fab1, YOTB, Vac1 and EEA1), phox and epsin N-terminal homology (ENTH) domain (Cullen et al., 2001; McLaughlin et al., 2002), and later the lipid binding potential of these proteins has been confirmed. The binding of PIs to these domains is highly reversible to favor dynamic responses and is generally of low-to-moderate affinity. Strikingly, most of the cytoskeletal proteins that bind to PIs, lack the conserved binding

motifs and interact through electrostatic interactions. However, how specificity of these electrostatic interactions is maintained is an outstanding question.

1.9.1 *Binding of phosphoinositols to actin-binding proteins*

Different ABPs have various mechanisms for interaction with PIP_2, by which they interact with membranes containing PIs. These mechanisms can be categorized into three classes of interactions. The first mechanism involves docking of a protein to a membrane in a manner that disrupts the interactions between the domains within monomer or homo-oligomers that mask binding sites of actin or membrane anchors. This model applies to WASP proteins, ERM proteins, talin, alpha-actinin and vinculin. This mechanism results in activation rather than inhibition of protein function.

Some of the cytoskeletal proteins have specific PI-binding sites, like spectrin, which has a PH domain that binds PI with a low affinity (Hyvonen et al., 1995). WASP and some of its close homologs also have a PH-like domain (referred to as WH1) that has been reported to bind PIs (Rohatgi et al., 2001). However, recent evidence shows that binding takes place via lysine-rich regions (Imai et al., 1999). Like WASP proteins, many other cytoskeletal proteins bind PIs via basic or aromatic residues rather than structured motifs. For some of the ABPs, the actin-binding site coincides with the PI-binding site and, hence, binding to PI dissociates actin competitively. Recent studies on yeast and chicken cofilins show that their actin and PI binding sites are not precisely coincident (Gorbatyuk et al., 2006; Ojala et al., 2001). Furthermore, PI binding promotes oligomerization of cofilin/ADFs and subsequently promotes actin-filament bundling (Pfannstiel et al., 2001). Likewise, profilin binds to PIP_2 with an extensive surface, and this binding increases the α-helical content of the protein (Raghunathan et al., 1992). On the contrary, for gelsolin and related proteins, binding to PI induces rearrangements of the actin-binding site or a local unfolding of the polypeptide within the actin biding domain to derange the surface required to bind actin (Lin et al., 1997). The third mode of binding, which is used by proteins like WASP, ERM, talin, α-actinin and vinculin, involves docking of the protein to the membrane in a manner that disrupts interactions between domains within the molecule resulting in masking of the actin-binding site (Steimle et al., 1999).

1.9.2 *Regulation of actin depolymerizing factors*

Cellular functions of ADFs are regulated by several factors, such as pH, phosphorylation, and interaction with PIs. Although a wealth of knowledge is available about the different domains involved in PI recognition (Cullen et al., 2001; McLaughlin et al., 2002) and binding, the exact mode of interaction of ADFs with PIs in *Apicomplexa* is still not understood (Misra et al., 2001). PI binding affects the actin-related functions of ADFs. In a mutational study on yeast cofilin, it has been shown that ADFs interact with PIs in a multivalent manner through a large positively charged surface at the C-terminal end of α-helix 3, which overlaps with the F-actin binding site, resulting in abrogation of ADF-F-actin interactions (Ojala et al., 2001). Binding is also dependent on salt and PI concentrations. The head group is the main interacting moiety, and the acyl groups do not interact with cofilin. The main residues involved in binding are E134, R135 and R138 (Zhao et al., 2010).

In an NMR study, it was suggested that the C-terminal part of chicken cofilin interacts with PIs (Gorbatyuk et al., 2006). In accordance to this, a dodecyldimethylaminoxid (LDAO) molecule was bound to the C-terminal region of *A. thaliana* cofilin crystal structure. It was hypothesized that this binding resembles the binding mode of PI (Leonard et al., 1997). The main residues involved in binding were K132 and H133, which are conserved in vertebrates but are not conserved in invertebrates. Interestingly, mutants of K132 and H133 showed a difference in the chemical shift of K125, which corresponds to R109 in yeast cofilin, shown to be involved in PI binding. However, common to all the studies is the fact that cofilins interact with highest affinity to PIP$_2$, which is most likely the physiologically relevant ligand. In another study, it was shown using peptide mapping that the N-terminal region of chicken cofilin, (residues D9-V36), is important for binding to PIs (Kusano et al., 1999) **(Figure 17)**. In apicomplexan parasites, the interplay between ADFs and actin is crucial. Thus, the regulation of ADFs by phosphorylation or by PI binding may play an important role in actin dynamics regulation of ADFs. To date, not much is known about the interaction of apicomplexan ADFs with PI. Interestingly, the crystal structure of *Pf*ADF1 has four sulphate molecules bound to Arg6, Arg21, Lys100 and Lys101, which may mimic the PI binding site to *Pf*ADF1 (Singh et al., 2011).
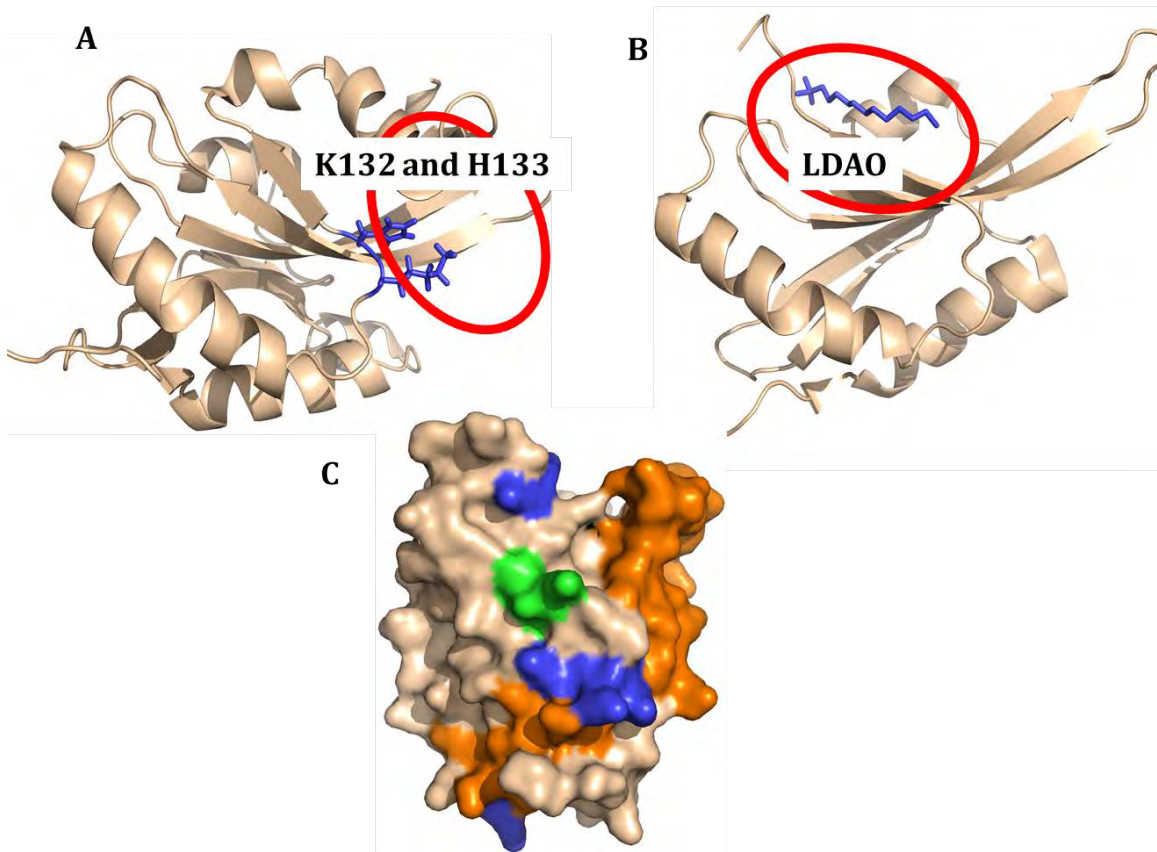
Figure 17: PI binding of cofilins.

(A NMR structure of chicken cofilin with the residues K132 and H133 coloured in blue that are predicted to be important for PI binding by NMR (Gorbatyuk et al., 2006). **(B))** X-ray crystal structure of At ADF bound to LDAO, assumed to occupy the same binding site as PI, i.e., at the C terminus (Leonard et al., 1997). **(C)** The positively charged surface of human cofilin 1 is indicated in blue. The residues corresponding to chicken cofilin which are studied to be involved binding to PIs are shown in green while coloured in orange are the residues important for PI binding as by shown peptide mapping studies (Gorbatyuk et al., 2006).

1.10 ***Capping proteins***

CPs, as the name suggests, are proteins that bind to the barbed end of actin filaments with high affinity and cap them. When CP is bound to the barbed end of an actin filament, there is no loss or addition of actin monomers to/from that end. In cells, CP is important for dynamics of actin filament assembly, which is important for cell shape maintenance and motility (Cooper et al., 1984; Cooper and Sept, 2008; Xu et al., 1999). CP was first characterized and purified from muscle cells, in 1960 by Maruyama and colleagues. The first non-muscle CP was purified from *Acanthamoeba* in 1980 (Ichetovkin et al., 2002; Yamashita et al., 2003). CPs are αβ heterodimers with an α subunit of 32-36 kDa and a β subunit of 28-

32 kDa. Highly conserved homologues of CPs are found in all eukaryotes and various cell and tissues in invertebrates (Casella et al., 1986).

Vertebrates have two isoforms of the α and β subunit, each, and an additional male germ cell specific isoform, while invertebrates only have one isoform for each subunit. The two isoforms of α, namely α1 and α2, are encoded by two genes, while β1 and β2 are produced from a single gene by alternative splicing (Hart et al., 1997). There is not much literature available on the distinct functions of the two isoforms of the α subunit.

1.10.1 *Structure of conventional capping proteins*

The X-ray crystal structure of the CP αβ heterodimer from chicken CapZ (Yamashita et al., 2003) gave new insight into the structure and function of CPs. The crystal structure reveals that CP has a pseudo two-fold rotational symmetry. Both subunits have very similar secondary and tertiary structures, although they do not have a high degree of amino acid sequence similarity. The overall structure resembles a mushroom; the stalk consists of six α-helices (three from each subunit), while the cap consists of a ten stranded antiparallel β-sheet (five from each subunit), on top of which lie the two C-terminal α-helices (from each of the subunits) running perpendicular to the β-sheet. The C terminus of both subunits consists of an amphipathic α-helix. In the β-subunit, the helix protrudes out of the protein, while in the α-subunit; it is folded onto the surface of the protein, making hydrophobic contacts **(Figure 18)**. The hydrophobic side of the C-terminal amphipathic helix of the β-subunit binds actin, and mutating the conserved hydrophobic residues in the C terminus of the β-subunit (Leu258, Leu262, Leu266) of CapZ leads to a significant decrease in capping affinity (Casella et al., 1986; Kim et al., 2004).

For chicken and yeast CP, the removal of C-terminal ends (residues R259-A286 for CapZ α-subunit and R244-N277 for the β-subunit) results in complete loss of capping activity. The individual subunit deletion mutant causes impaired barbed end capping, but to a different extent. Removal of only the α C-terminal end reduces capping affinity by 5000-fold, while removal of only the β C-terminal end reduces the affinity by only 300-fold. Also, single mutations of highly conserved residues of the α-subunit (W271R and R259A) were sufficient to decrease binding affinity respectively (Wear and Cooper, 2004). Along these

lines, a synthetic peptide corresponding only to the C-terminal 30 amino acids of yeast CP α-subunit was enough to inhibit actin polymerization (Kim et al., 2010). Similarly, a peptide corresponding to the C-terminal 28 residues of the β-subunit of CapZ could weakly cap the filament end, albeit with reduced activity compared to wild type CP. These results suggest that CP uses the two C-terminal ends of both subunits independently to cap the F-actin end (Barron-Casella et al., 1995; Kim et al., 2004; Kim et al., 2010; Wear et al., 2003).

The α and β subunits of CP share very low sequence identity, and a twofold rotational symmetry suggests a unique way of actin regulation. Yet, residues that are important for maintaining the architecture are conserved or equivalently substituted between the two subunits and also among the same subunits of different isoforms or species. These observations have inspired to propose a tentacle model of binding of CPs to actin, which initially predicted that capping activity of CP involves the C-terminal α-helices of both subunits. The C-terminal regions are mobile, extended, and flexible so that they can reach the two actin subunits at the barbed end. However, according to a recent EM study, three highly conserved basic residues in the α-tentacle (K256, R260, R266) likely play a major role in making electrostatic interactions with a cluster of acidic residues on the interface of the actin molecule. This acidic cluster is exclusively exposed at the barbed end of the filament. Consistent with this hypothesis, substitution of all three amino acids with glutamate or alanine caused dramatically reduced capping activity (Narita et al., 2006). A more recent study showed that K268, which is also in this cluster of basic residues, is even more important in terms of binding affinity than R266. In addition, another residue lying on the surface of the α-subunit of CapZ, E200, has been predicted to be involved in a salt-bridge interaction with actin, and the importance of this residue was also confirmed by mutation experiments (Kim et al., 2004). Despite the limited resolution of the EM density for the β-tentacle, the data support the assumption of its translocation to bind to actin by hydrophobic interactions, as described above. Based on structural observations and taken the results of mutation studies into account, a new actin-CP binding model was proposed (Wear and Cooper, 2004). This model is in accordance with previous results, where the α-tentacle was reported to contribute more to capping affinity than the β-tentacle. In the first step, the barbed end is thought to be recognized even without the influence of the β-tentacle, consistent with the observation that deleting the β-tentacle did not alter the on-

rate of capping, but deletion of the α-tentacle reduced the on-rate of by 20-fold. This binding already covers the surface of both actin protomers at the barbed end, preventing the dissociation and attachment of actin monomers. During the second step, the flexible β-tentacle binds one barbed end promoter, which reduces the off-rate and thus acting mainly as a lock, as suggested before (Wear et al., 2003).
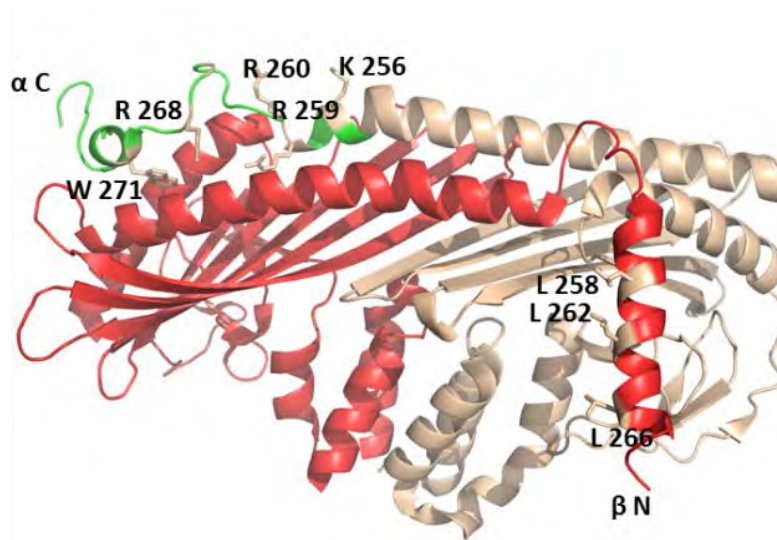
Figure 18: Structure of CapZ.

(A) Crystal structure of chicken CP α1/β1 (CapZ). The α-subunit is shown in red with its proposed 28-residue tentacle (R259 - A286) in white. The β-subunit is shown in brown with its proposed 34-residue tentacle (R244 - N277) in green, which is protruding from the body of the heterodimer and is mobile and flexible. (PDB 1IZN) (Yamashita et al., 2003).

1.10.2 *Apicomplexan capping proteins*

Apicomplexan parasites have single copy of each capping protein subunit (Gardner et al., 2002). The genes of both CP subunits are transcribed in all stages of life cycle, implying essentiality in all stages (Ganter et al., 2009). It has been shown that the β-subunit transcript from *P. berghei* is upregulated in sporozoites, suggesting that it plays an important role in the transmission of sporozoites from the mosquito to the mammalian host (Matuschewski et al., 2002). Like most of the ABPs, subunits of CP in apicomplexan parasites are also the most divergent among this protein family, but a majority of conserved residues responsible for structural maintenance and actin binding are also either conserved or conservatively substituted (Ganter et al., 2009).

Also a CPβ functional mutant parasite line was generated, and these parasites were found to be viable and infectious in the pathogenic erythrocytic stage, merozoite, in the mammalian host, while in the sporozoites stage in the mosquito vector they displayed a severe deficiency in gliding motility. Hence, CPβ functional mutant parasite results in lack the capacity to invade cells resulting into complete attenuation of the life cycle progression. Additionally, it was shown that highly susceptible C57BL/6 mice could not be infected with malaria either by CPβ functional mutant parasite mosquito host or by direct intravenous injection of CPβ functional mutant sporozoites, thus supporting the essentiality of CPβ in sporozoite stage of the *Plasmodium* life cycle (Ganter et al., 2009). This study indicates that the α and β subunits in apicomplexan parasites might have functions independent of each other, which has not yet been reported for any CP from any other species.

2 Materials

2.1 *Laboratory equipment*

Equipment	Manufacturer
ÄKTA explorer	GE Healthcare, Sweden
ÄKTA purifier	GE Healthcare, Sweden
Analytical balance	Sartorius, Germany
Astacus distillation unit	MembraPure, Germany
Avanti J26-XP centrifuge	Beckman Coulter, USA
Biacore T100	GE Healthcare, Sweden
CERTOMAT^R IS benchtop incubator	Sartorius, Germany
CFX96 RealTime System	Bio-Rad, Germany
ChiraScan Plus spectrophotometer	Applied Photophysics, UK
DynaPro NanoStar™	Wyatt, Germany
Electrophoresis unit	Bio-Rad, Germany
Gel documentation system	PEQ Lab, Germany
Genie vortex	Scientific Industries, Germany
Gyromini™ nutating mixer	Labnet International, Germany
Heraeus™ FRESCO21™ centrifuge	Thermo Scientific, Germany
Laminar air flow chamber	KOJAIR, Finland
Mastercycler^R gradient	Eppendorf, Germany
MiniDAWN™ TREOS detector	Wyatt, Germany
Multitron Pro shaker	Infors, Germany
Nanodrop 2000 spectrophotometer	Thermo Scientific, Germany
Optilab^R T-rEX refractometer	Wyatt, Germany

pH meter	Mettler Toledo, Germany
Sonopuls Sonifier	Bandelin, Germany
Systec VX150 autoclave	Systec, Germany
Tabletop centrifuge 5810-R	Eppendorf, Germany
TECAN infinite M200 fluorometer	TECAN, Germany
Thermomixer comfort	Eppendorf, Germany
Tube rotator	Stuart, UK
VARIOMAG^R magnetic shaker	Thermo Scientific, Germany

2.2 *Laboratory consumables*

Consumable	Company
Amicon-Ultra centrifugal filter units	Millipore, Ireland
Assay plates (96-well)	Greiner Bio-One, Germany
Dialysis membranes	Carl Roth, Germany
Disposable plastic cuvettes	Carl Roth, Germany
Erlenmeyer flasks	Schott Duran, Germany
Falcon tubes	Greiner Bio-One
Gravity-flow columns	Bio-Rad, Germany
Inoculation loops	Greiner Bio-One
Low 96-well clear plate	Bio-Rad, Germany
Microcentrifuge tubes	Eppendorf, Germany
Microseal adhesive films	Bio-Rad, Germany
Mini PROTEAN^R TGX™ precast gels	Bio-Rad, Germany
PCR tubes	Brand, Germany

Pipette tips	Sartorius, Germany
Plastic Petri dishes	Sarstedt, Germany
Plastic syringes	Braun Melsungen, Germany
Serological pipettes	Greiner Bio-One
Slide-A-Lyzer mini dialysis units	Thermo Scientific, Germany
Syringe filters	Millipore, Germany
Vivaspin 20 concentrators (MWCO: 10 & 30K)	Sartorius Stedim Biotech, Germany
PD-10 columns	GE Healthcare, UK

2.2.1 *Chemicals*

Chemicals used in this study were of analytical grade and were purchased from Carl Roth (Germany), Sigma Aldrich (Germany), Roche Diagnostics (Germany), Calbiochem (Germany), GE Healthcare (Sweden), Avanti Polar lipids (USA) and AppliChem (Germany), unless stated otherwise.

Kits, spin columns and reagents

QIAprep[R] Spin mini-prep kit	Qiagen, Germany
QIAquick[R] Gel Extraction Kit	Qiagen, Germany
QIAquick[R] PCR Purification Kit	Qiagen, Germany
Quick-Load DNA Ladder	New England Biolabs, Germany
PageRuler prestained protein ladder	Thermo Scientific, Lithuania

Plasmids

pETNKI_his_SUMO33_LIC_kan_*Pf*ADF1- contains DNA sequence of *Pf*ADF1 (obtained from SGC, Karolinska Institute) cloned into pETNKI_his_SUMO33_LIC_kan vector (obtained from Netherlands Cancer Institute, Amsterdam).

pETNKI_his_SUMO33_LIC_kan_*Pb*ADF2- contains DNA sequence of *Pb*ADF2 cloned into pETNKI_his_SUMO33_LIC_kan vector.

pNIC_*Pb*CPα- contains DNA sequence of *Plasmodium berghei* CPα (*Pb*CPα)subunit cloned pNIC which was obtained from SGC, Karolinska Institute.

2.2.2 *Growth media and antibiotics*

LB medium	Carl Roth, Germany
Ampicillin	Carl Roth, Germany
Chloramphenicol	Carl Roth, Germany
Kanamycin	Carl Roth, Germany

2.2.3 *Bacterial strains*

Cloning strain:	
NEB5α *Escherichia coli* (E.coli)	New England Biolabs, Germany
Expression strains:	
BL21 CodonPlus (DE3) RIPL	New England Biolabs, Germany
Rosetta (DE3)	Agilent Technologies, Germany
	Novagen, Germany

2.2.4 *Materials for chromatography*

Resins:	
Ni-NTA agarose	GE Healthcare, Sweden
Columns:	
HisTrapFF (1ml) column	GE Healthcare, Sweden

Hi-Load 16/60 Superdex 200 column	GE Healthcare, Sweden
Hi-Load 16/60 Superdex 75 column	GE Healthcare, Sweden
Superdex 200 10/300 GL	GE Healthcare, Sweden
Superdex 75 10/300 GL	GE Healthcare, Sweden

2.2.5   *Lysogeny broth medium*

Lysogeny broth (LB) medium is the most widely used, nutritionally-rich medium for the growth of bacteria. The composition of LB medium (BERTANI, 1951) is as follows:

Tryptone	10 g
Yeast extract	5 g
NaCl	10 g
Distilled water	1000 ml

The medium was sterilized using an autoclave at 121°C for 15 min, and stored at 4°C until used.

2.2.6   *Auto-induction medium*

Auto-induction (AI) medium, allows spontaneous induction of protein expression, isopropyl β-D-1-thioglactopyranoside (IPTG)-inducible *E. coli* strains, when the cells reach high density close to saturation phase. The medium contains a limited amount of glucose, which prevents uptake of lactose until it is depleted. The glucose is metabolized during the initial phase of bacterial cell growth and depleted in mid to late log phase. At this stage, lactose is taken up by the cells and converted to the natural inducer, allolactose by β-galactosidase. The allolactose causes the release of lactose repressor from its binding sites in the DNA and induces the expression of T7 polymerase, which in turn induces the expression of target proteins (Studier, 2014). Following is the composition of AI medium used in this study:

ZY medium	958.0 ml
1M $MgSO_4$	2.0 ml
1000X trace metals	0.2 ml
50X 5052	20.0 ml
50X M	20.0 ml

ZY medium:

Tryptone   10 g

Yeast extract   5 g

1 l of distilled water was added, and the medium was sterilized in an autoclave.

50X 5052:

100% Glycerol   25.0 ml

Glucose   2.5 g

α-Lactose   10.0 g

The volume was made up to 100 ml with distilled water, and the solution was mixed with a magnetic stirrer overnight for the sugars to get completely dissolved.

50X M:

Na_2HPO_4 17.75 g

KH_2PO_4 17.00 g

NH_4Cl 13.40 g

Na_2SO_4 3.55 g

The volume was adjusted to 100ml with distilled water and the solution autoclaved.

1000X Trace metals

50 mM $FeCl_3$

20 mM $CaCl_2$

10 mM $MnCl_2$

10 mM $ZnSO_4$

2 mM $CoCl_2$

2 mM $CuCl_2$

2 mM $NiCl_2$

2 mM Na_2MoO_4

2 mM Na_2SeO_3

2 mM H_3BO_3

2.2.7 *M9 minimal medium*

Minimal M9 medium was used for expression and purification of labeled ^{15}N and ^{13}C *Pf*ADF1 supplemented with ^{15}N NH_4Cl and ^{13}C glucose was used. Following is the composition of minimal medium used in this study:

Na_2HPO_4	12.8 g
KH_2PO_4	3.0 g
NaCl	0.5 g
^{15}N NH_4Cl	1.0 g

950 ml of distilled water was added, the pH was adjusted to 7.4, and the medium was sterilized using an autoclave.

^{13}C Glucose	2.0 g
$MgSO_4.7H_2O$	0.4940 g
$CaCl_2.2H_2O$	0.0152 g
Thiamine	0.0100 g
$FeSO_4.7H_2O$	0.0100 g

50 ml of distilled water was added and the solution was filtered using 0.22 µM filter into the media and stored at 4 °C until used.

2.2.8 *List of buffers*

6x Sodium dodecyl sulfate polyacrylamide gel electrophoresis (SDS-PAGE) loading buffer	375 mM tris(hydroxymethyl)amino-methane(Tris)-HCl (pH 6.8), 12 % (w/v) SDS, 60 % (v/v) glycerol, 600 mM dithiotheritol (DTT), 0.06 % (w/v) bromophenol blue
SDS-PAGE Coomassie staining solution	30 % ethanol (v/v), 10 % acetic acid (v/v), 0,25 % (w/v) Coomassie Brilliant blue R
SDS-PAGE destaining solution	30 % ethanol (v/v), 10 % acetic acid

	(v/v)
SDS-PAGE running buffer	25 mM Tris base, 192mM Glycine, 0.1 % (w/v) SDS
G-buffer	2 mM Tris-HCl (pH 8.0 at RT), 0.2 mM ATP, 0.1mM $CaCl_2$, 1 mM DTT
F-buffer	G-buffer + 200mM KCl, 4mM $MgCl_2$, 1mM ATP
Lysis buffer	20 mM Tris pH 8.0, 50 mM NaCl, 5mM βME,
ADF1 buffer	20 mM HEPES (4-(2-hydroxyethyl)-1-piperazineethanesulfonic acid) pH 7.0, 50 mM NaCl, 1 mM TCEP (tris(2-carboxyethyl)phosphine)
ADF2 buffer	20 mM Tris pH 8.0, 50 mM NaCl, 5mM βME
Elution buffer	20 mM Tris pH 8.0, 50 mM NaCl, 5mM βME, 300mM Imidazole
Dilaysis buffer	20 mM Tris pH 8.0, 50 mM NaCl, 1 mM TCEP
Cross linking buffer (CL buffer)	20 mM MES pH 6.5, 50 mM Nacl, 1 mM TCEP
NMR buffer	20 mM Bis Tris pH 6.5, 50 mM Nacl, 1

	mM TCEP
Circular Dichorism buffer (CD buffer)	20 mM Phosphate buffer pH 7.0, 50 mM NaF, 1 mM TCEP
Native gel buffer (NG buffer)	Tris 195 mM, Glycine 25 mM , Ethylene glycol tetraacetic acid (EGTA) 0.2 mM, ATP 0.2 mM, DTT 0.5 mM, 20% v/v Glycerol
CPα buffer	20 mM HEPES pH 7,5, 100 mM NaCl, 1 mM DTT

2.3 ***Bioinformatics tools***

Following tools were used to analyse the amino acid sequences of the proteins studied. Sequence similarities, conservation of protein sequence and regions with flexibility and disorder were analysed using the programs described below.

2.3.1 *T-coffee*

T-coffee (Tree-based Consistent Objective For alignment Evaluation) is a multiple sequence alignment program. This program has two main features; first it provides a simple and flexible means of generating multiple alignments using heterogeneous data sources. The data from these sources are provided to T-coffee via a library of pair-wise alignments. Secondly, its optimization method finds multiple alignment that best suitable the pair wise alignment (Magis et al., 2014).

2.3.2 *BLAST*

Basic local alignment search tools (Altschul et al., 1990), Blastp and Blastn were used to search for sequences similar to the given sequence for amino acids and nucleotides respectively. The BLAST tools were mainly used to check the similarity between the *Pf*ADF1, *Pb*ADF2 and proteins available at the nucleotide database of the National Center for Biotechnology Information (NCBI).

2.3.3   *ExPASy tools*

A few tools of the Expert Protein Analysis System (Artimo et al., 2012) such as Translate and Protparam were routinely used in this study. Translate was used to translate a nucleotide sequence into a protein sequence. ProtParam was used to compute parameters such as molecular weight, theoretical isoelectric point, hydrophobicity and extinction co-efficient from an amino acid sequence.

3 Methods

3.1.1 *Overexpression of recombinant PfADF1, PbADF2 and PbCPα*

Recombinant proteins were produced in *E.coli* using the pETNKI-his-SUMO3-LIC-*Pf*ADF1, SUMO3-LIC-*Pb*ADF2, and *pNIC-PbCPα* expression vectors. The plasmids were transformed into ultra-competent RIPL cells for *Pf*ADF1 and Rosetta for *Pb*ADF2 and *Pb*CPα. As all the constructs used for protein expression in this study carry a kanamycin resistance gene (kanR), 100 μg/ml kanamycin was maintained in all the cultures. Selected transformants were inoculated into LB medium and allowed to grow overnight at 37 °C, shaking at 180 revolutions per minute (rpm), in a Certomat IS benchtop incubator (primary culture).

For overexpression of *Pf*ADF1 and *Pb*ADF2, AI medium for 36 h at 20 °C was used. A required volume of primary culture, to get an A_{600} (light absorbance at 600 nm) of 0.6 was inoculated into 1000 ml auto-induction medium (secondary culture), and the culture was allowed to grow in a shaker incubator at 20 °C at 180 rpm for 36 h.

For over expression of *Pb*CPα, LB medium was used. For induction of the protein expression of *Pb*CPα, 0.1 mM IPTG was used, following which the culture was grown overnight at 20 °C.

3.1.2 *^{15}N and ^{13}C labelling of PfADF1*

Overexpression of labeled *Pf*ADF1 (^{15}N and ^{13}C) for NMR experiments was performed in M9 minimal supplemented with ^{15}N NH_4Cl and ^{13}C glucose. Protein expression was induced with 0.1 mM IPTG, following which the culture was grown for 4 h at 37 °C. Cells were harvested at 3000 g for 20 min at 4 °C. The cell pellet was stored at -20 °C until the start of purification (Dutta et al., 2003).

3.1.3 *Purification of recombinant PfADF1, ^{15}N and ^{13}C labeled PfADF1, and PbADF2*

All purifications described in this thesis were performed in the cold room (5-10°C), and protein samples were always handled on ice. Two conceptually different chromatographic methods were used. The cell pellets were resuspended in lysis buffer containing protease inhibitors (a complete EDTA-free protease inhibitor cocktail tablet per 50 ml of lysis buffer). The resuspended cells were sonicated at 30% amplitude (3 cycles) for 15 min with a Sonopuls HD 2070 system from Bandelin. The lysates were clarified by centrifuging at

30000 g for 45 min at 4 °C. The clarified lysates were loaded using a gravity flow column onto Ni-NTA agarose matrix pre-equilibrated with at least 10 ml of lysis buffer. Prior to elution of the protein in elution buffer (lysis buffer supplemented with 300 mM of imidazole), the matrix was washed with 20 ml of lysis buffer supplemented with 20 mM of imidazole and 100 mM of NaCl to remove the un-specifically bound protein. Following elution the protein was cleaved with SENP2 protease at 4 °C overnight under dialysis to remove imidazole in dialysis buffer (20 mM Tris-HCl pH 8.0, 50 mM NaCl, 5 mM βME). The dialyzed protein was passed through NiNTA agarose matrix to remove the cleaved tag, uncleaved protein, and the His-tagged protease. Partially purified protein fractions from affinity chromatography were pooled and concentrated. The concentrated sample was filtered using a filtering device with 0.22 μm pore-size and loaded onto a Hi-Load 16/60 Superdex 75 column, pre-equilibrated with ADF1 buffer (20 mM HEPES pH 7.0, 50 mM NaCl, 1mM TCEP) and ADF2 buffer (20 mM Tris-Cl pH 8.0, 50 mM NaCl, 1mM TCEP) for *Pf*ADF1 and *Pb*ADF2, respectively. Protein fractions of the peak were pooled, concentrated using an Amicon® Ultra centrifugal device with a 3 kDa molecular weight cutoff membranes (3MWCO), and the concentration was estimated by determining UV absorbance at 280 nm (A_{280}) using a Nanodrop spectrophotometer and employing a theoretical extinction coefficient based on the amino acid composition (Gill and von Hippel, 1989). The theoretical molar extinction coefficients of for *Pf*ADF1 is 10220 M^{-1} cm^{-1}, and for *Pb*ADF2 14565 M^{-1} cm^{-1} at A_{280}. Both proteins were flash frozen in liquid nitrogen and stored in aliquots at -80 °C. Protein samples were used for subsequent biophysical analysis and crystallization experiments. Mass spectrometry analysis to identify the proteins was carried out in Biocenter Oulu Proteomics Core Facility, Department of Biochemistry, University of Oulu (Oulu, Finland).

3.1.4 *Purification of recombinant PbCPα*

A cell pellet was resuspended in 20 ml of CPα buffer (20 mM HEPES pH 7.5, 100 mM NaCl, 1 mM DTT) supplemented with a protease inhibitor cocktail tablet (Roche). The cells were kept on ice and lysed by sonication at 30% amplitude (3 cycles), cycle 3 using a Sonopuls HD 2070 system from Bandelin for 20 min. The sample was centrifuged at 30000 g for 45 min in order to separate the soluble protein fraction from the cell debris. The C-terminus of *Pb*CPα has a 6xHis-tag to allow for affinity purification. The supernatant was loaded onto a

Ni-NTA column pre-equilibrated with CPα buffer and incubated for 1 h. To remove unspecifically bound molecules, the column was washed with 10 ml of *Pb*CPα buffer containing 20 mM imidazole, followed by 10 ml of CPα buffer containing 50 mM imidazole. Finally, *Pb*CPα was eluted with CPα buffer supplemented with 300 mM imidazole. To remove the imidazole, the sample was dialysed overnight in 2 l CPα buffer. The protein sample was then further purified by size exclusion chromatography using a Hi-Load 16/60 Superdex 200 column equilibrated in CPα buffer, containing 1 mM TCEP instead of DTT. The theoretical molar extinction coefficient of *Pb*Cpα is 34084 M^{-1} cm^{-1} at A_{280}. The eluted *Pb*CPα was flash frozen in liquid nitrogen and stored in aliquots at -80°C. Mass spectrometry analysis to identify the proteins was carried out in Biocenter Oulu Proteomics Core Facility, Department of Biochemistry, University of Oulu (Oulu, Finland).

3.1.5 *Purification of pig skeletal muscle α actin*

Actin was purified from pig muscle acetone powder, provided by J. Vahokoski from the Department of Biochemistry, University of Oulu, Finland. The fibrous part of the acetone powder was grinded on ice using a pastel and mortar, 20 ml ice-cold G-buffer was added per gram of acetone powder and stirred on ice for 30 min. The sample was centrifuged for 15 min at approximately 14000 g. After decanting the supernatant, 4 mM $MgCl_2$ and 100 mM KCl (final concentrations) were added and stirred slowly for 1 h at room temperature (RT) to induce actin polymerization. Then, solid KCl was added to a final concentration of 800 mM and stirred slowly for 1 h at 4°C. The polymerized actin was sedimented by centrifugation for 3 h at approximately 219000 g. Following this, the supernatant was discarded, and the pellet was resuspended by gentle homogenization in ice-cold G-buffer, followed by dialysis in 2 l G-buffer at 4°C overnight. The next day, non-depolymerized actin was removed by centrifugation for 1 h at approximately 219000 g. The supernatant was concentrated and further purified by size exclusion chromatography using a Hi-Load 16/60 Superdex 200 column equilibrated in G-buffer. Finally, the eluted G-actin was stored in dialysis, and the G-buffer was changed daily, containing freshly added ATP and DTT. Actin concentration was measured by absorbance at 290 nm [Abs_{290} (1 mg/ml) = 0.63].

3.1.6 *Fluorescence spectroscopy*

Fluorescence is one of the two phenomena of luminescence that occurs from electronically excited singlet states of a chromophore. When a fluorophore absorbs photons of certain energy, singlet electronic high energy states S1, S2, etc. are populated within which a number of sub vibrational energy levels 0, 1, 2, etc. exists. A rapid relaxation process called internal conversion occurs from the higher vibrational states to the lowest vibrational level of S1. The return of electrons from singlet-excited states to the ground state is spin-allowed and occurs by the emission of photons which is called fluorescence. Partial energy dissipation during the internal conversions causes the fluorescence to occur at lower energies or longer wavelengths (Stokes' shift) (Jameson et al., 2003). This spectroscopic method is exploited to study the polymerization property of actin.

For many experiments, it is advantageous to be able to follow the course of actin polymerization which helps to understand the kinetics of actin polymerization in the presence of ABPs. Actin can be stored in monomeric form by removing all the salts, below the critical concentration, and by maintaining a slightly alkaline condition. Actin solution can be induced to form filaments by adding a buffer mix containing salts at the physiological range. Additionally, actin can be labeled with a fluorophore, pyrene, at Cys-374, and native actin co-polymerizes with the labeled actin, which allows following of the fluorescence as the polymer forms. Furthermore pyrene-labeled actin has been reported to have identical time course of polymerization, elongation rate constants and critical concentration for polymerization (Cooper et al., 1983). With this method, fluorescence intensity for actin solution, doped with a small amount of pyrene actin, can be measured in real time and thus is well suited for kinetic assays. Here, polymerization was measured with an excitation wavelength of 365 nm (bandwidth 9 nm) and emission wavelength of 407 nm (bandwidth 20 nm), using a TECAN Infinity M200 plate reader. Polymerization was induced by addition of 1/10 volume of 10X F-buffer (200 mM KCl, 4 mM $MgCl_2$ and 1 mM ATP – final concentrations) at 25 °C. The fluorescence signal arising from pyrene actin polymerization was monitored for 1 h.

3.1.6.1 Polymerization assays

Possible aggregates were removed from the purified G-actin solution by centrifugation at approximately 219000 g for 30 min. For all experiments, 4 µM purified G-actin containing 5% pyrene-labeled actin was used in a final reaction volume of 200 µl in a 96-well microplate. Polymerization of G-actin was induced by adding 200 mM KCl, 4 mM MgCl$_2$ and 1 mM ATP (final concentrations). In order to follow the effect of *Pf*ADF1, *Pb*ADF2 and *Pb*CPα, polymerization was induced in presence of 0.5-4 µM *Pf*ADF1, 4 and 8 µM *Pb*ADF2, 1-50 nM CapZ and 1-500 nM *Pb*CPα. Different concentrations of respective proteins were mixed with G-actin just before inducing polymerization with F-buffer. All samples were measured twice and prepared independently to observe reproducibility. The data were exported to Origin for analysis. For *Pf*ADF1 the steady state fluorescence units were plotted against the protein concentration which was fitted with first order exponential decay function to obtain the binding affinity.

3.1.6.2 Nucleotide exchange assay

The exchange of the nucleotide is a potential regulatory step in the assembly of actin filaments. The rapid turnover of actin filaments results in ADP-actin monomers, the regulatory effect exerted by the ABPs on the exchange of ADP would determine the direction of actin polymerization. The nucleotide bound to the actin monomers can exchange with the nucleotides in the medium, with highest affinity for ATP followed by 1,N^6–etheno-ATP (ε-ATP) and ADP. Effects of *Pf*ADF1 and *Pb*ADF2 on nucleotide exchange were measured by monitoring the increase in fluorescence upon exchange of ADP to ε-ATP on G-actin.

Possible aggregates were removed from the purified G-actin solution by centrifugation at approximately 219000 g for 30 min. A reaction volume of 150 µl and an actin concentration of 4 µM were used. Various concentrations of *Pb*ADF2, *i.e* 1, 2, 4, 8, 16, 20 µM were tested, while *Pf*ADF1 was only used at 4 µM. The reaction was measured for 15 min using a Tecan Infinity M200 plate reader, with an excitation wavelength of 360 nm (bandwidth 9 nm) and emission wavelength of 410 nm (bandwidth 20 nm). All samples were measured in triplicate and prepared independently. The data were exported to Origin for analysis. The linear part of each curve was fitted using linear fitting, and the slope was calculated. The calculated slope was plotted against protein the concentration to obtain a binding curve,

which was fitted using the first order exponential decay function to obtain the binding affinity.

3.1.6.3 Seeded actin polymerization assay

Purified G-actin was centrifuged at approximately 219000 g for 30 min to remove any possible aggregates. For all experiments, 4 µM purified G-actin containing 5 % pyrene-labeled actin was used in a final reaction volume of 200 µl in a 96-well microplate. The reactions were pipetted in a 96-well microplate and adjusted to a final volume of 200 µl. Actin seeds were used at a final concentration of 2 µM and prepared as 10 µM from purified G-actin by adding 200 mM KCl, 4 mM MgCl$_2$ and 1 mM ATP (final concentrations) to induce polymerization and incubated for 3 h at RT. When pipetting the actin seeds, the pipet tips were cut approximately 2-3 mm from the end to increase the diameter, in order to reduce shearing forces during pipetting. *Pb*CPα was added to the actin seeds and incubated for 15 min. Finally, 2 µM monomeric G-actin containing 5% pyrene-labeled actin was added together with 200 mM KCl, 4 mM MgCl$_2$ and 1 mM ATP (final concentrations). All samples were measured twice and prepared. The data were exported to Origin for analysis, where slope of the individual curves was calculated and plotted against the concentration of the proteins to obtain a binding curve.

3.1.6.4 Tryptophan fluorescence assay

Most of the intrinsic fluorescence of the protein is due to tryptophan emission. Tryptophan has an absorption at 280-290 nm and emission from 300-350 nm. Hence, intrinsic protein fluorescence can be used to diagnose changes in protein conformations. *Pf*ADF1 has one tryptophan at position 26 which makes it ideally suited for tryptophan fluorescence assays. Fluorescence was measured for *Pf*ADF1 at a concentration of 8 µM in ADF1 buffer (20 mM HEPES pH 7, 50 mM NaCl, 1 mM TCEP) with excitation at 290 nm and emission from 300 to 420 nm. Following this, tryptophan fluorescence was measured for protein samples with 1:1 to 1:25 PIP$_2$ molar ratio. The protein and lipid mixture was centrifuged to get rid of any aggregates before measurements. The data were analyzed using Origin. The peak maxima were plotted against the PIP$_2$ concentration, and the data were fitted using 1st order exponential decay to yield the binding curve.

3.1.7 *Actin co-sedimentation assay*

The binding of a protein to F-actin can be analyzed by a co-sedimentation assay. In this *in vitro* assay, actin is polymerized, incubated with a specific protein proposed to bind to filaments, followed by an ultracentrifugation step to sediment the actin filaments and a subsequent separation and analysis of the pellet and the supernatant fractions.

Purified G-actin was centrifuged at approximately 219000 g for 30 min to remove any possible aggregates. Actin at a concentration of 4 μM in the presence of *Pf*ADF1, *Pb*ADF2 (1–20 μM) and *Pb*CPα was polymerized by adding 1X F-buffer from stock of 10X F-buffer to the reaction and incubated for 1 h at RT. Polymerized actin was sedimented by centrifugation at approximately 219000 g for 2 h. The supernatant was withdrawn and the pellet carefully washed with 100 μl F-buffer, or G-buffer in case of the actin control, before being resuspended in 100 μl of the respective buffer. Supernatant and pellet fractions were analyzed by SDS-PAGE.

3.1.8 *Lipid vesicle preparation*

100 μl of PIP_2-C18 (1 mg/ml stock in ethanol) and/or 28 μl dimyristoylphosphatidalcholine (DMPC) (9.4 mg/ml in chloroform) were mixed and evaporated in stream a of nitrogen gas. Following this, residual lipids were dissolved in 500 μl of 20 mM HEPES pH 7 and 1 mM DTT, resulting in a solution of 1mM DMPC or DMPC-PIP_2 vesicles. Further, the solution was sonicated at RT for 30 min to yield a clear solution indicating uni-lamellar DMPC or DMPC-PIP_2 vesicles (Steimle et al., 1999).

3.1.9 *Band shift assay*

Specific protein ligand interactions change the migration pattern of the proteins in non-denaturing condition; this was used to investigate the interaction between PIs and ADFs (Arnold et al., 1995). 20 μM ADFs (*Pf*ADF1, *Pb*ADF2) were incubated at 1:1 protein to lipid vesicle ratio and analyzed on native gel at 4 °C overnight, using NG buffer at pH 7.5 (Tris 195 mM, Glycine 25 mM , EGTA 0.2 mM, ATP 0.2 mM, DTT 0.5 mM, 20% v/v glycerol).

3.1.10 *Circular dichroism spectroscopy*

(CD) Circular dichroism spectroscopy is a well-known technique for examining the secondary structure of a protein in solution (Kelly et al., 2005; Kelly and Price, 2000). CD refers to the differential absorption of left (L) and right (R) circularly polarized components

of plane polarized light which is a property of chiral or asymmetric molecules. If L and R are absorbed to a different extent, the transmitted light will possess elliptical polarization. A CD instrument measures the difference in absorbance between the L and R circularly polarized components (ΔA) and reports in terms of ellipticity (θ) in degrees ($\theta = 32.98\ \Delta A$). The CD spectrum is a measure of ellipticity of a sample as a function of wavelength. It is possible to estimate the overall secondary structure content of a protein from the far UV-CD (typically 240 to 180 nm), as different regular secondary structures found in proteins show distinct spectra (Sreerama and Woody, 1994). Different CD spectra can be made comparable by normalizing to the mean residual ellipticity (MRE). Here, CD was measured using a ChiraScan Plus CD spectrophotometer at 20 °C. A spectrum from the corresponding buffer was measured for all the samples and used for background correction.

For characterization of *Pf*ADF1 and *Pb*ADF2 PIP$_2$ interactions, SRCD (synchrotron radiation circular dichorism) data were collected at AU-CD beam line on ASTRID2 in Aarhus, Denmark. *Pf*ADF1 and *Pb*ADF2 were dialyzed in CD buffer (20 mM phosphate buffer, 50 mM NaF, 1mM TCEP) and diluted to 1 mg/ml and 1.16 mg/ml respectively. Proteins were incubated with DMPC and DMPC-PIP$_2$ vesicles for 30 min, and the spectra were measured for protein alone and protein-vesicle complexes. For CD measurements, *Pf*ADF1 was dialyzed in CD buffer overnight and diluted in the same to a concentration of 0.25 mg/ml. *Pf*ADF1 alone was measured as control. Protein and lipids were mixed to equimolar and 15:1 PIP$_2$ to *Pf*ADF1 molar ratio, and spectra were collected. To measure the stability of the protein in the presence of PIP$_2$, temperature scans were performed from 20 to 80 °C, for *Pf*ADF1 at 0.25 mg/ml alone and presence of 1:1 and 1:15 protein to PIP$_2$ molar ratio, using a heating rate of 1 °C/min.

For all the spectra measured, the corresponding buffers were subtracted. The unit was converted from millidegrees to MRE and plotted using Origin. The spectra were deconvoluted at the Dichroweb server (Lobley et al., 2002) using the CDSSTR algorithm (Compton and Johnson, 1986). In order to calculate the T_m from the temperature scan, the MRE at 208 nm was plotted against temperature, and the data were fitted using the Boltzmann equation.

3.1.11 *EDC crosslinking*

For 1-ethyl-3-(3-dimethyl aminopropyl) carbodiimide (EDC) crosslinking experiments, actin (100 μM), *Pf*ADF1 (120 μM) and *Pb*ADF2 (120 μM) were dialyzed in CL buffer (20 mM MES pH 6.5, 50 mM NaCl, 1 mM TCEP), following which actin was mixed with one of the ADFs in the presence of 10 mM EDC and incubated at RT for 1 h. The samples were gel filtered in G-buffer supplemented with 50 mM NaCl using Hi-Load Superdex 10/300 GL, pre-equilibrated with the same buffer. The complex eluted as a single peak, which was further analyzed by SDS-PAGE and static light scattering (SLS).

3.1.12 *Static light scattering*

SLS is used to determine the absolute molecular mass of macromolecules in solution. The sample is exposed with a low intensity laser of wavelength 690 nM, which is scattered by the sample and is recorded as a function of the scattering angle. It gives information regarding molecular mass, the second viral coefficient (A_2), and root mean square of the radius. A_2 determines the strength of interaction between the molecule and solvent, and thus gives important information about aggregation.

SLS was carried out in chromatography mode using a mini-DAWN TREOS multi-angle static light scattering (MALS) detector (Wyatt) and an Optilab Rex differential refractometer (Wyatt) in the flow path of an ÄKTA purifier (GE Healthcare). For calibration, bovine serum albumin (BSA) was used as standard in the same buffer as the sample, *i.e.* G-buffer. 100 μl BSA were injected into the Superdex 200 10/300GL column attached to the ÄKTA purifier. Once the correct molecular mass for BSA was determined, 100 μl 4 mg/ml *Pb*ADF2-actin EDC cross-linked in G-buffer supplemented with 50 mM NaCl were injected into the column for analytical size-exclusion chromatography, followed by data collection. Similarly, for the estimation of oligomeric state of *Pb*CPα, 100 μl at 6.5 mg/ml gel filtered *Pb*CPα was injected into Superdex 200 10/300GL column equilibrated with CPα buffer (20 mM HEPES, pH 7.5, 100 mM NaCl, 1 mM DTT). The results were analysed using the ASTRA software version 5.3.4.11. The processing involved selection of baselines in the UV and three LS signals, assignment of peaks based on how well the signals overlay and calculation of absolute molecular mass. Either refractive index or UV absorbance was used as the source of concentration.

3.1.13 *Small-angle X-ray scattering*

Small angle X-ray scattering (SAXS) is used for determination of low-resolution three-dimensional structures of biological macromolecules in terms of averaged particle size and shape. SAXS is based on the principle of elastic scattering of x-ray photons by particles in an illuminated volume. Basically, a monochromatic focused beam of X-rays hit the solution containing the molecule of interest, which is a protein in this study, and the scattered intensity [I(s)] is recorded as a function of momentum transfer, $s = 4\pi sin\theta/\lambda$ here θ is the angle between the incident and scattered radiation. Provided that the scattering is isotropic, the recorded image is radially averaged to obtain the scattering curve. The scattering curve can be used to estimate the global structure and conformation of the protein and also to extract a few crucial parameters such as the molecular mass (MM), radius of gyration (R_g), hydrated particle volume (V_P) and maximum intramolecular distance of the particle (D_{max}) (Skou et al., 2014).

Actin, *Pf*ADF1 and *Pb*ADF2 were purified according to sections 3.1.4 and 3.1.1, respectively. Respective proteins were mixed in 1:1.2 (100 µM of actin and 120 µM of ADFs) molar ratios and gel filtered in G-buffer supplemented with 50 mM NaCl using a Superdex 200 10/300 GL column. Peak fractions were collected and analysed on SDS-PAGE. The fractions containing the desired complexes were concentrated and filtered using 0.22 µM filters. SAXS data were collected for the purified *Pf*ADF1-actin, *Pb*ADF2-actin complexes, *Pf*ADF1 in ADF1 buffer, *Pb*ADF2 in ADF2 buffer, and actin in G-buffer at MAX LAB I1911-4, Lund and X33 beamline DESY, Hamburg. *Pf*ADF1 alone was measured at 2 and 4.77 mg/ml, Actin was measured at 1 and 2.7 mg/ml, *Pb*ADF2 was measured at 2.2 and 3.75 mg/ml, the *Pf*ADF1-actin complex was measured at 1.1 and 3.6 mg/ml, and the *Pb*ADF2-actin complex was measured at 0.6, 1.1, and 2 mg/ml.

Data analysis was performed using the ATSAS package (Petoukhov and Svergun, 2013). PRIMUS (Konarev *et al.*, 2003) was used for subtracting, averaging the data. R_g was calculated using Guiner approximation (Glatter *et al.*, 1977, Svergun, 1992) using PRIMUS. The output from PRIMUS was used to obtain distance distribution (p_r) and maximum dimension of the molecule (D_{max}) using GNOM (Svergun, 1992). The output of GNOM was used to build low-resolution *ab initio* models using DAMMIN (Svergun, 1999), DAMMIF (Franke *et al.*, 1990). The resulting models were visualized and compared using Pymol.

3.1.14 *NMR experiments*

2D ^{1}H-^{15}N HSQC (heteronuclear single quantum coherence) NMR experiments were performed on a Varian ^{Unity}INOVA instrument, equipped with cryogenic Z-axis PFG triple resonance probe at a proton frequency of 600 MHz at EMBL Heidelberg. The 2D ^{1}H-^{15}N HSQC spectrum represents the signal from a proton that is bound to a nitrogen atom (H^N), which is basically the backbone amide group (- CONH - of a peptide bond), the primary amine group of asparagine, glutamine and secondary amine group of histidine and tryptophan. Typically, HSQC experiments are performed in the presence and absence of the ligand, correlating H^1 and N^{15} resonances in a two dimensional NMR spectrum, and the chemical shift perturbations that are observed can be mapped to the sequential protein resonance assignment, if it is available. This spatially highlights the protein ligand binding site. Affinity information in the form of a NMR-K_d can be obtained from ligand titration (Carlomagno, 2005). However, two dimensional experiments are time consuming, and the isotope labelling required N^{15}, and possibly C^{13} is expensive.

(Double labeled and triple labelled, N^{15}, C^{13} *Pf*ADF1, was purified was purified as in section using NMR buffer). HSQC data collected for labeled *Pf*ADF1 (100 μM) mixed with 10 % D_2O following which the protein was titrated with varying molar concentration ratios of PIP$_2$ (1:1.2). Overlay of the spectra was done using the CCP4 NMR specview software. 3D ^{1}H-^{15}N-^{13}C protein backbone was assigned by Dr. Bernd Simon from EMBL Heidelberg.

3.1.15 *Microscale thermophoresis*

Microscale thermophloresis (MST) is a technique used for determination of affinities between two biomolecules. It exploits the phenomena of directed movements of molecules in temperature gradient. A change in conformation due to binding of an analyte and a ligand results in change in the relative movement along the temperature gradient, which is used to determine the binding affinities (Seidel et al., 2013).

Actin (20 nM) was fluorescently labelled using NT-647 using a Monolith NT protein labeling kit. Subsequently, it was incubated with varying concentrations of *Pf*ADF1 ranging from 2.3 nM to 75 μM and *Pb*ADF2 ranging from 2.5 nM to 82 μM. The assay was performed in G-buffer supplemented with 0.5 mg/ml BSA and 0.05 % Tween-20. Low-binding tubes were used for these experiments. Prior to the experiment, the appropriate concentration of actin needed was decided by performing a fluorescence scan, and 20 nM was chosen, which gave

an approximate count of 2000 units. MST power of 20 % and LED power 60 % were used. The thermophoretic mobility against concentration gives the binding curve, which is fitted with quadratic solution for the fraction of fluorescent molecules that formed the complex, calculated from law of mass action.

3.1.16 *Surface plasmon resonance*

Surface plasmon resonance (SPR) is used to determine the binding constants of two molecules. In a typical SPR study (Johnsson et al., 1991), the ligand is immobilized on the metal coated surface of surface SPR chips, followed by injection of the analyte. When the ligand binds to the analyte, change in refractivity/reflectivity properties of the metal is expressed in response units (RU). During the event of binding the analyte upon injection first saturates the ligand and then is washed off with buffer without the analyte resulting in dissociation of complex indicated by decrease of SPR signal. SPR experiments were performed on a Biacore T100 instrument from GE Healthcare, using an HPA chip for the immobilization of the ligand.

For measuring the binding coefficient between ADF and lipid vesicles, an HPA chip was activated with 5 % Triton, following which lipid vesicles were immobilized on the chip. DMPC alone was immobilized to a level of 4813 RU and DMPC-PIP$_2$ to a level of 2186 RU on different flow channels. BSA (0.1 mg/ml) was then injected onto the lipid surface, which yielded a response of 96 RU. Following this, *Pf*ADF1 and *Pb*ADF2 were passed through the channels and the response was observed. A concentration range of 1-10 μM *Pf*ADF1 and *Pb*ADF2 was used for the binding assay. After the binding event, the flow cannel was washed with buffer before the next injection. The maximum response after the binding event was plotted against the protein concentration using Origin, followed by fitting using the law of mass action equation.

4 Results

Plasmodium expresses two isoforms of both actin and ADF, of which actin1 and *Pf*ADF1 are expressed during all its life stages, while actin2 and *Pb*ADF2 are expressed only in its sexual stages (Doi et al., 2010). The current thesis work was set to probe the differential functions of the two ADFs in order to understand the need for the presence of the two isoforms of both actin and ADF.

4.1 *Purification of ADFs*

*Pf*ADF1 and *Pb*ADF2 eluted from size exclusion chromatography (SEC) at volumes of 84.1 ml and 80.2 ml, respectively. Their respective molecular weights were estimated to be 13.8 kDa and 16.5 kDa, using the calibration plot of the Hi-Load 16/60 Superdex 75 column. The samples corresponding to the SEC peaks appeared as single band on SDS-PAGE, indicating high purity **(Figure 19)**.
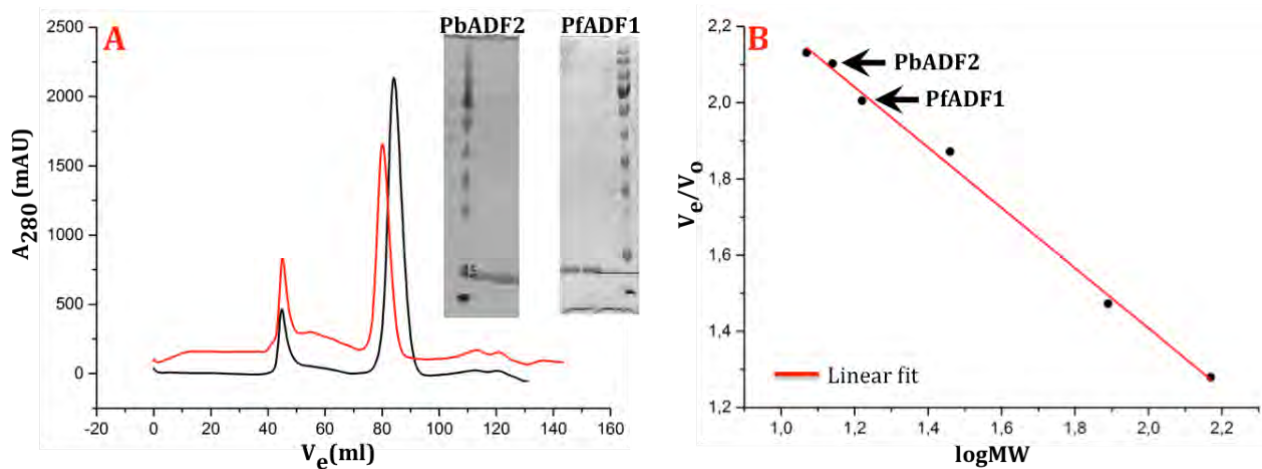
Figure 19: SEC profile of PfADF1 and PbADF2.

(A) Chromatogram of *Pf*ADF1 (black) and *Pb*ADF2 (red) with peaks at 84.1 ml and 80.2 ml respectively on Hi-Load 16/60 Superdex 75 column. SDS-PAGE shows a single band for the respective proteins (inset). **(B)** Shows the calibration curve of standard proteins (β-amylase, cytochrome-c and albumin) resolved by the Hi-Load 16/60 prep grade Superdex 75 column. Ve/Vo of *Pb*ADF2 and *Pf*ADF1 are shown with arrows.

4.2 *Purification of pig skeletal muscle α-actin*

Plasmodium actin filaments are short and unstable, and their polymerization assays have not been established. Therefore, heterologous actin *i.e.*, pig skeletal muscle α-actin, was

used to investigate the actin-binding activity of *Pb*ADF2 and *Pf*ADF1. SDS-PAGE analysis of the purified α-actin fractions corresponding to a peak at 62 ml in SEC showed a single band at an apparent molecular weight of 42 kDa, corresponding to the actin monomer **(Figure 20)**. To keep the purified actin monomeric and properly folded, it was maintained in the G form by constant dialysis against G-buffer with fresh ATP and DTT.
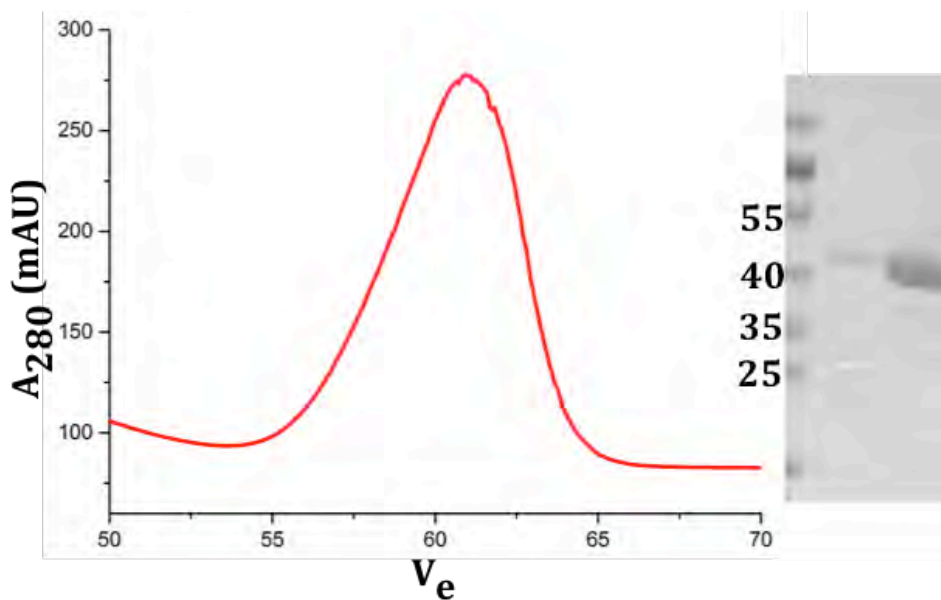
Figure 20: SEC profile of pig skeletal muscle α-actin.

SEC profile showing a peak at an elution volume of 62 ml from Hi-Load 16/60 Superdex 200 column. SDS-PAGE shows a single band with an approximate molecular weight of 42 kDa.

4.3 *Characterization of the interaction of PbADF2 and PfADF1 with actin*

4.3.1 *Binding of PbADF2 and PfADF1 to actin*

A co-sedimentation assay was performed to test the interaction of *Pb*ADF2 with actin. In the control reactions, actin was seen in the supernatant and pellet fractions in the presence and absence of F buffer, *vice versa*. *Pb*ADF2 alone in F-buffer was found in the supernatant. Upon increasing concentrations of *Pb*ADF2 (1, 4, 8, and 20 μM), an increase in the amount of actin in the supernatant was observed. At a 1:1 molar ratio of actin to *Pb*ADF2, approximately half of actin was seen in the pellet and the other half in the supernatant, indicating that *Pb*ADF2 depolymerizes filamentous actin and/or sequesters monomeric actin. Nevertheless, trace amounts of *Pb*ADF2 were also seen in the pellet, indicating that *Pb*ADF2 binds both forms of actin **(Figure 21)**.
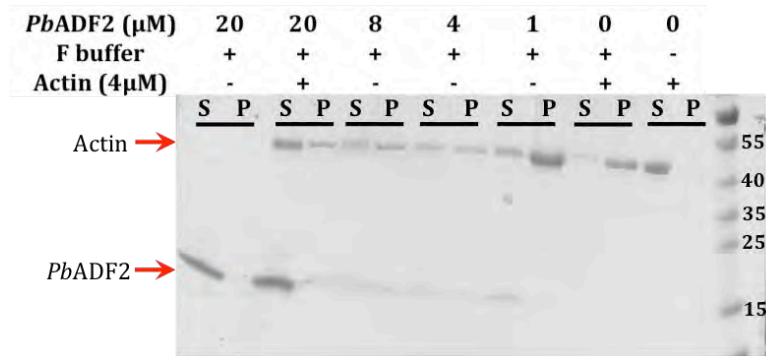
Figure 21: Actin co-sedimentation assay with PbADF2.

Supernatant (S) and pellet (P) fractions of the actin co-sedimentation assay with *Pb*ADF2 analyzed by SDS-PAGE. The presence and absence of actin and F-buffer are represented as + and − above the gel, respectively. The concentration of *Pb*ADF2 in each of the samples is also shown. A clear increase in the concentration of actin in the supernatant fractions upon addition of *Pb*ADF2 can be seen.

Similarly, the binding of *Pf*ADF1 to actin was also assessed using a co-sedimentation assay. The control reactions for actin and *Pf*ADF1 individually in F-buffer showed actin in the pellet fraction and *Pf*ADF1 in the supernatant fraction. Similarly to *Pb*ADF2, increasing the concentration of *Pf*ADF1 (4, 8, 20, and 40 µM) in the reaction resulted in an increase in the amount of actin in the supernatant fraction **(Figure 22)**. Unlike reported before (Schüler et al., 2005a), *Pf*ADF1 was also observed in the pellet fractions at 1:2 and higher actin:ADF ratios, indicating that it also interacts with F-actin.
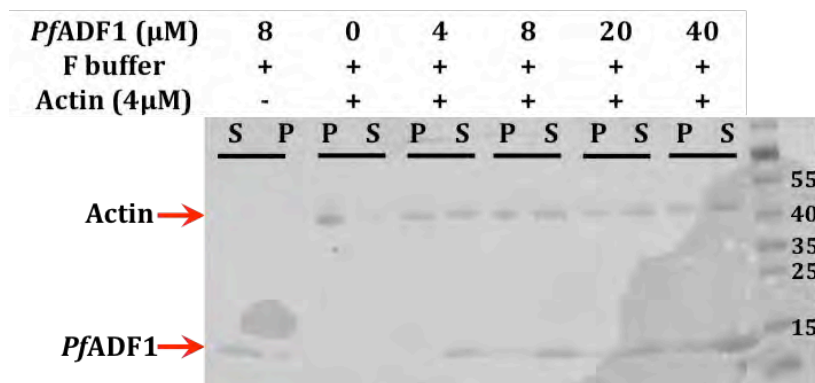
Figure 22: Actin co-sedimentation assay with PfADF1.

Supernatant (S) and pellet (P) fractions of actin co-sedimentation assay with *Pf*ADF1 analyzed by SDS-PAGE are shown. The presence and absence of actin and F-buffer are represented as + and − above the gel, respectively. The concentration of *Pf*ADF1 in each of the samples is also shown. A clear increase in the concentration of actin in the supernatant fractions upon addition of *Pf*ADF1 can be seen.

4.3.2 *Role of PbADF2 in actin polymerization*

To understand the effect of *Pb*ADF2 on actin polymerization kinetics, a pyrene actin fluorescence assay was performed. Actin polymerization was induced in the absence and presence of *Pb*ADF2 (4 and 8 µM). *Pb*ADF2 inhibited polymerization completely, suggesting that *Pb*ADF2 is a strong monomer sequestering protein **(Figure 23)**.
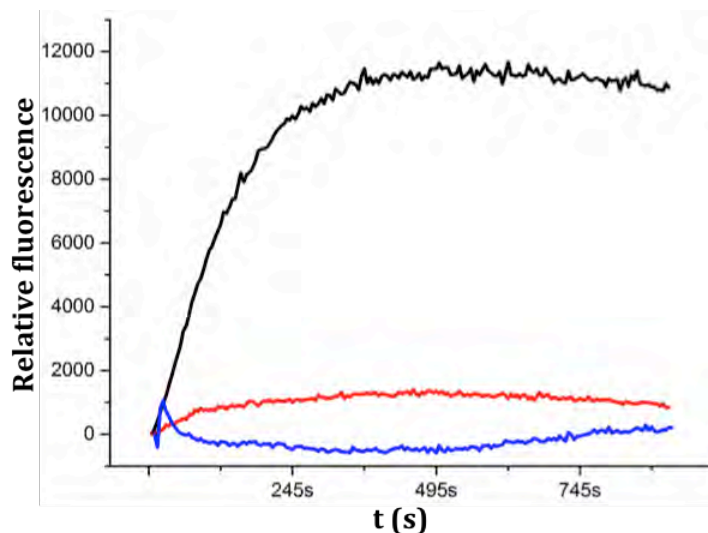
Figure 23: Actin polymerization assay in presence of PbADF2.

Actin (4 µM) was polymerized alone (black) and in the presence of 4 (red) and 8 µM (blue) PbADF2. Actin polymerization in the presence of PbADF2 was completely inhibited.

4.3.3 *Role PfADF1 in actin polymerization*

The effect of *Pf*ADF1 on actin polymerization was also assessed using the pyrene actin polymerization assay. 2 µM actin was polymerized in the presence of various concentrations of *Pf*ADF1 (0.5, 1, 1.5, 2, 3, and 4 µM), and the increase in pyrene fluorescence was monitored. With low concentrations of *Pf*ADF1, the rate of elongation initially increased, and then decreased with increasing concentrations. Besides affecting the elongation rate, the final steady state concentration of actin decreased in the presence of *Pf*ADF1 in a concentration dependent manner **(Figure 24)**. Thus *Pf*ADF1 not only binds to F-actin but also affects the elongation rate of actin polymerization and steady state concentration. The fluorescence units at the steady state were plotted against *Pf*ADF1 concentrations and fitted using the first order exponential decay equation. A K_d of 1.13 +/- 0.055 µM was obtained for F-actin binding with a chi squared value of 0.99.
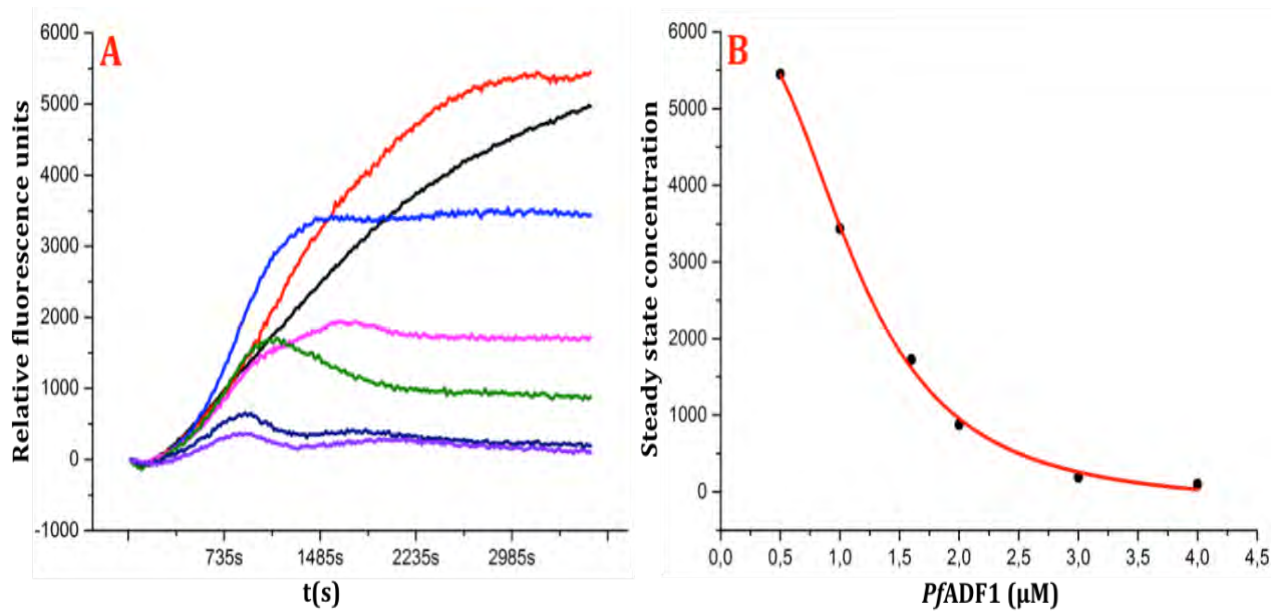
Figure 24: Actin polymerization assay in the presence of PfADF1.

(A) 2 µM G-actin (5% pyrene-labeled) was polymerized at RT in F-buffer in the absence and presence of different *Pf*ADF1 concentrations (red 0.5, blue 1, pink 1.5, green 2, dark blue 3, and violet 4 µM). **(B)** The steady state fluorescence units were plotted against *Pf*ADF1 concentration and a nonlinear fit (1st order exponential decay) was made to get a binding curve.

4.3.4   *Effect of PbADF2 and PfADF1 on G-actin nucleotide exchange*

Conventional ADFs decrease the rate of nucleotide exchange from ADP to ATP, resulting in a decrease in the pool of polymerizable G-actin (Nishida, 1985). The effect of *Pf*ADF1 and *Pb*ADF2 on nucleotide exchange from ADP to ϵ-ATP was tested by monitoring the change in fluorescence of ϵ-ATP upon incorporation into G-actin. On contrary to conventional ADFs, *Pf*ADF1 accelerates nucleotide exchange on G-actin (Schüler *et al.*, 2005). Therefore, *Pf*ADF1 was used as a control sample, and the earlier results could be reproduced **(Figure 25)**. Increasing concentrations of *Pb*ADF2 (2, 4, 8, 16, and 20 µM), accelerated the nucleotide exchange rate on G-actin from ADP to ϵ-ATP in a concentration dependent manner with a saturation at 16 µM *Pb*ADF2 **(Figure 25)**. Thus, both *Plasmodium* ADFs accelerate nucleotide exchange on G-actin, in contrast to other characterized ADFs.

4.3.5   *Microscale thermophoresis binding analysis of actin-PbADF2 and actin-PfADF1 complex*

Polymerization and co-sedimentation assays indirectly but clearly demonstrate that *Pb*ADF2 and *Pf*ADF1 both bind to G-actin. MST was employed to characterize the interaction

of G-actin with *Pb*ADF2 and *Pf*ADF1 in more detail. Labeled actin (20 nM) was incubated with various concentrations of *Pf*ADF1 (2.3 nM to 75 µM) and *Pb*ADF2 (2.5 nM to 82 µM) separately, and thermophoresis was measured. The experiment showed two states, bound and unbound, and K_ds of 2.5 µM and 2.6 µM were calculated for *Pb*ADF2 and *Pf*ADF1, respectively **(Figure 26)**. The result confirms that the both *Plasmodium* ADFs bind directly to ATP-actin with comparable affinities, providing evidence for sequestering activities. The results are in line with previous reports, where it has been shown that *Plasmodium* ADFs bind ADP–actin with a higher affinity compared to ATP-actin, which in most of the cases have been reported to be in range from 0.5 – 1 µM (Yadav et al., 2011).
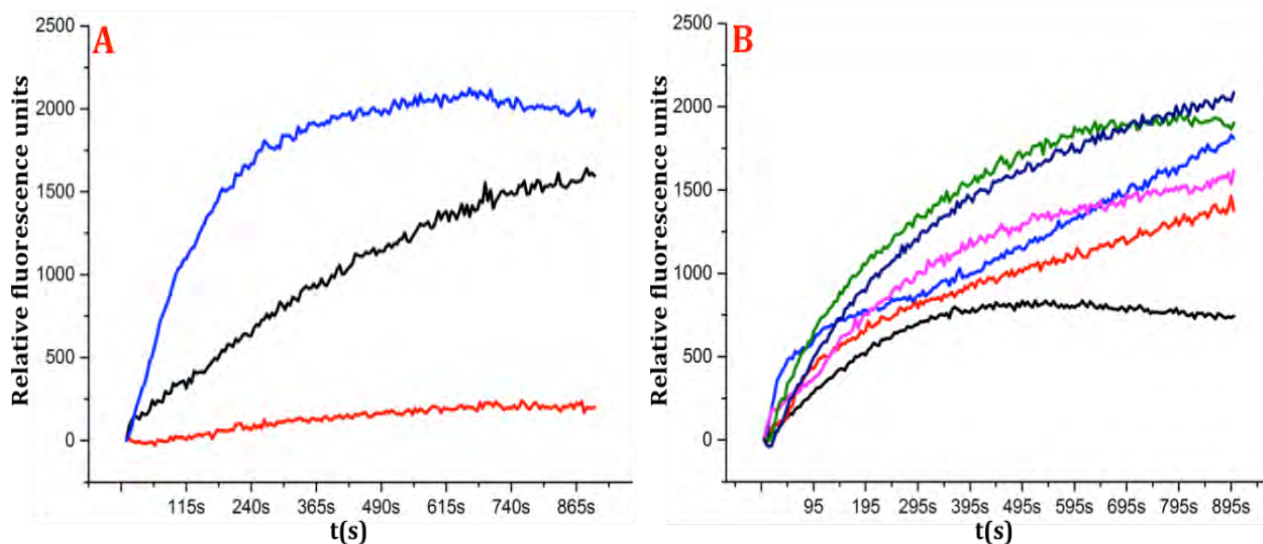
Figure 25: PfADF1 and PbADF2 accelerate the rate of nucleotide exchange on G-actin.

(A) Nucleotide exchange rate of G-actin (4 µM) alone (black) and in the presence of 4 µM *Pf*ADF1 (blue) was measured. The red curve is only 4 µM *Pf*ADF1 as a negative control. **(B)** The effect of *Pb*ADF2 on nucleotide exchange of G-actin was monitored by adding various concentrations of *Pb*ADF2 (red 2, blue 4, pink 8, green 16, and violet 20 µM). Both *Pf*ADF1 and *Pb*ADF2 accelerate the rate of nucleotide exchange.
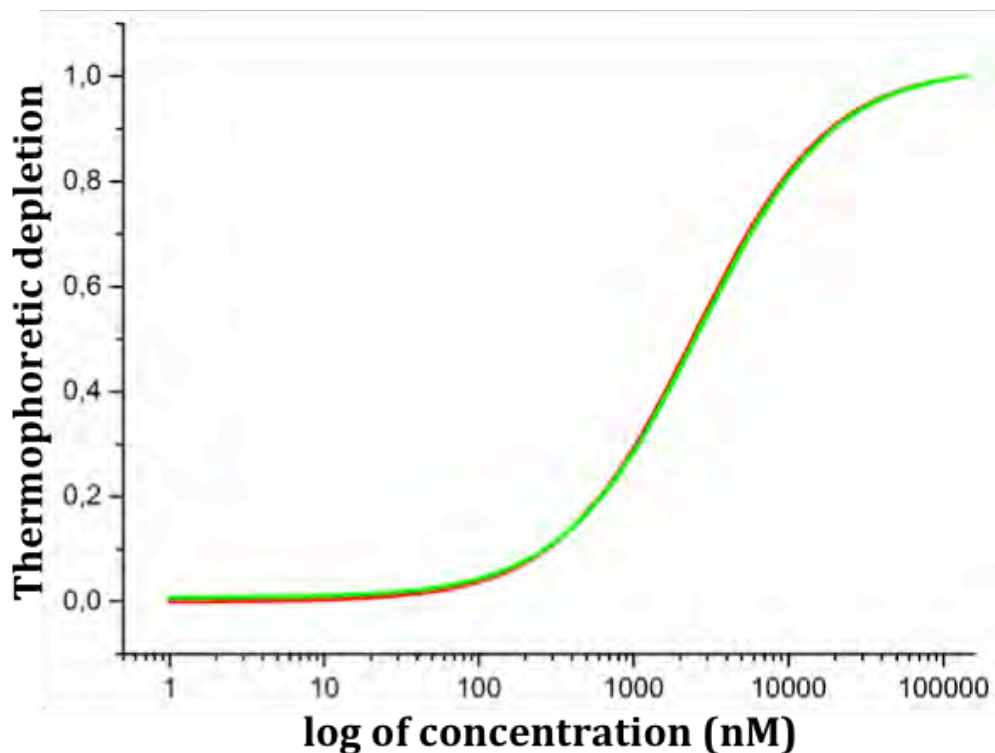
Figure 26: Interaction of PbADF2 and PfADF1 with G-actin.

Unlabeled *Pb*ADF2 (2.5 nM - 82 µM) and *Pf*ADF1 (2.3 nM to 75 µM) were titrated with labeled actin at a concentration of 20 nM and incubated for 5 min. Subsequently, thermophoresis was measured. Log of protein concentrations were plotted against thermophoresis using a non-linear fit (green: *Pf*ADF1; red: *Pb*ADF2). *Pf*ADF1 and *Pb*ADF2 interact with a K_d 2.5 and 2.6 µM with actin, respectively.

4.4 <u>*Structural characterization of the PfADF1- and PbADF2–actin complexes*</u>

4.4.1 *Purification of the PbADF2- and PfADF1-actin complexes*

The SEC profile of both *Pf*ADF1- and *Pb*ADF2-actin complexes showed three peaks. SDS-PAGE analysis showed that the samples from the first peak contain complex of *Pb*ADF2-actin and *Pf*ADF1-actin (elution volumes 13.7 and 13.5 ml respectively), while the second and third peaks contain actin and the ADFs, respectively. The molecular weights estimated using a standard calibration curve are 54.9 kDa for *Pf*ADF1-actin and 57.5 kDa for *Pb*ADF2-actin **(Figure 27)**. The estimated molecular weights are close to the expected molecular weight of the complexes *i.e.* 55.9 kDa for *Pf*ADF1-actin and 58.7 kDa for *Pb*ADF2-actin.
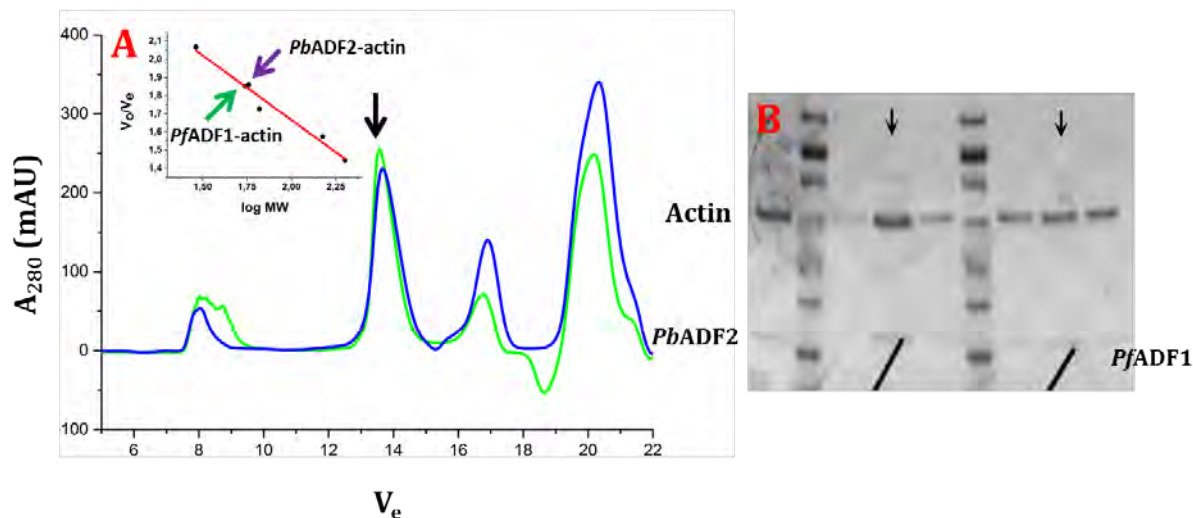
Figure 27: Purification of PbADF2-actin and PfADF1-actin complexes.

(A) SEC profiles of sample with *Pb*ADF2-actin (green) and *Pf*ADF1-actin (blue) resolved using a Superdex 200 10/300 GL column. The inset shows calibration curve of standard proteins carbonic anhydrase, cytochrome c, bovine serum albumin, alcohol dehrdrogenase and data points corresponding to respective complexes **(C)** SDS-PAGE analysis of the samples from the SEC peak fractions. The peak fractions corresponding to the actin-ADF complex are shown with arrow mark.

4.4.2 *SAXS analysis of the PbADF2-actin complex*

Analysis of the *Pb*ADF-actin SAXS data with GNOM (Svergun, 1992), showed a bilobal shape, indicating the formation of the complex. The complex has an R_g of 3.4 nm, while actin alone has an R_g of 2.9 nm and *Pb*ADF2 1.7 nm. The Porod volumes calculated from the SAXS data were also in good agreement; the complex had a Porod volume of 94.4 nm^3, while actin and *Pb*ADF2 alone have volumes of 72.05 nm^3 and 24.81 nm^3, respectively. The D_{max} was calculated to be 10.77 for the complex, 9.05 for actin, and 6.09 for *Pb*ADF2. After the initial processing by GNOM, an *ab initio* model was built using DAMMIF (Franke *et al.*, 1990). No symmetry constrains were applied in the model building. The model from DAMMIF has a good fit to the data with a chi squared value of 1.8. The crystal structure of actin-twinfilin, where twinfilin was replaced with the X-ray crystal structure of *Pb*ADF2 was superimposed on the *ab initio* model (Paavilainen et al., 2008; Singh et al., 2011) **(Figure 28)**.
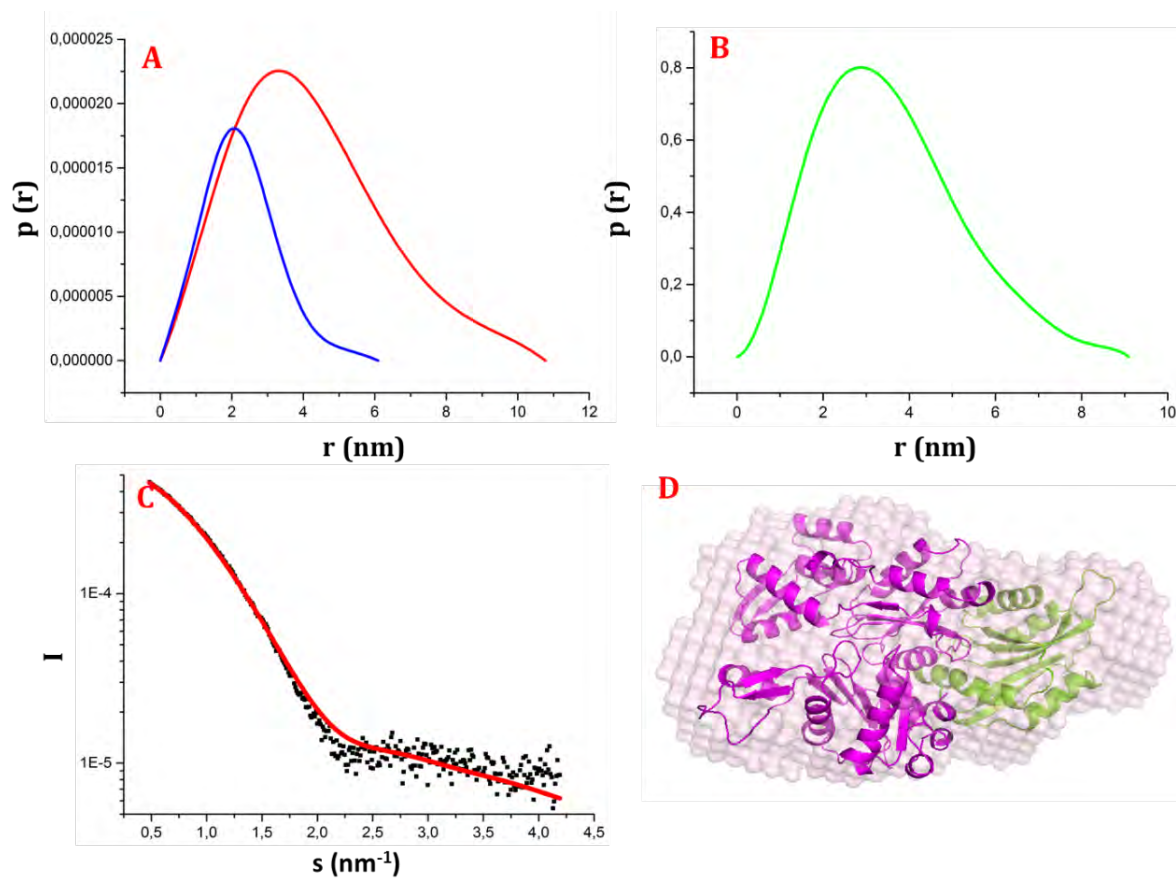
Figure 28: Solution structure of the PbADF2-actin complex.

(A) Distance distribution function of *Pb*ADF2 (blue) and *Pb*ADF2-actin complex (red). **(B)** Distance distribution function of actin (green). **(C)** Scattering curve of *Pb*ADF2-actin complex. Raw data points are indicated in black, while red represents the fit of the *ab initio* model to the raw data. **(D)** Superposition of the *ab initio* model of actin-*Pb*ADF2 generated from DAMMIF (Franke *et al.*, 1990) (pink) with the crystal structure of actin bound to C-twinfilin (3DAW) (Paavilainen et al., 2008) (magenta), where the C-twinflin chain has been replaced by *Pb*ADF2 crystal structure (green).

4.4.3 *SAXS analysis of the PfADF1-actin complex*

SAXS data for the purified *Pf*ADF1-actin complex showed an R_g of 7.9 nm, D_{max} of 27.81 nm and Porod volume of 521 nm^3. The scattering curve had a peak at 1.1 nm^{-1} corresponding to 57 Å lattice size, which indicates polymerization of actin, apparently due to inefficient sequestering of actin monomers by *Pf*ADF1 **(Figure 29).**
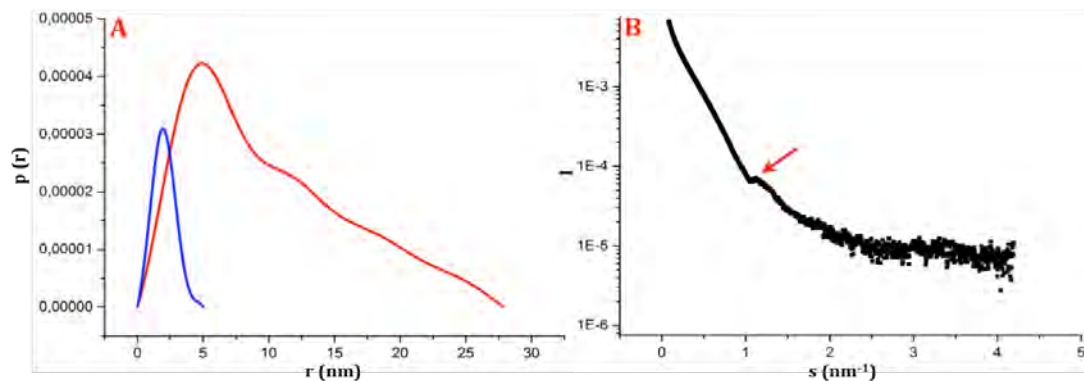
Figure 29: PfADF1 does not form stable complex with G-actin in vitro.

(A) Distance distribution function of *Pf*ADF1 (blue) and *Pf*ADF1-actin complex (red). **(B)** Experimental scattering curve of *Pf*ADF1-actin complex showing a peak at 1.1 nm depicted with red arrow, which is the characteristic of filamentous actin signifying that actin and *Pf*ADF1 does not form a stable complex *in vitro*.

4.4.4 *Cross-linking of PbADF2-actin and PfADF1-actin*

With the aim to obtain crystal structures of the complexes of actin and *Plasmodium* ADFs, cross-linking with EDC was performed. The cross-linked complexes were purified, and SEC analysis showed peaks at elution volumes of 14.7 ml and 14.4 ml for the *Pb*ADF2-actin and *Pf*ADF1-actin complexes, respectively **(Figure 30)**. The estimated molecular weights were 54.9 kDa and 58.8 kDa for the complexes, respectively. The samples were analyzed by SDS-PAGE.
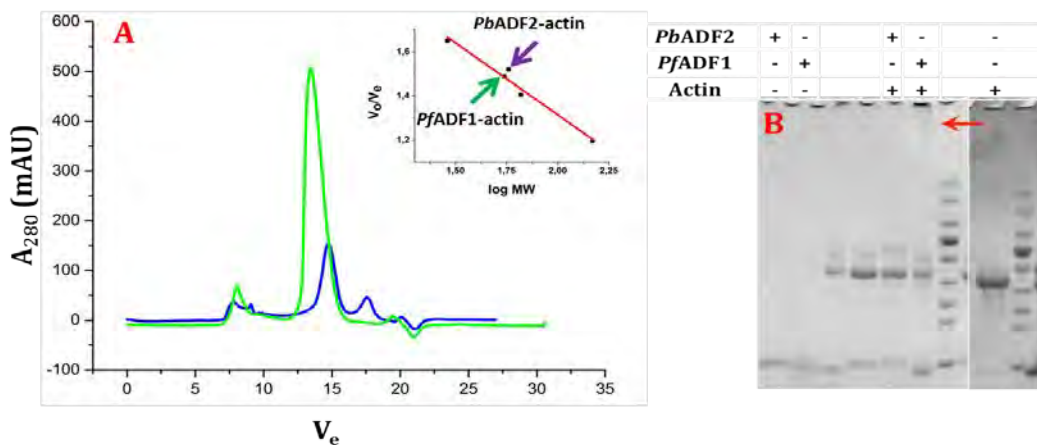
Figure 30: EDC crosslinking of actin with PfADF1 and PbADF2.

(A) SEC profile of cross-linked *Pb*ADF2-actin (green) and *Pf*ADF1-actin (blue) using a HiLoad Superdex 75 10/300 GL column. The inset shows a calibration curve for the Hi-Load Superdex 75 10/300 GL column and depicted with arrows the V_e/V_o of *Pb*ADF2-actin and *Pf*ADF1-actin. (B) SDS-PAGE analysis of EDC cross-linked actin-ADF complexes. Highlighted with the red arrow is the sample containing actin-*Pf*ADF1 indicating inefficient monomer sequestering.

4.5   *Characterization of PfADF1-PIP$_2$ binding*

The homologs of ADFs have been shown to be negatively regulated by phosphoinositides, hence influencing actin dynamics. In the current study, experiments were performed with the aim to explore and understand the interaction of *Plasmodium* ADFs with phosphoinositides. The results are summarized in the following sections.

4.5.1   *Preliminary characterization of the PfADF1-PIP$_2$ interaction*

Preliminary interaction studies of both parasite ADFs with PIs were performed using a band shift assay. *Pf*ADF1 and *Pb*ADF2 in the absence and presence of vesicles with PIP$_2$ (DMPC+PIP$_2$) and without PIP$_2$ (DMPC) were analyzed on native gel. A clear difference was observed in the migration pattern of *Pf*ADF1 alone or in the presence of vesicles without PIP$_2$ in comparison to the sample with PIP$_2$. Although *Pf*ADF1 alone, with a pI close to the running buffer, does not migrate far into the gel, differences could be observed in the running pattern in the presence and absence of PIP$_2$. In the presence of PIP$_2$, the sample migrates further into the native gel as a smear, and the main band disappears, indicating specific interactions between *Pf*ADF1 and PIP$_2$. *Pb*ADF2 migrates on the native gel as a sharp band and also shows a slight shift in the migration profile in the presence of PIP$_2$, similar to *Pf*ADF1 **(Figure 31)**. However, the shift for *Pb*ADF2 is not as clear as in the case of *Pf*ADF1.
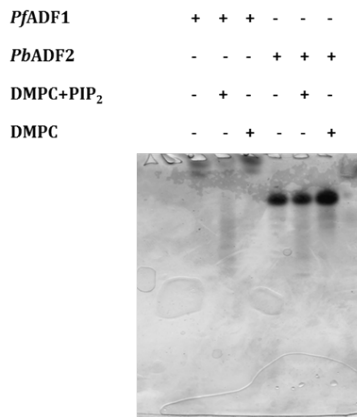
Figure 31: Band shift analysis of PfADF1 and PIP$_2$ interaction.

Migration profiles of *Pf*ADF1 and *Pb*ADF2 alone, in presence of PIP$_2$-DMPC and DMPC containing vesicles. Both, *Pf*ADF1 alone and in absence of PIP$_2$ migrates simiarly while in presence of PIP$_2$ contining vesicles the main band disappears indicating *Pf*ADF1 interacts specifically with PIP$_2$. *Pb*ADF2 migrates similarly in all conditions, indicating a weaker interaction.

69

The specificity of the ADF-PIP$_2$ interaction was confirmed by SPR. Lipid vesicles formed of DMPC-PIP$_2$ and DMPC were immobilized on different flow channels and used as ligands, while the ADFs were used as analytes. Increasing concentrations of *Pf*ADF1 and *Pb*ADF2 (0.1–10 μM) in 20 mM Tris-HCl, 50 mM NaCl, 1 mM DTT buffer at pH 7.5 were injected over the immobilized lipid vesicle surfaces, and responses were recorded. The maximum response at each concentration of *Pf*ADF1 and *Pb*ADF2 was plotted against protein concentrations, and the data fitting was done by using the law of mass action. For *Pf*ADF1, maximum responses of 560 and 127.8 RU were observed for DMPC-PIP$_2$ vesicles and DMPC vesicles, respectively **(Figure 32)**. The SPR results showed that *Pf*ADF1 specifically interacts with PIP$_2$ containing vesicles, thus supporting the results from the gel shift assay. On the contrary, *Pb*ADF2 showed only responses of 170 and 10 RU for DMPC vesicles and DMPC-PIP2 vesicles, respectively **(Figure 33)**. This may be indicative of a low affinity of *Pb*ADF2 to PIP$_2$-DMPC or inaccessibility of *Pb*ADF2 binding site.

Binding of profilin to PIP$_2$ results in an increase of the α-helical content of the protein (Raghunathan et al., 1992). To investigate if the binding to lipids affects the secondary structure of the *Pf*ADF1 and *Pb*ADF2, SRCD data were collected for proteins alone, in the presence of DMPC-PIP$_2$ vesicles and DMPC alone. The SRCD data for the proteins alone showed curves characteristic of a typical folded mixed α-β protein with large negative peaks at 208 and 222 nm and a positive peak at 190 nm. The SRCD spectra of *Pf*ADF1 in presence of PIP$_2$ vesicles show change in the shape of curve, suggesting specific interaction with PIP$_2$. On contrary, SRCD spectra of *Pb*ADF2 doesn't show any change in presence or absence of PIP$_2$, indicating weak or no interaction **(Figure 34)**.

 In line with this observation, changes in the CD spectra of *Pf*ADF1 in the presence of soluble PIP$_2$ with a short 8-carbon tail were also observed **(Figure 34)**. In the presence of PIP$_2$, changes were observed in the shape of the curve, in particular in the ratio of the peaks at 208 to 222 nm, suggesting that the interaction with PIP$_2$ affects the secondary structure of *Pf*ADF1. Deconvolution of the data showed a small increase in the in the α-helical content of *Pf*ADF1 upon PIP$_2$ binding (**Table 1**).
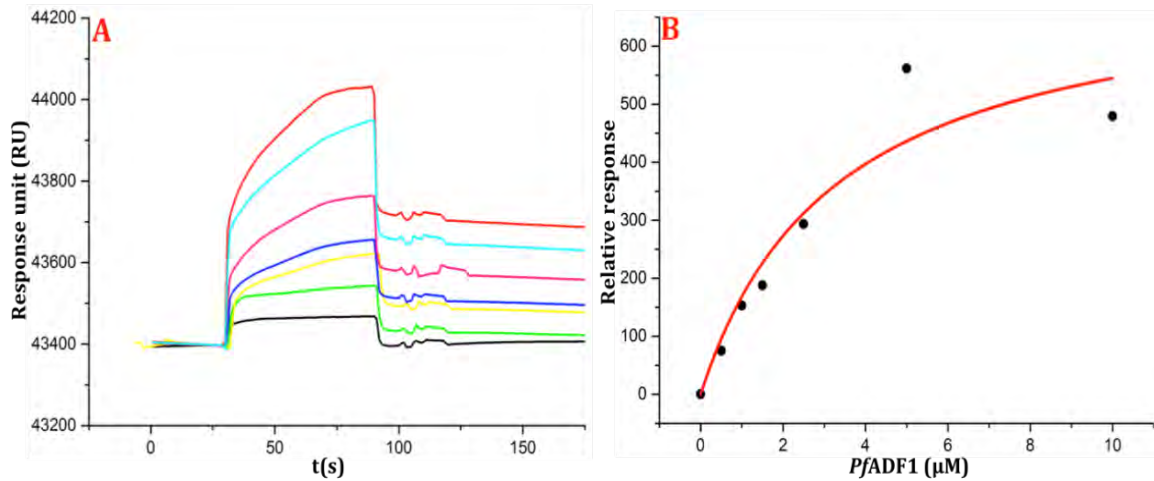
Figure 32: SPR analysis of PfADF1 binding to DMPC-PIP$_2$ vesicles.

(A) Binding of *Pf*ADF1 to DMPC-PIP$_2$ vesicles immobilized on an HPA chip. The concentrations used were 0 (black), 0.5 (green), 1 (yellow), 1.5 (blue), 2.5 (pink), 5 (red), and 10 µM (cyan). **(B)** The maximum response was plotted against the *Pf*ADF1 concentration (black dots), and fitting was perfomed using the law of mass action to obtain a binding curve (red).
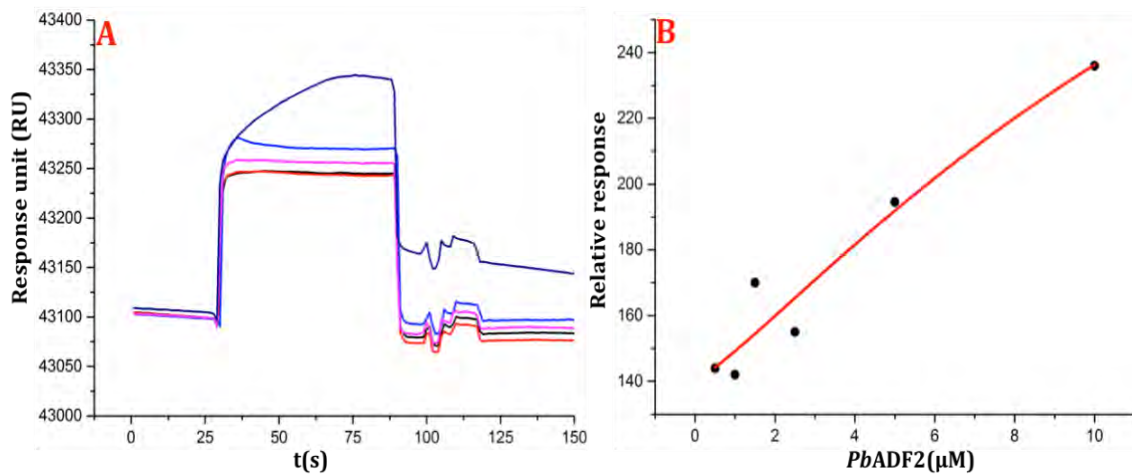
Figure 33: SPR analysis of PbADF2 in the presence of DMPC-PIP$_2$ vesicles.

(A) Binding of *Pb*ADF2 (0.5-10 µM) to DMPC-PIP$_2$ vesicles immobilized on an HPA chip. **(B)** The maximum response was plotted against the *Pb*ADF2 concentrations (black dots), and fitting was performed using the law of mass action to obtain binding curve (red).
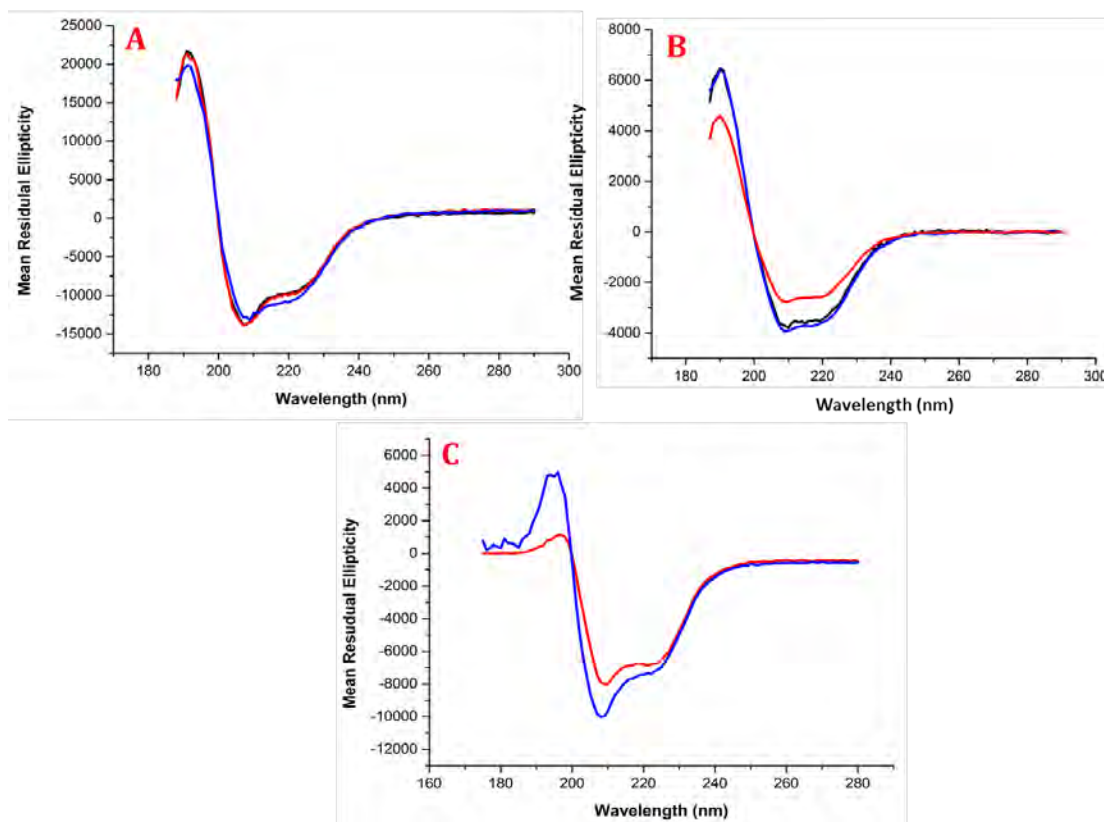
Figure 34: CD analysis of PfADF1-PIP$_2$ interaction.

(A) The curves show the SRCD spectra of *Pf*ADF1 alone (red), in presence of DMPC vesicles (black) and DMPC-PIP$_2$ vesicles (blue). **(B)** The curves show the SRCD spectra of *Pb*ADF2 alone (red), in presence of DMPC vesicles (black) and DMPC-PIP$_2$ vesicles (blue). **(C)** The CD spectra of *Pf*ADF1 alone (red) and in presence of 1:1 soluble PIP$_2$ (blue) are shown, indicating a change in the secondary structure.

	α- helix (%)	β- sheet (%)	Random coil (%)
*Pf*ADF1	29	15	49
*Pf*ADF1 PIP$_2$ (1:1)	30	15	45

Table 1: Calculated secondary structure content of *Pf*ADF1 alone and in the presence of PIP$_2$ (1:1molar ratio).

4.5.2 *Mapping of residues on PfADF1 for PIP$_2$ binding*

In order to map the residues involved in the *Pf*ADF1-PIP$_2$ interaction, NMR titration experiments were performed. Yeast cofilin was used as a positive control, as it has previously been shown to interact with PIP$_2$ (Ojala et al., 2001) using mutational studies. Upon titration, the protein maintained its fold, and overlay of both spectra showed chemical shifts mainly in three residues, confirming the binding of yeast cofilin to PIP$_2$. Further, 2D ^{1}H-^{15}N HSQC data were collected for *Pf*ADF1 at a concentration of 100 μM in the absence

and presence of PIP$_2$ (1:1.2 protein to PIP$_2$ molar ratio). *Pf*ADF1 alone showed a good peak dispersion, indicating a folded protein. When titrated with increasing concentrations of PIP$_2$, small changes in the spectra were observed up to a *Pf*ADF1:PIP$_2$ molar ratio of 1:0.8, and at a molar ratio of 1:1.2, some peaks disappeared and new intense peaks started appearing **(Figure 35)**. The changes appearing in the spectra upon titration yet again confirmed interaction between *Pf*ADF1 and PIP$_2$.

Furthermore, 3D ^{13}C, ^{14}N and ^{1}H assignment of *Pf*ADF1 was done in order to identify the residues that had undergone changes. The initial experiments showed that the peaks in two regions, residues 20-28 and 60-64, were missing in the original native spectra. The rest of the peaks could be assigned. When the 3D native *Pf*ADF1 spectrum was compared with the *Pf*ADF1–PIP$_2$ titrated spectra, chemical shifts were observed mainly in residues Arg88, Met18 and Lys19, confirming the role of these residues in the interaction with PIP$_2$ **(Figure 35)**.
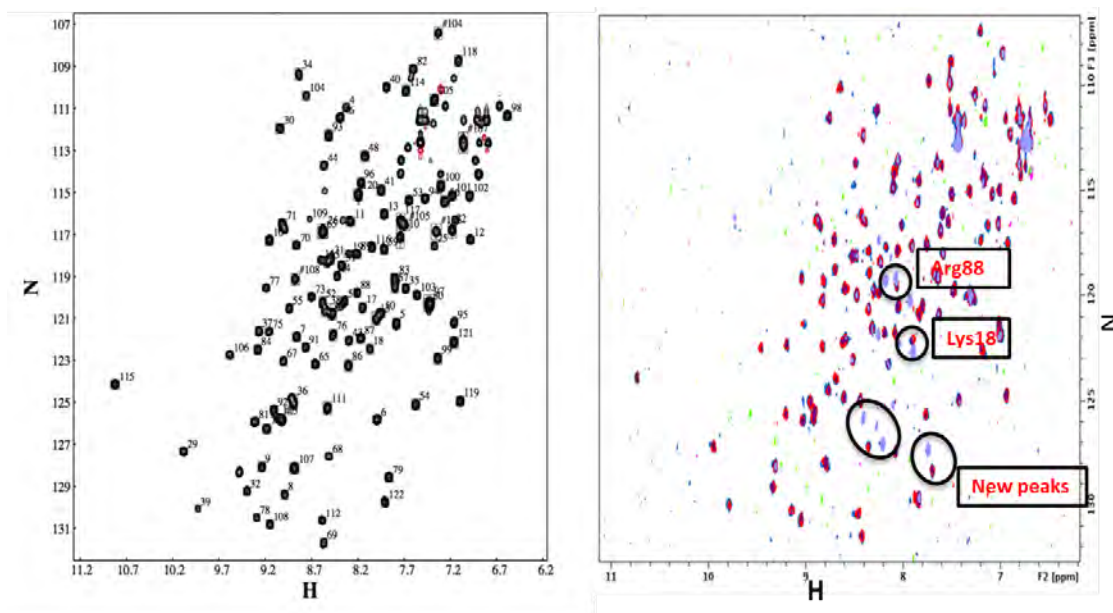
Figure 35: Mapping of residues on PfADF1 involved in PIP$_2$ binding.

(A) Backbone assignment of 100 μM of *Pf*ADF1 C^{13}, N^{15} and 10% D$_2$O. Most of the residues were assigned, except for the flexible N terminus and residues 20-28, 60-64 (due to line broadening). **(B)** Overlay of 100 μM of *Pf*ADF1 alone (blue) titrated with different concentrations of PIP$_2$ (protein: PIP$_2$ molar ratio: 1:0.2, red; 1:0.5, purple; 1:1, violet).

4.5.3 *Role of residues 20-28 in PIP₂ binding*

To assess whether the missing peaks in the original spectra and the appearance of new peaks upon PIP$_2$ titration can be linked to structural rearrangements upon the *Pf*ADF1-PIP$_2$ interaction, a multiple sequence alignment for the stretch of residues missing, *i.e.* 20-RKTCGWII-28, in *Pf*ADF1 was performed against sequences from *T. gondii* ADF, vertebrate destrin, human cofilin 1 and chicken cofilin-2, using T-coffee **(Figure 36)**. This stretch of residues overlaps with residues, which have been proposed to undergo a transition between extended and helical conformations (Goldenberg and Avila, 2011; Hatanaka et al., 1996). Hence, this missing stretch of residues also might play an important role in either interaction with or recognition of PIP$_2$.

.
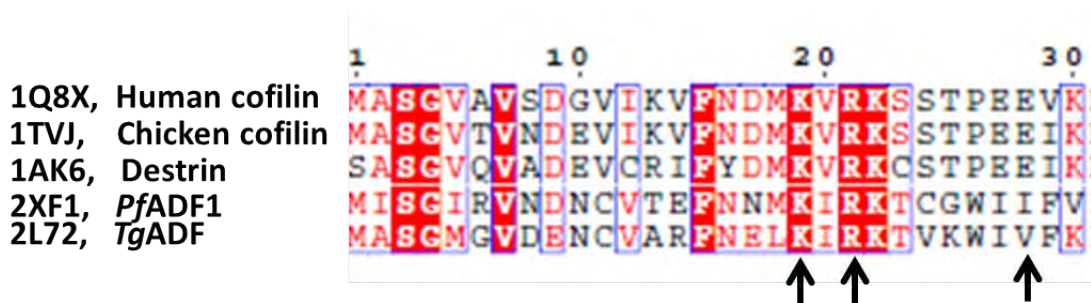
Figure 36: Multiple sequence alignment of residues 1-30 of PfADF1 against other ADFs.

A multiple sequence alignment was performed for the residues 1-30 of *Pf*ADF1 with sequences from *T. gondii* ADF, vertebrate destrin, human cofilin-1 and chicken cofilin-2. The residues marked with black arrows have been implicated to be important for translocation of ADFs to the nucleus and undergo changes in conformation from helix to an extended conformation.

Furthermore, it was observed that the above mentioned stretch of residues has a tryptophan at position 26, hence tryptophan fluorescence assays were performed to investigate if the interaction with PIP$_2$ changes the local environment of this tryptophan. Measurements were performed for *Pf*ADF1 (8 µM) alone and with increasing concentrations of PIP$_2$. Tryptophan fluorescence increased in a PIP$_2$-concentration dependent manner upon titration. A clear saturation was observed at a ratio of 1:15 *Pf*ADF1:PIP$_2$. The data were plotted using Origin, and a binding curve was obtained by fitting the data using the Hill's equation **(Figure 37)**. These results confirm that the loop residues 20-RKTCGWII-28 play an important role in the interaction with PIP$_2$. The increase in the fluorescence could be reasoned due to this stretch of residues undergoing change in the environment upon binding.
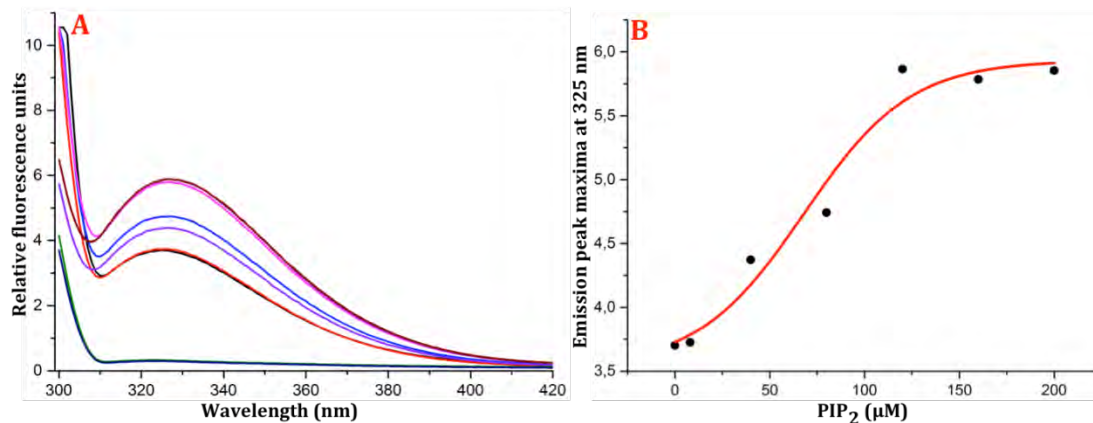
Figure 37: Tryptophan fluorescence measurements of PfADF1 with PIP₂.

(A) Tryptophan fluorescence was scanned for excitation wavelength 290 nm and emission wavelength from 300 to 420 nm of *Pf*ADF1 (8 μM). An increase in tryptophan fluorescence was observed upon addition of PIP$_2$, and a clear saturation was reached at 1:15 *Pf*ADF1 to PIP$_2$ molar ratio. **(B)** The emission peak maxima, observed at 325 nm, were plotted against the PIP$_2$ concentration (black dots). The data were fitted using the Hill's equation to obtain a binding curve (red).

4.5.4 *PIP₂ interaction stabilizes PfADF1*

Furthermore, as the tryptophan fluorescence experiments show saturation at 1:15 protein to ligand, CD was measured with *Pf*ADF1 to PIP$_2$ ratios of 1:1 and 1:15. It was also assessed, whether the thermal stability of *Pf*ADF1 was affected by the interaction with PIP$_2$.

Deconvolution of the CD data of *Pf*ADF1 alone and *Pf*ADF1:PIP$_2$ at a 1:15 molar ratio showed that the α-helical content in the PIP$_2$-saturated protein increased from 29 to 35% **(Table 2)**. The θ_{222}:θ_{208} increased from 0.734 for protein alone to 0.814 for protein saturated with PIP$_2$, which represents change in the helical content of the protein. Hence, the results from the CD experiments clearly show that the interaction with PIP$_2$ increases the helical content of *Pf*ADF1 **(Table 2).**

Furthermore, the T$_m$ for *Pf*ADF1 alone was calculated to be 63.5 °C and in presence of 1:1 protein to PIP$_2$ the T$_m$ increased to 67 °C. At 1:15 protein to PIP$_2$, though the T$_m$ reduced to 62 °C, yet an increase in the negative value of MRE is observed indicating a transition to β-structures, predicting induction of a non-native but still ordered conformation in the protein upon heating in presence of PIP$_2$. Temperature scan of 1:1 *Pf*ADF1 to PIP$_2$ loses its β-structure at 70 °C, while when saturated with ligand (1:15) the nonnative structure is not

lost. These experiments together predict that the protein is stabilized upon interaction with PIP$_2$ **(Figure 38)**.
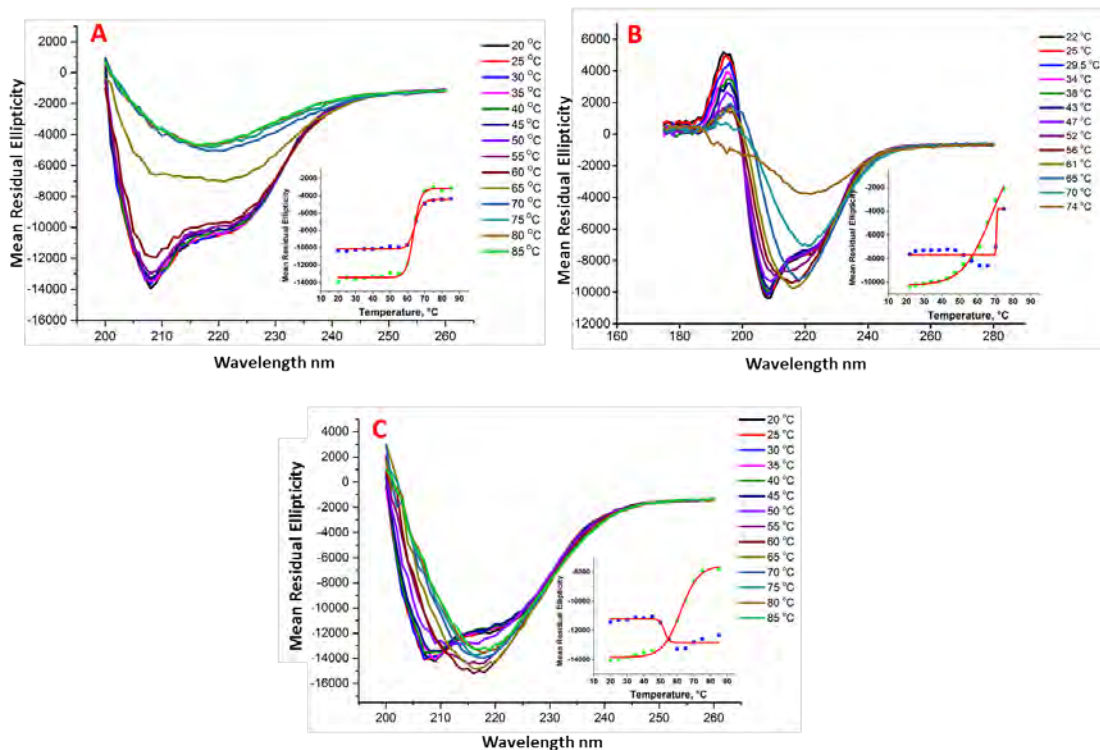
Figure 38: Thermal melting curves PfADF1 in absence and presence of PIP2.

(A) CD spectra of *Pf*ADF1 (0.25 mg/ml) from wavelength 180 to 260 nm with increasing temperature from 20 to 85 °C. The inset shows decrease of MRE at 208 (green dots) and (blue dots) 222 nm. **(B)** CD spectra of *Pf*ADF1 (0.25 mg/ml) to PIP$_2$ 1:1 molar ratio with increasing temperatures from 21 to 74 °C. The inset shows decrease of MRE at 208 (green dots) and (blue dots) 222 nm. **(C)** CD spectra with increasing temperatures from 20 to 80 °C for *Pf*ADF1 (0.25 mg/ml) to PIP$_2$ 1:15 molar ratio. The inset shows decrease of MRE at 208 nm (green dots) and increase (blue dots) 222 nm. The data were buffer subtracted, converted to MRE and plotted using origin.

	α- helix (%)	β- sheet (%)	Random coil (%)
*Pf*ADF1	29	15	49
*Pf*ADF1 PIP$_2$ (1:15)	35	15	45

Table 2: Calculated secondary structure contents of PfADF1 alone and in the presence of PIP2 (1:15 molar ratio).

4.6   *Plasmodium capping protein α subunit forms functional homodimers*

4.6.1   *Purification of the Plasmodium capping protein α subunit*

The SEC profile of *Pb*CPα and chicken CapZ shows that the proteins elute as single peaks at elution volumes of 79 and 78 ml, respectively **(Figure 39)**. The sizes of the eluted proteins, as calculated from the calibration curve, corresponded to 74 and 71 kDa for *Pb*CPα and CapZ, respectively, indicating dimerization of both the homodimeric *Pb*CPα and the heterodimeric CapZ **(Figure 39)**. Mass spectrometry of the purified *Pb*CPα protein was used to confirm its identity.
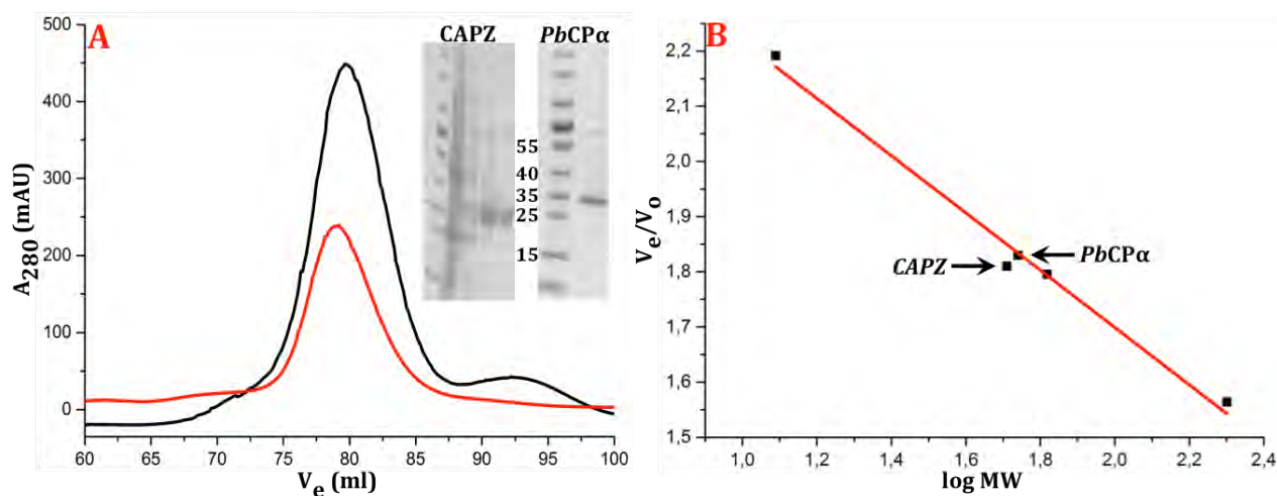
Figure 39: SEC of PbCPα and CAPZ subunit.

(A) Chromatogram of *Pb*CPα (black) and CapZ (red) on Hi Load 16/60 prep grade Superdex 75 column. The proteins eluted as single peaks at volumes 79 (*Pb*CPα) and 78 ml (CapZ). *Pb*CPα appears as a single band while CapZ heterodimer appears as double band on SDS-PAGE (inset). **(B)** The calibration curve of the Hi Load 16/60 prep grade Superdex S200 10/300 column. Marked are the elution volumes of *Pb*CPα and CapZ.

For determination of the accurate molecular mass of *Pb*CPα, SLS analysis was performed. BSA was used for calibration. *Pb*CPα (6.5 mg/ml) was injected to a Superdex S200 10/300 column equilibrated with CP buffer. The molecular weight was determined to be 68 kDa from the signal of refractive index, which corresponds to a *Pb*CPα dimer **(Figure 40)**.
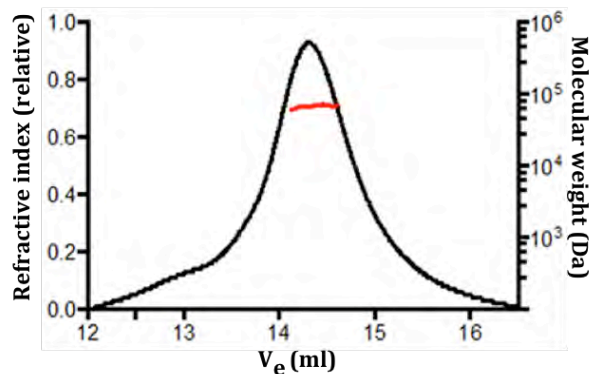
Figure 40: SLS analysis for accurate mass determination.

SEC was performed on *Pb*CPα (6.5 mg/ml) using Superdex 200 10/300 GL column and molecular mass measured using static light scattering signal. The elution volume is plotted against the refractive index signal and the red line indicates molar mass as function of elution volume.

4.6.2   *Biochemical characterization of PbCPα*

4.6.2.1 Binding of *Pb*CPα to actin

Binding of *Pb*CPα to actin was assessed using a co-sedimentation assay. The control reactions show that actin in F-buffer was in the pellet fraction, and *Pb*CPα alone in F-buffer was detected only in the supernatant fractions. *Pb*CPα (1-20 µM) caused small but detectable shift of actin from the pellet to the supernatant, indicating that it affects the filament length distribution. Additionally, trace amounts of *Pb*CPα were also detected in the pellet, demonstrating that it interacts with F-actin **(Figure 41)**.
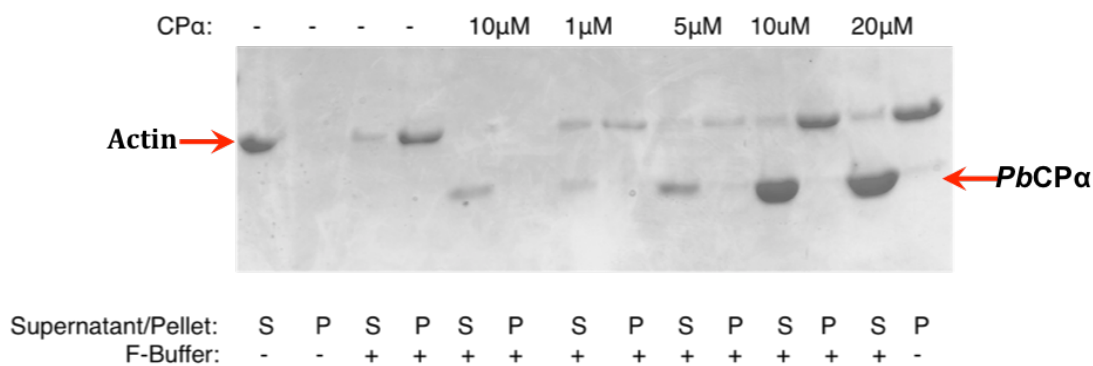
Figure 41: Co-sedimentation assay with PbCPα.

Actin (5 µM) was polymerized in the absence and presence of various concentrations of *Pb*CPα (1 – 20 µM) and incubated for 1 h at RT. The supernatant (S) and pellet (P) fractions were separated and analyzed on SDS PAGE. Upon addition of *Pb*CPα, a clear shift of actin from the pellet fraction to the supernatant was observed, indicating that *Pb*CPα binds to actin.

78

4.6.2.2 Effect of *Pb*CPα and CapZ on actin polymerization

Pyrene actin polymerization assay was used to test the effects of *Pb*CPα and CapZ on actin filament dynamics. Actin (5% pyrene labelled) at a concentration of 4 µM was polymerized in the presence of 1-50 nM CapZ and 1-500 nM of *Pb*CPα. Discrete effects were observed for CapZ and *Pb*CPα. Addition of CapZ resulted in an acceleration of actin polymerization, precisely affecting the elongation rate, likely due to stabilization of nuclei **(Figure 42)**, which is in accordance to the reported result (Caldwell et al., 1989), while *Pb*CPα does not affect the rate of polymerization, thus showing that dimeric *Pb*CPα lacks the ability to enhance actin polymerization **(Figure 43)**. The slopes of the individual curves were plotted against various CapZ concentrations, and fitting was performed using a non-linear equation (Michaelis-Menten).

4.6.2.3 CapZ and *Pb*CPα bind to actin filament barbed end

Since no nucleation activity was seen for *Pb*CPα, we next tested if *Pb*CPα affects the elongation rate of pre-formed actin filaments. The control reaction of actin alone (2 µM preformed filaments and 2 µM G-actin) shows absence of nucletion, as expected. Upon addition of 0.1 to 5 nM of CapZ, the polymerization rate decreased **(Figure 44)**. Addition of 0.25 – 5 µM *Pb*CPα also resulted in reduced polymerization, though the concentration required was higher for *Pb*CPα, which could be reasoned because of the truncated C terminus, which has been shown to be important of the capping activity (Wear. M. A,*et al.*,2009; Kim, K,*et al.*, 2004)**(Figure 45)**. The assay confirms that both CapZ and *Pb*CPα bind to the barbed end of actin filament. Slopes of the individual curves were plotted against the protein concentrations and non–linear fitting (1st order exponential decay equation) was performed.
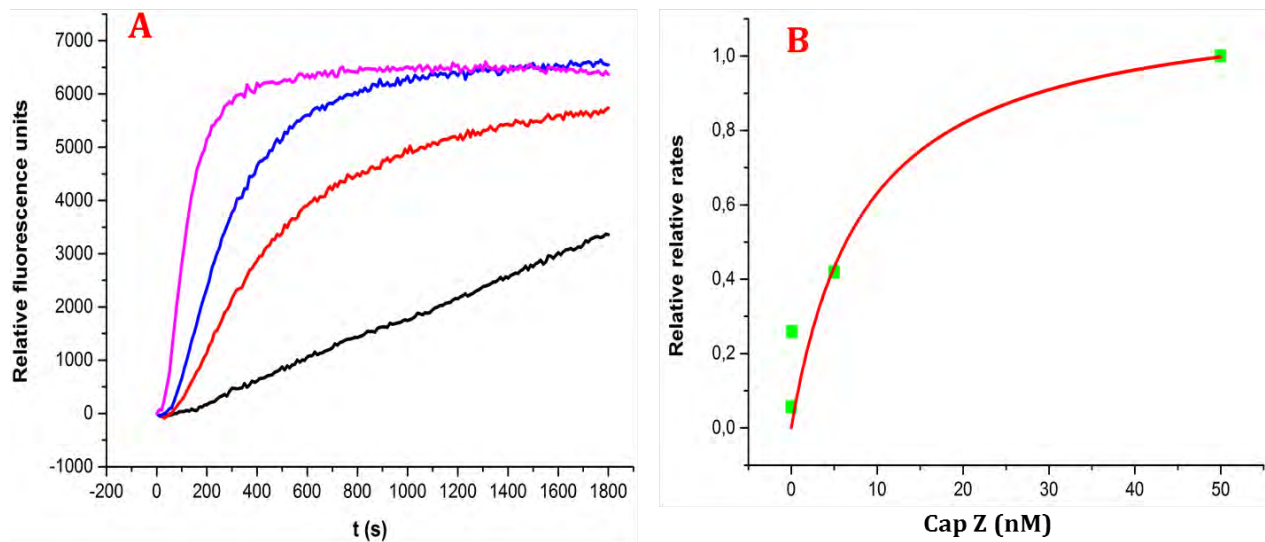
Figure 42: Actin polymerization assays in the presence of CapZ.

(A) Polymerization of 4 µM (5% pyrene labelled) of actin in the absence and presence of various concentrations of CapZ (red 1 nM, blue 5 nM and pink 50 nM). CapZ accelerated the actin polymerization. **(B)** The slope of the individual curves (green dots) was plotted against their respective CapZ concentrations, and non-linear fitting (Michaelis-Menten equation) was performed (red line) to obtain a binding curve.
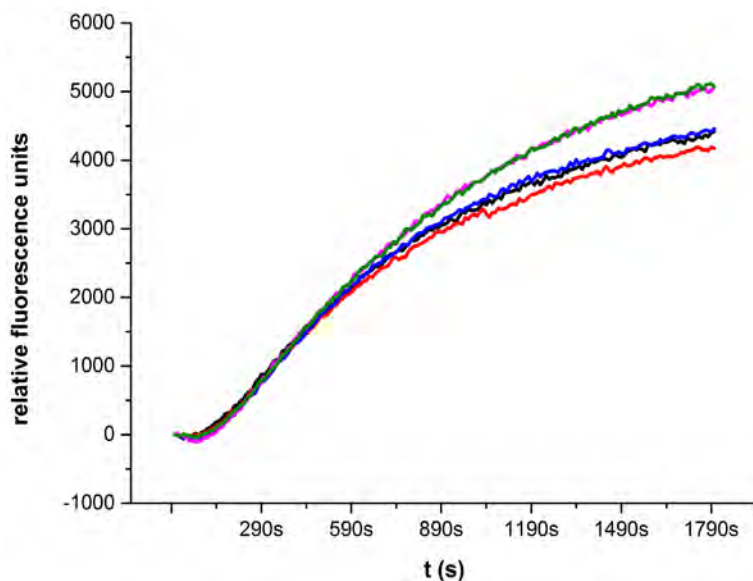
Figure 43: Actin polymerization assays in the presence of PbCPα.

Polymerization of 4 µM (5% pyrene labelled) of actin in the absence and presence of various concentrations of *Pb*CPα (red 1 nM, blue 5 nM, pink 50 nM and green 500 nM) was followed for 1 h at RT.
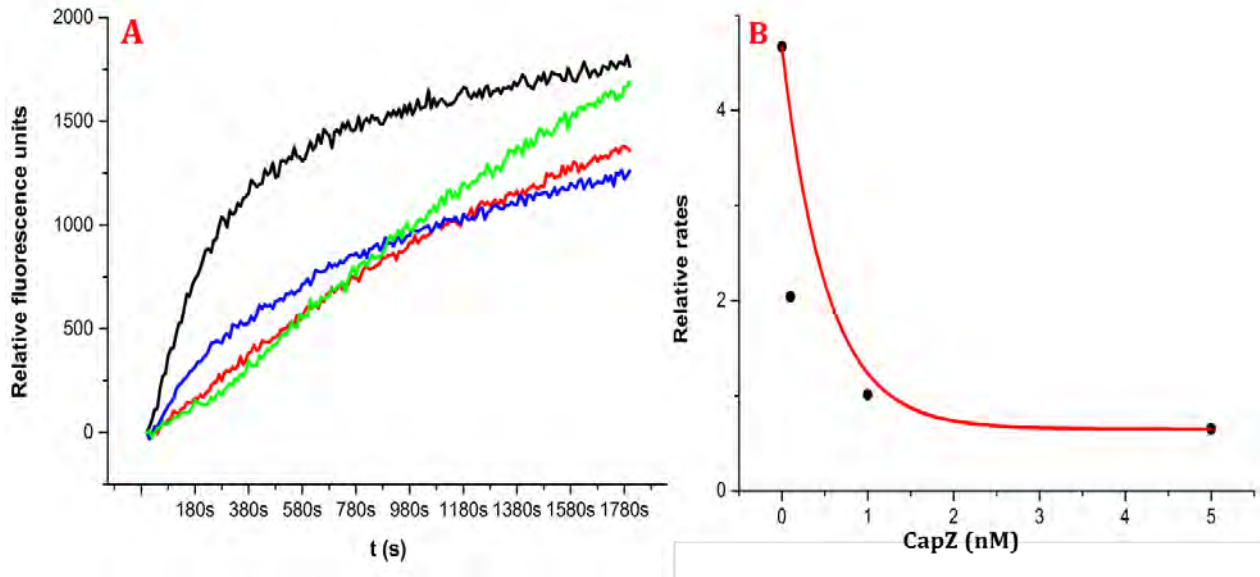
Figure 44: Seeded actin polymerization assay in the presence of CapZ.

(A) Polymerization was followed for 2 µM G-actin incubated with different concentrations of CapZ (0 µM black, blue 0.1 nM, red 1 nM and green 5 nM) in the presence of actin seeds (2 µM) by adding 1x F buffer. Polymerization was followed for 1 h at RT. **(B)** Slope of the individual curves was plotted against different CapZ concentration (black dots), and non-linear fitting was performed (1st order exponential decay equation) (red line).
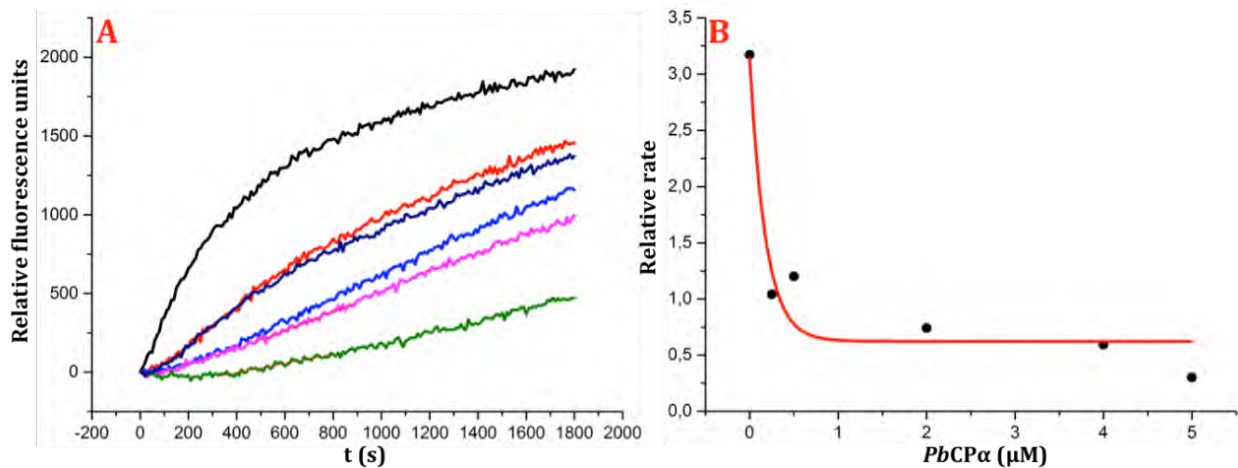
Figure 45: Seeded actin polymerization assay in the presence of PbCPα.

(A) Polymerization was followed for 2 µM G-actin incubated with different concentrations of *Pb*CPα (black 0 µM, red 0.25 µM, violet 0.5 µM, blue 2 µM, pink 4 µM and green 5 µM) in the presence of actin seeds (2 µM) by adding 1x F buffer. Polymerization was followed for 1 h at RT. **(B)** Slope of individual curves was plotted against different *Pb*CPα concentrations (black dots) and non-linear fitting was performed (1st order exponential decay equation) (red line).

81

4.6.3   *Solution structure of the PbCPα homodimer*

SAXS data were collected for dimeric *Pb*CPα which was purified in CP buffer as mentioned in section 3.1.16. The initial processing by GNOM (Svergun, 1992) shows that the molecule has Rg of 4.32 nm and Dmax was calculated to be 12.2. *Ab initio* model building was done by DAMMIF (Franke *et al.*, 1990) which suggests a 2-fold symmetry and shows a good fit to the data with a chi square value 1.164. No symmetry constrains were applied for model building. The *ab initio* model fits well to the homodimer structure model which was generated based on X-ray crystal structure of CapZ **(Figure 46)**.
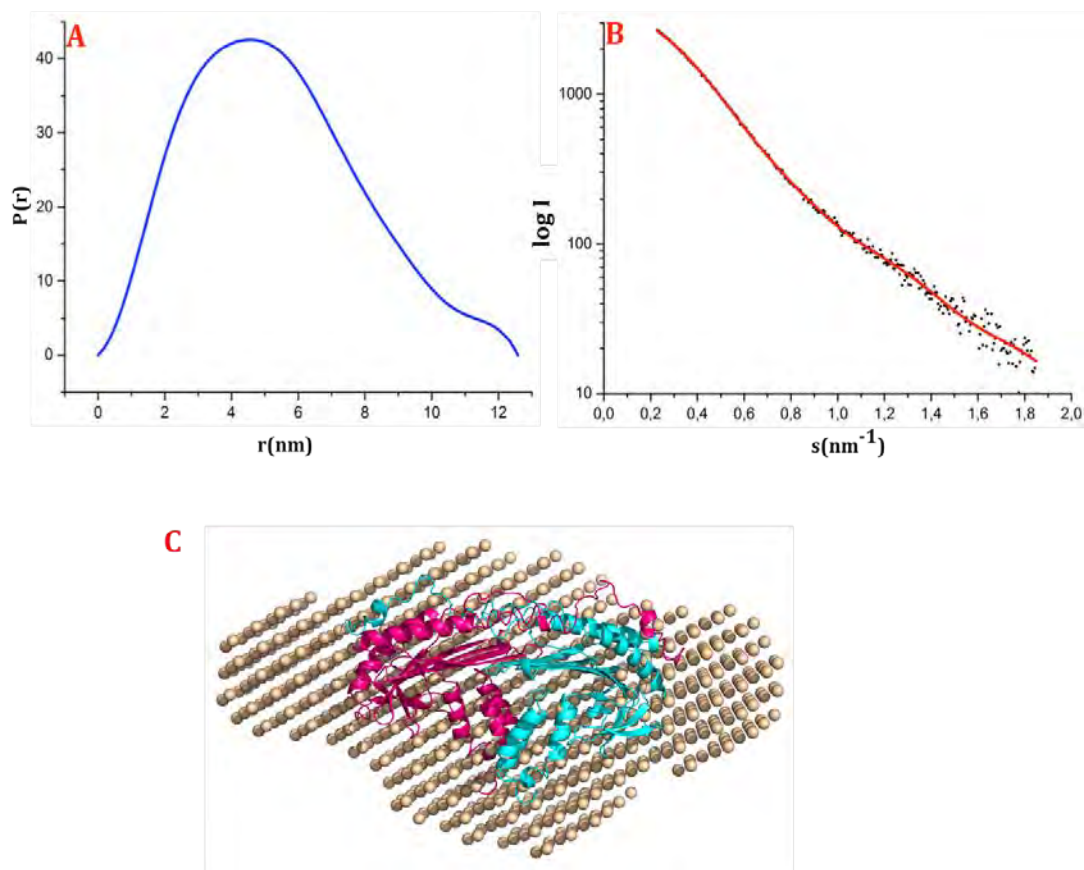
Figure 46: SAXS structure of the PbCPα homodimer.

(A) Distance distribution function of the *Pb*CPα. **(B)** Scattering curve of *Pb*CPα. The raw data is shown in black, while the red shows the fit of the *ab initio* model to the raw data. **(C)** Superposition of the *ab initio* SAXS model (in brown) of *Pb*CPα and to CPα dimer model based on the CapZ X-ray crystal structure.

5   Discussion

Functional differences in Plasmodium ADFs contribute to the unique actin filament dynamics of the parasite

Plasmodium ADFs play an important role in actin filament dynamics. *Plasmodium* spp. express two isoforms of both actin and ADFs (Wesseling et al., 1988). *Plasmodium* actin 1 and 2 have divergent expression profiles and biochemical properties. Additionally, actin 2 as well as ADF2 are both expressed in the sexual stages of the parasite, while actin 1 and ADF1 are expressed throughout the life cycle of the parasite, which hints towards a stage specific function of the ADFs (Schüler et al., 2005a). Comparison of the crystal structures shows that the two isoforms of ADFs are divergent, the most striking difference being in the length of the F-loop and the C terminus, which are shorter in ADF1 in comparison to ADF2 (Singh et al., 2011). The structural differences in the two ADFs also convert into functional divergence. Both ADFs can bind to G-actin. Though the filament binding and severing properties of ADF1 have been questioned previously, our experiments clearly show that ADF1 binds actin filaments, albeit at a lower affinity than ADF2. In actin polymerization assays, ADF1 at lower concentrations accelerated the rate of polymerization, but had the opposite effect at higher concentrations. This likely results from severing of filaments resulting in more barbed ends at lower concentrations of ADF1, resulting in an increased pool of polymerizable actin, while higher ADF1 concentrations result in rapid depolymerization, possibly accompanied by monomer sequestering.

 In contrast to conventional ADFs, *Plasmodium* ADF1 accelerates nucleotide exchange from ADP to ATP in the actin active site cleft. In this respect, ADF1 functions like profilin rather than classical ADFs. Moreover, it has been shown that actin 1 inherently forms short transient filaments, which may lead to need of several profilin-like proteins to rapidly reload polymerizable ATP-actin monomers.

ADF2 in structure and function resembles canonical ADFs, functions as a depolymerizing factor, monomer sequestering protein and severs filamentous actin. Both ADF2 and actin 2 are expressed in the insect cell stage, indicating that ADF2 might interact specifically with actin 2. Moreover, though both ADF1 and ADF2 bind to G-actin with similar affinities, as shown by MST experiments, yet ADF1 does not form a stable complex in solution. The SAXS

results show formation of a stable ADF2–actin complex, whereas in spite of repeated efforts, a stable complex for ADF1–actin was not obtained. Instead, the experiment showed a typical profile for filaments, indicating inefficient monomer sequestering by ADF1. Additionally, in a crosslinking reaction, though a complex could be obtained for ADF1–actin, the analysis by SDS-PAGE demonstrates also presence of filaments, confirming the SAXS results. ADF2 in cross linking experiments forms a stable complex with actin, as expected. These results together suggest that ADF1 binds actin with a high off-rate, leading to a transient complex. ADF N-terminal residues are essential for filament severing (Abe et al., 1990). The ADF1 construct used in this study has a complete N terminus, which is missing in most other published works. Our results show that ADF1 does bind to F-actin. Several reports have shown that the C terminal and F-loop regions of ADFs are important for F-actin binding (Galkin et al., 2011). These regions are spatially very close to each other, and hence, are recognized as the molecular surface of ADF binding to F-actin (Ono et al., 2001). The pyrene fluorescence assay on contrary to the earlier reports, were no severing has been observed (Schüler et al., 2005a), shows that *Pf*ADF1 does show severing activity in a concentration dependent manner. The steady state concentration of actin decreases upon increasing ADF concentration. These observations indicate that the N terminus of ADF1 is important for its severing activity and might indicate the presence of two F-actin binding sites on *Pf*ADF1, 1st the C terminal conventional binding site and 2nd the N terminal region.

PIP$_2$ blocks the ADF1 actin binding site

Plasmodium is characterized by the presence of peculiar actin and ADFs. Therefore, understanding the regulation of ADFs would help to understand how these unique proteins function. PIP$_2$ is an important regulator of ADFs and therefore also actin dynamics (Gorbatyuk et al., 2006; Kusano et al., 1999). From the results here, it is clear that like conventional ADFs, *Plasmodium* ADFs also interact with PIP$_2$. Additionally, the results clearly demonstrate that the interaction is specific and results in an ordering and stabilization of the ADF structure.

The preliminary results, demonstrating the interaction between ADF1 and PIP$_2$ were further confirmed by ^{15}N HSQC NMR titration experiments, which indicated Arg88, Met18 and Lys19, as the most important interacting residues. Moreover, residues 88 correspond to

the conserved basic residues of α-helix 3 that interact with actin in the Twf-C–actin complex. Hence, our results indicate that the actin and PIP_2 binding sites on *Pf*ADF1 are overlapping, and the binding of actin and PIP_2 to *Pf*ADF1 is mutually exclusive.

For chicken cofilin, residues 9-25 have been identified for binding both to PIP_2 and actin (Kusano et al., 1999). In agreement with these results, the NMR data show that residues Met18 and Lys19 also experienced shift upon titration with PIP_2. Together, these data hint towards the N-terminal region of *Pf*ADF1 being the second binding site for PIP_2.

Upon titration with PIP_2, new peaks appeared, which could not be assigned, as the assignment was done only in the absence of PIP_2. Furthermore, from the protein only spectra, residues 20-28 were missing. This stretch of residues on *Pf*ADF1 has a tryptophan, and in good agreement with this observation, an increase in tryptophan fluorescence was observed upon addition of PIP_2, which indicates a direct effect on the only tryptophan (Trp26) of *Pf*ADF1, which lies in the missing region of the original spectra. It is possible that this loop (residues 20-28) gets more ordered in the presence of PIP_2, which would explain the seen increase in the tryptophan fluorescence signal and the helical content of *Pf*ADF1.

In chicken cofilin, Lys132 and His133 are the most important interacting residues with PIP_2. Additionally, several residues at the C terminus, specific to vertebrate ADFs, were shown to be involved in PIP_2 interaction (Gorbatyuk et al., 2006). In the absence of these residues in *Pf*ADF1, the loop region 20-28 might act as the main PIP_2 interacting site.

Interaction of ABPs and PIP_2 has been reported to be mediated by localized unfolding of the protein for profilin and vinculin (Wirth et al., 2010). Weaker signal in our NMR studies could also hint towards localized unfolding of some regions of *Pf*ADF1, and folding of other parts hence making the interacting sites inaccessible for binding to actin. The appearance of additional peaks in the NMR spectra may be due to the loop 20-28 getting structured.

Plasmodium capping protein α subunit forms functional homodimers in solution

CPs have been reported always as heterodimers, consisting of an α and a β subunit (Yamashita et al., 2003). Reverse genetics studies have shown that the *Plasmodium* CP β subunit is dispensable for the parasite propagation in the mammalian host (Ganter et al., 2009). This led to the idea that *Apicomplexa* in the absence of CPβ have only CPα subunits to perform the vital functions *in vivo*. The results show the very first evidence of *Pb*CPα

existing as a homodimer. SLS, SAXS and SEC of *Pb*CPα subunit show a molecular weight of 66 kDa, which corresponds to a dimer in solution with a shape similar to the CapZ heterodimer. The existence of a homodimer is more likely also, as the monomer would expose the large hydrophobic dimerization interface to solvent.

Further, it was questioned whether the homodimer is functional, and co-sedimentation and actin polymerization assays were performed. These clearly suggest that the *Pb*CPα homodimer has capping activity *in vitro*. In the co-sedimentation assay, *Pb*CPα co-sedimented with F-actin, indicating its interaction with filaments. In addition, *Pb*CPα caused a shift of actin from the pellet to the supernatant. This shift probably occurs as the barbed end is blocked, resulting in a rise of the C_c at the pointed end and an increase of monomers in solution. Further, it also could be that due to change in the length distribution of actin filaments very short filaments still remain in the supernatant. This effect has been directly shown by microscopy for chicken CapZ (Cooper et al., 1984; Cooper and Pollard, 1985) and *Pb*CPαβ (Wetzel et al., 2003). To further investigate the role of CPα, polymerization assays were performed. These observations were further clarified by a seeded polymerization assay, where *Pb*CPα caused a clear reduction of the polymerization rate due to barbed end capping. Taken together, the results imply that homodimeric *Pb*CPα displays a characteristic actin capping activity.

For CapZ, the detected shift of actin during the co-sedimentation assay was stronger than for *Pb*CPα, and CapZ could not be detected in the pellet. The difference in the behavior of both proteins in the co-sedimentation assay is in accordance with the difference observed during the polymerization assays. First, *Pb*CPα is much less efficient in reducing the polymerization rate than CapZ. In addition, CapZ efficiently facilitated the formation of actin nuclei, which is presumably due to the ability to stabilize transient oligomers (Casella et al., 1986). Therefore, CapZ would promote the formation of many, but rather short polymers, instead of being associated with long filaments. In contrast to CapZ, *Pb*CPα did not show nucleation activity under the conditions tested here. It is conceivable that the nucleation activity is required for efficiently shifting the actin filament length distribution during co-polymerization. This hypothesis explains why *Pb*CPα was also found associated with long actin filaments. Hence, the lack of nucleation activity, together with the less efficient capping

activity, are probably the reasons for the differences observed for the co-sedimentation assay results of *Pb*CPα compared to CapZ.

The nucleation activity of CapZ might also explain the strange results of the seeded polymerization experiment. Capping the barbed ends reduces the polymerization rate. This accounts for the preformed actin seeds as well as for newly formed filaments. On the other hand, as the CapZ concentration rises, transient actin oligomers are being stabilized, which promotes filament formation and increases the rate, as seen in the nucleation assay. These two counteracting processes might be the reason for the discontinuous trend of actin polymerization when the CapZ concentration rises. This is further supported by the observation that *Pb*CPα, which did not promote nucleation, shows a continuous reduction of F-actin elongation in a concentration-dependent manner.

For the capping activity of CPs, the C terminal tails are important. Basic residues of the α subunit C terminus interact with acidic amino acids of the penultimate and last actin promoters. The C terminus of the β subunit then occupies a hydrophobic pocket on the terminal promoter. This binding model assigns a central role for the C terminus, and a deletion of the C terminus in CapZ leads to a 5000-fold decrease in capping activity (Cooper and Sept, 2008; Narita and Maeda, 2007; Narita et al., 2006). The lack of the last 20 amino acid residues in our *Pb*CPα construct may explain the need of higher concentrations for exhibiting capping activity by *Pb*CPα on heterologous actin.

6 Conclusions and future perspectives

The machinery involved in cell locomotion is powered by actin, which forms long polymers for generation of force required for movement. Despite the wealth of knowledge available on actin and actin related processes, they remain still to be characterized in the divergent malarial parasite. The parasite actin dynamics is unique in involving a very small set of regulatory proteins, only short transient filaments, and actin with low sequence identity compared to all other actins. The work in this thesis was aimed to characterize the effect of parasites ADFs and capping proteins, two most important actin regulators, on actin filament dynamics.

Plasmodium expresses two ADFs with divergent expression profiles; ADF1 is the all-time ADF in *Plasmodium* while ADF2 is expressed only in the sexual stages. This work focusses on the divergent roles of the ADFs on actin filament dynamics, which would help us to understand the need of two ADFs in the parasite and regulation of ADFs by membrane PIs.

To address this question, various biophysical techniques were employed, and our results show that ADF2 acts primarily as a monomer sequestering protein and can bind and sever actin filaments. Though both the ADFs bind to G-actin, with comparable affinities, yet the actin-ADF1 complex is transient in nature, indicating a high dissociation rate. The results show that ADF1 does bind to F-actin and severs filaments in absence of the F-loop. Furthermore, ADF1 interacts with PIs specifically and *via* the actin binding site. Additionally, our results here give preliminary evidence that the binding might involve transition of the loop following the α-helix1 to helical structure. In the future, to understand the ADF1 and F-actin interaction, exact mapping of the additional parasite specific F-actin binding and severing sites would be necessary. Also studies aimed to understand the interplay between actin and membrane bound ADFs would give an additional insight into the process of actin filament dynamics.

We show here that *Plasmodium* CPα forms homodimers, which are able to cap actin filaments. This result suggests that in the parasite the two subunits of CPs might have independent functions, and notably in line to our results it was shown previously that CPβ functional mutant in mosquito vector lack efficiency to invade, while CPα was found essential in the erythrocyte stages. Though the results show that CPα forms dimers *in vitro,*

future studies directed to understand if CPα could exist as mixture of monomer and dimer or as heterodimer at specific stages during parasite life cycle *in vivo* need to be addressed.

7 Appendix

Risk and safety statements

Following is the list of potentially hazardous materials and their respective hazard and precautionary statements as introduced by the Globally Harmonized System of Classification and labeling of chemicals (GHS).

Compound	Chemical Abstracts Service No.	Hazard Statement	GHS hazard	Precautionary Statements
Ampicillin	69-52-3	H334, H317	GHS08	P280,P261,P302+P352,P342+P311
β-mercaptoethanol	60-24-2	H301, H310, H330, H315, H318, H410	GHS05,06,09	P280,P273,P302+P352,P304+350+ 351+P338+P310
$CaCl_2$	10043-52-4	H319	GHS07	P280,P305+351+P338
Chloramphenicol	56-75-7	H350, H361	GHS08	P281, P308+P313,P501
Citric acid	5949-29-1	H319	GHS07	P305+P351+P338
DTT	3483-12-3	H302, H315, H319, H335	GHS07	P280,P301+P312,P302+352,P403+ P233
EDTA	60-00-4	H319	GHS07	P264,P280,P305+P351+P338
Ethanol	64-17-5	H225	GHS02	P210

Ethidium Bromide	1239-45-8	H302, H330, H341	GHS06,08	P260,P281,P284,P310
Hydrochloric acid	7647-01-0	H314, H335	GHS05,07	P261,P280,P310,P305+P351+P338
Imidazole	288-32-4	H310, H314, H361	GHS05,06,08	P260,P281,P303+P361+P353,P301 +P330+P331,P305+351+P338,P30 8+P313
Isopropanol	67-63-0	H225, H319, H336	GHS02,07	P210,P233,P305+P351+P338
Kanamycin	25389-94-0	H360	GHS08	P281,P260,P308+P313
NaOH	1310-73-2	H290, H314	GHS05	P280,P303+P361+P353,P301+P33 0+P331,0P305+P331+P358,P301+ P406
NiSO$_4$	10101-97-0	H302, 332,H 315,H 334,H 317,H 341,H 350,H 360,H 372,H 410	GHS07,08,09	P280,P201,P302+352,P308+P313, P342+P311
SDS	151-21-3	H228, H302, H311, H315, H319,	GHS02,06	P210,P261,P280,P312,P305+P351 +P338

		H335		
TCEP	51805-45-9	H314		P280,P305+P351+P338,P310
Tris	1185-53-1	H315, H319, H335	GHS07	P261,P305+P351+P338

GHS hazard statement

H225	Highly flammable liquid and vapour
H228	Flammable solid
H290	Corrosive to metals
H301	Toxic if swallowed
H302	Harmful if swallowed
H310	Fatal in contact with skin
H311	Toxic in contact with skin
H314	Causes skin burn and eye damage
H315	Causes skin irritation
H317	May cause allergic skin reaction
H318	Causes eye damage
H319	Causes eye irritation
H330	Fatal if inhaled
H332	Harmful if inhaled
H334	May cause breathing difficulty
H335	May cause respiratory irritation
H336	May cause dizziness
H341	May cause genetic disease
H350	May cause cancer
H360	May damage fertility or the unborn child
H361	Suspecting of damaging fertility or the unborn child
H372	Causes damage through prolonged repeated exposure
H410	Toxic effect to aquatic life

GHS precautionary statement

P201	Obtain special instruction before use
P210	Keep away from heat/spark/open flames/hot surfaces – No smoking
P233	Keep container tightly closed
P260	Do not breath dust/fume/gas/mist/vapor/spray
P261	Avoid breathing dust/fume/gas/mist/vapor/spray
P264	Wash… thoroughly after handling
P273	Avoid release to environment
P280	Wear protective gloves/protective clothing/eye protection/face protection
P281	Use personal protective equipment as requirement
P284	Wear respiratory protection
P310	Immediately call a POISON CENTRE
P312	Call a POISON CENTRE or doctor if unwell
P406	Store in a corrosive resistant/… container with a resistant inner lining
P501	Dispose of contents/container too
P301+P312	If swallowed call a POISON CENTRE or doctor
P302+P352	If on skin wash with soap and water
P304+P340	If inhaled: keep the victim in fresh and comfortable position for breathing
P304+P341	If breathing is difficult remove the victim in fresh and comfortable position for breathing
P308+P313	If exposed or concerned: get medical attention
P342+P311	If experiencing respiratory symptom- call POISON Centre or doctor
P403+P233	Store in a well-ventilated place-Keep the container tightly closed
P301+P330+P331	If swallowed – rinse mouth
P303+P361+P353	If on skin- remove clothing and wash immediately
P305+P351+338	If in eyes- rinse with water cautiously several time

GHS and hazard symbols

Oxidizing   **Flammable**   **Very toxic**   **Harmful**   **Corrosive**   **Explosive**

Hazard symbols for formulations and respective risk labels (according to Health and Safety Executive UK, http://www.hse.gov.uk)

GHS02   GHS03   GHS05   GHS06   GHS07   GHS08   GHS09

GHS pictograms (Source: United Nations Economic Commission for Europe).

8 References

Abe, H., T. Endo, K. Yamamoto, and T. Obinata. 1990. Sequence of cDNAs encoding actin depolymerizing factor and cofilin of embryonic chicken skeletal muscle: two functionally distinct actin-regulatory proteins exhibit high structural homology. *Biochemistry*. 29:7420-7425.

Allen, M.L., J.M. Dobrowolski, H. Muller, L.D. Sibley, and T.E. Mansour. 1997. Cloning and characterization of actin depolymerizing factor from Toxoplasma gondii. *Mol Biochem Parasitol*. 88:43-52.

Altschul, S.F., W. Gish, W. Miller, E.W. Myers, and D.J. Lipman. 1990. Basic local alignment search tool. *J Mol Biol*. 215:403-410.

Andenmatten, N., S. Egarter, A.J. Jackson, N. Jullien, J.P. Herman, and M. Meissner. 2013. Conditional genome engineering in Toxoplasma gondii uncovers alternative invasion mechanisms. *Nat Methods*. 10:125-127.

Anderson, R.A., and V.T. Marchesi. 1985. Regulation of the association of membrane skeletal protein 4.1 with glycophorin by a polyphosphoinositide. *Nature*. 318:295-298.

Andrianantoandro, E., and T.D. Pollard. 2006. Mechanism of actin filament turnover by severing and nucleation at different concentrations of ADF/cofilin. *Mol Cell*. 24:13-23.

Arnold, M., P. Ringler, and A. Brisson. 1995. A quantitative electrophoretic migration shift assay for analyzing the specific binding of proteins to lipid ligands in vesicles or micelles. *Biochim Biophys Acta*. 1233:198-204.

Artimo, P., M. Jonnalagedda, K. Arnold, D. Baratin, G. Csardi, E. de Castro, S. Duvaud, V. Flegel, A. Fortier, E. Gasteiger, A. Grosdidier, C. Hernandez, V. Ioannidis, D. Kuznetsov, R. Liechti, S. Moretti, K. Mostaguir, N. Redaschi, G. Rossier, I. Xenarios, and H. Stockinger. 2012. ExPASy: SIB bioinformatics resource portal. *Nucleic Acids Res*. 40:W597-603.

Bamburg, J.R., and B.W. Bernstein. 2008. ADF/cofilin. *Curr Biol*. 18:R273-275.

Bamburg, J.R., H.E. Harris, and A.G. Weeds. 1980. Partial purification and characterization of an actin depolymerizing factor from brain. *FEBS Lett*. 121:178-182.

Barron-Casella, E.A., M.A. Torres, S.W. Scherer, H.H. Heng, L.C. Tsui, and J.F. Casella. 1995. Sequence analysis and chromosomal localization of human Cap Z. Conserved residues within the actin-binding domain may link Cap Z to gelsolin/severin and profilin protein families. *J Biol Chem*. 270:21472-21479.

Baum, J., T.W. Gilberger, F. Frischknecht, and M. Meissner. 2008a. Host-cell invasion by malaria parasites: insights from Plasmodium and Toxoplasma. *Trends Parasitol*. 24:557-563.

Baum, J., A.T. Papenfuss, B. Baum, T.P. Speed, and A.F. Cowman. 2006. Regulation of apicomplexan actin-based motility. *Nat Rev Microbiol*. 4:621-628.

Baum, J., C.J. Tonkin, A.S. Paul, M. Rug, B.J. Smith, S.B. Gould, D. Richard, T.D. Pollard, and A.F. Cowman. 2008b. A malaria parasite formin regulates actin polymerization and localizes to the parasite-erythrocyte moving junction during invasion. *Cell Host Microbe*. 3:188-198.

Belmont, L.D., A. Orlova, D.G. Drubin, and E.H. Egelman. 1999. A change in actin conformation associated with filament instability after Pi release. *Proc Natl Acad Sci U S A*. 96:29-34.

BERTANI, G. 1951. Studies on lysogenesis. I. The mode of phage liberation by lysogenic Escherichia coli. *J Bacteriol*. 62:293-300.

Black, M.W., and J.C. Boothroyd. 2000. Lytic cycle of Toxoplasma gondii. *Microbiol Mol Biol Rev*. 64:607-623.

Blanchoin, L., and T.D. Pollard. 2002. Hydrolysis of ATP by polymerized actin depends on the bound divalent cation but not profilin. *Biochemistry*. 41:597-602.

Bobkov, A.A., A. Muhlrad, D.A. Pavlov, K. Kokabi, A. Yilmaz, and E. Reisler. 2006. Cooperative effects of cofilin (ADF) on actin structure suggest allosteric mechanism of cofilin function. *J Mol Biol*. 356:325-334.

Bork, P., C. Sander, and A. Valencia. 1992. An ATPase domain common to prokaryotic cell cycle proteins, sugar kinases, actin, and hsp70 heat shock proteins. *Proc Natl Acad Sci U S A*. 89:7290-7294.

Bowman, G.D., I.M. Nodelman, Y. Hong, N.H. Chua, U. Lindberg, and C.E. Schutt. 2000. A comparative structural analysis of the ADF/cofilin family. *Proteins*. 41:374-384.

Burridge, K., and J.R. Feramisco. 1981. Non-muscle alpha actinins are calcium-sensitive actin-binding proteins. *Nature*. 294:565-567.

Cai, L., T.W. Marshall, A.C. Uetrecht, D.A. Schafer, and J.E. Bear. 2007. Coronin 1B coordinates Arp2/3 complex and cofilin activities at the leading edge. *Cell*. 128:915-929.

Caldwell, J.E., S.G. Heiss, V. Mermall, and J.A. Cooper. 1989. Effects of CapZ, an actin capping protein of muscle, on the polymerization of actin. *Biochemistry*. 28:8506-8514.

Carlier, M.F., V. Laurent, J. Santolini, R. Melki, D. Didry, G.X. Xia, Y. Hong, N.H. Chua, and D. Pantaloni. 1997. Actin depolymerizing factor (ADF/cofilin) enhances the rate of filament turnover: implication in actin-based motility. *J Cell Biol*. 136:1307-1322.

Carlomagno, T. 2005. Ligand-target interactions: what can we learn from NMR? *Annu Rev Biophys Biomol Struct*. 34:245-266.

Carruthers, V.B., O.K. Giddings, and L.D. Sibley. 1999. Secretion of micronemal proteins is associated with toxoplasma invasion of host cells. *Cell Microbiol*. 1:225-235.

Carruthers, V.B., and L.D. Sibley. 1997. Sequential protein secretion from three distinct organelles of Toxoplasma gondii accompanies invasion of human fibroblasts. *Eur J Cell Biol*. 73:114-123.

Casella, J.F., D.J. Maack, and S. Lin. 1986. Purification and initial characterization of a protein from skeletal muscle that caps the barbed ends of actin filaments. *J Biol Chem*. 261:10915-10921.

Compton, L.A., and W.C. Johnson. 1986. Analysis of protein circular dichroism spectra for secondary structure using a simple matrix multiplication. *Anal Biochem*. 155:155-167.

Cooper, J.A., J.D. Blum, and T.D. Pollard. 1984. Acanthamoeba castellanii capping protein: properties, mechanism of action, immunologic cross-reactivity, and localization. *J Cell Biol*. 99:217-225.

Cooper, J.A., and T.D. Pollard. 1985. Effect of capping protein on the kinetics of actin polymerization. *Biochemistry*. 24:793-799.

Cooper, J.A., and D. Sept. 2008. New insights into mechanism and regulation of actin capping protein. *Int Rev Cell Mol Biol*. 267:183-206.

Cooper, J.A., S.B. Walker, and T.D. Pollard. 1983. Pyrene actin: documentation of the validity of a sensitive assay for actin polymerization. *J Muscle Res Cell Motil*. 4:253-262.

Cullen, P.J., G.E. Cozier, G. Banting, and H. Mellor. 2001. Modular phosphoinositide-binding domains--their role in signalling and membrane trafficking. *Curr Biol*. 11:R882-893.

Daher, W., F. Plattner, M.F. Carlier, and D. Soldati-Favre. 2010. Concerted action of two formins in gliding motility and host cell invasion by Toxoplasma gondii. *PLoS Pathog*. 6:e1001132.

Daher, W., and D. Soldati-Favre. 2009. Mechanisms controlling glideosome function in apicomplexans. *Curr Opin Microbiol*. 12:408-414.

Dancker, P., I. Low, W. Hasselbach, and T. Wieland. 1975. Interaction of actin with phalloidin: polymerization and stabilization of F-actin. *Biochim Biophys Acta*. 400:407-414.

Dobrowolski, J., and L.D. Sibley. 1997. The role of the cytoskeleton in host cell invasion by Toxoplasma gondii. *Behring Inst Mitt*:90-96.

Dobrowolski, J.M., V.B. Carruthers, and L.D. Sibley. 1997. Participation of myosin in gliding motility and host cell invasion by Toxoplasma gondii. *Mol Microbiol*. 26:163-173.

Dodatko, T., A.A. Fedorov, M. Grynberg, Y. Patskovsky, D.A. Rozwarski, L. Jaroszewski, E.

Aronoff-Spencer, E. Kondraskina, T. Irving, A. Godzik, and S.C. Almo. 2004. Crystal structure of the actin binding domain of the cyclase-associated protein. *Biochemistry*. 43:10628-10641.

Doi, Y., N. Shinzawa, S. Fukumoto, H. Okano, and H. Kanuka. 2010. ADF2 is required for transformation of the ookinete and sporozoite in malaria parasite development. *Biochem Biophys Res Commun*. 397:668-672.

Dominguez, R., and K.C. Holmes. 2011. Actin structure and function. *Annu Rev Biophys*. 40:169-186.

dos Remedios, C.G., D. Chhabra, M. Kekic, I.V. Dedova, M. Tsubakihara, D.A. Berry, and N.J. Nosworthy. 2003. Actin binding proteins: regulation of cytoskeletal microfilaments. *Physiol Rev*. 83:433-473.

Dubremetz, J.F., and G. Torpier. 1978. Freeze fracture study of the pellicle of an eimerian sporozoite (Protozoa, Coccidia). *J Ultrastruct Res*. 62:94-109.

Dutta, A., B.J. Rao, and K.V. Chary. 2003. Overexpression and purification of isotopically labeled Escherichia coli MutH for NMR studies. *Protein Expr Purif*. 29:252-258.

Fedorov, A.A., P. Lappalainen, E.V. Fedorov, D.G. Drubin, and S.C. Almo. 1997. Structure determination of yeast cofilin. *Nat Struct Biol*. 4:366-369.

Figueroa, J.V., E. Precigout, B. Carcy, and A. Gorenflot. 2004. Identification of a coronin-like protein in Babesia species. *Ann N Y Acad Sci*. 1026:125-138.

Foth, B.J., M.C. Goedecke, and D. Soldati. 2006. New insights into myosin evolution and classification. *Proc Natl Acad Sci U S A*. 103:3681-3686.

Foussard, F., Y. Gallois, G. Tronchin, R. Robert, and G. Mauras. 1990. Isolation of the pellicle of Toxoplasma gondii (Protozoa, Coccidia): characterization by electron microscopy and protein composition. *Parasitol Res*. 76:563-565.

Galkin, V.E., A. Orlova, D.S. Kudryashov, A. Solodukhin, E. Reisler, G.F. Schroder, and E.H. Egelman. 2011. Remodeling of actin filaments by ADF/cofilin proteins. *Proc Natl Acad Sci U S A*. 108:20568-20572.

Galkin, V.E., A. Orlova, G.F. Schroder, and E.H. Egelman. 2010. Structural polymorphism in F-actin. *Nat Struct Mol Biol*. 17:1318-1323.

Ganter, M., H. Schüler, and K. Matuschewski. 2009. Vital role for the Plasmodium actin capping protein (CP) beta-subunit in motility of malaria sporozoites. *Mol Microbiol*. 74:1356-1367.

Gardner, M.J., N. Hall, E. Fung, O. White, M. Berriman, R.W. Hyman, J.M. Carlton, A. Pain, K.E. Nelson, S. Bowman, I.T. Paulsen, K. James, J.A. Eisen, K. Rutherford, S.L. Salzberg, A. Craig, S. Kyes, M.S. Chan, V. Nene, S.J. Shallom, B. Suh, J. Peterson, S. Angiuoli, M.

Pertea, J. Allen, J. Selengut, D. Haft, M.W. Mather, A.B. Vaidya, D.M. Martin, A.H. Fairlamb, M.J. Fraunholz, D.S. Roos, S.A. Ralph, G.I. McFadden, L.M. Cummings, G.M. Subramanian, C. Mungall, J.C. Venter, D.J. Carucci, S.L. Hoffman, C. Newbold, R.W. Davis, C.M. Fraser, and B. Barrell. 2002. Genome sequence of the human malaria parasite Plasmodium falciparum. *Nature*. 419:498-511.

Ghosh, M., X. Song, G. Mouneimne, M. Sidani, D.S. Lawrence, and J.S. Condeelis. 2004. Cofilin promotes actin polymerization and defines the direction of cell motility. *Science*. 304:743-746.

Gill, S.C., and P.H. von Hippel. 1989. Calculation of protein extinction coefficients from amino acid sequence data. *Anal Biochem*. 182:319-326.

Goldenberg, S., and A.R. Avila. 2011. Aspects of Trypanosoma cruzi stage differentiation. *Adv Parasitol*. 75:285-305.

Gonzalez, V., A. Combe, V. David, N.A. Malmquist, V. Delorme, C. Leroy, S. Blazquez, R. Menard, and I. Tardieux. 2009. Host cell entry by apicomplexa parasites requires actin polymerization in the host cell. *Cell Host Microbe*. 5:259-272.

Goode, B.L., J.J. Wong, A.C. Butty, M. Peter, A.L. McCormack, J.R. Yates, D.G. Drubin, and G. Barnes. 1999. Coronin promotes the rapid assembly and cross-linking of actin filaments and may link the actin and microtubule cytoskeletons in yeast. *J Cell Biol*. 144:83-98.

Gorbatyuk, V.Y., N.J. Nosworthy, S.A. Robson, N.P. Bains, M.W. Maciejewski, C.G. Dos Remedios, and G.F. King. 2006. Mapping the phosphoinositide-binding site on chick cofilin explains how PIP2 regulates the cofilin-actin interaction. *Mol Cell*. 24:511-522.

Graceffa, P., and R. Dominguez. 2003. Crystal structure of monomeric actin in the ATP state. Structural basis of nucleotide-dependent actin dynamics. *J Biol Chem*. 278:34172-34180.

Hakansson, S., A.J. Charron, and L.D. Sibley. 2001. Toxoplasma evacuoles: a two-step process of secretion and fusion forms the parasitophorous vacuole. *Embo j*. 20:3132-3144.

Hart, M.C., Y.O. Korshunova, and J.A. Cooper. 1997. Vertebrates have conserved capping protein alpha isoforms with specific expression patterns. *Cell Motil Cytoskeleton*. 38:120-132.

Hatanaka, H., K. Ogura, K. Moriyama, S. Ichikawa, I. Yahara, and F. Inagaki. 1996. Tertiary structure of destrin and structural similarity between two actin-regulating protein families. *Cell*. 85:1047-1055.

Hayward, S., and H.J. Berendsen. 1998. Systematic analysis of domain motions in proteins from conformational change: new results on citrate synthase and T4 lysozyme. *Proteins*. 30:144-154.

Head, J.F., N. Swamy, and R. Ray. 2002. Crystal structure of the complex between actin and human vitamin D-binding protein at 2.5 A resolution. *Biochemistry*. 41:9015-9020.

Heaslip, A.T., J.M. Leung, K.L. Carey, F. Catti, D.M. Warshaw, N.J. Westwood, B.A. Ballif, and G.E. Ward. 2010. A small-molecule inhibitor of T. gondii motility induces the posttranslational modification of myosin light chain-1 and inhibits myosin motor activity. *PLoS Pathog*. 6:e1000720.

Hegge, S., S. Munter, M. Steinbuchel, K. Heiss, U. Engel, K. Matuschewski, and F. Frischknecht. 2010. Multistep adhesion of Plasmodium sporozoites. *FASEB J*. 24:2222-2234.

Hellman, M., V.O. Paavilainen, P. Naumanen, P. Lappalainen, A. Annila, and P. Permi. 2004. Solution structure of coactosin reveals structural homology to ADF/cofilin family proteins. *FEBS Lett*. 576:91-96.

Herman, I.M. 1993. Actin isoforms. *Curr Opin Cell Biol*. 5:48-55.

Hertzog, M., C. van Heijenoort, D. Didry, M. Gaudier, J. Coutant, B. Gigant, G. Didelot, T. Preat, M. Knossow, E. Guittet, and M.F. Carlier. 2004. The beta-thymosin/WH2 domain; structural basis for the switch from inhibition to promotion of actin assembly. *Cell*. 117:611-623.

Hliscs, M., J.M. Sattler, W. Tempel, J.D. Artz, A. Dong, R. Hui, K. Matuschewski, and H. Schüler. 2010. Structure and function of a G-actin sequestering protein with a vital role in malaria oocyst development inside the mosquito vector. *J Biol Chem*. 285:11572-11583.

Holmes, K.C., D. Popp, W. Gebhard, and W. Kabsch. 1990. Atomic model of the actin filament. *Nature*. 347:44-49.

Hu, K., J. Johnson, L. Florens, M. Fraunholz, S. Suravajjala, C. DiLullo, J. Yates, D.S. Roos, and J.M. Murray. 2006. Cytoskeletal components of an invasion machine--the apical complex of Toxoplasma gondii. *PLoS Pathog*. 2:e13.

Humphries, C.L., H.I. Balcer, J.L. D'Agostino, B. Winsor, D.G. Drubin, G. Barnes, B.J. Andrews, and B.L. Goode. 2002. Direct regulation of Arp2/3 complex activity and function by the actin binding protein coronin. *J Cell Biol*. 159:993-1004.

Huynh, M.H., and V.B. Carruthers. 2006. Toxoplasma MIC2 is a major determinant of invasion and virulence. *PLoS Pathog*. 2:e84.

Hyvonen, M., M.J. Macias, M. Nilges, H. Oschkinat, M. Saraste, and M. Wilmanns. 1995. Structure of the binding site for inositol phosphates in a PH domain. *EMBO J*. 14:4676-4685.

Ichetovkin, I., W. Grant, and J. Condeelis. 2002. Cofilin produces newly polymerized actin filaments that are preferred for dendritic nucleation by the Arp2/3 complex. *Curr Biol*. 12:79-84.

Ignatev, A., S.P. Bhargav, J. Vahokoski, P. Kursula, and I. Kursula. 2012. The lasso segment is required for functional dimerization of the Plasmodium formin 1 FH2 domain. *PLoS One*. 7:e33586.

Imai, K., S. Nonoyama, H. Miki, T. Morio, K. Fukami, Q. Zhu, A. Aruffo, H.D. Ochs, J. Yata, and T. Takenawa. 1999. The pleckstrin homology domain of the Wiskott-Aldrich syndrome protein is involved in the organization of actin cytoskeleton. *Clin Immunol*. 92:128-137.

Irobi, E., A.H. Aguda, M. Larsson, C. Guerin, H.L. Yin, L.D. Burtnick, L. Blanchoin, and R.C. Robinson. 2004. Structural basis of actin sequestration by thymosin-beta4: implications for WH2 proteins. *EMBO J*. 23:3599-3608.

Jameson, D.M., J.C. Croney, and P.D. Moens. 2003. Fluorescence: basic concepts, practical aspects, and some anecdotes. *Methods Enzymol*. 360:1-43.

Johnsson, B., S. Lofas, and G. Lindquist. 1991. Immobilization of proteins to a carboxymethyldextran-modified gold surface for biospecific interaction analysis in surface plasmon resonance sensors. *Anal Biochem*. 198:268-277.

Kabsch, W., H.G. Mannherz, and D. Suck. 1985. Three-dimensional structure of the complex of actin and DNase I at 4.5 A resolution. *Embo j*. 4:2113-2118.

Kabsch, W., H.G. Mannherz, D. Suck, E.F. Pai, and K.C. Holmes. 1990. Atomic structure of the actin:DNase I complex. *Nature*. 347:37-44.

Kappe, S., T. Bruderer, S. Gantt, H. Fujioka, V. Nussenzweig, and R. Menard. 1999. Conservation of a gliding motility and cell invasion machinery in Apicomplexan parasites. *J Cell Biol*. 147:937-944.

Keeley, A., and D. Soldati. 2004. The glideosome: a molecular machine powering motility and host-cell invasion by Apicomplexa. *Trends Cell Biol*. 14:528-532.

Kelly, S.M., T.J. Jess, and N.C. Price. 2005. How to study proteins by circular dichroism. *Biochim Biophys Acta*. 1751:119-139.

Kelly, S.M., and N.C. Price. 2000. The use of circular dichroism in the investigation of protein structure and function. *Curr Protein Pept Sci*. 1:349-384.

Khaitlina, S.Y., and H. Strzelecka-Golaszewska. 2002. Role of the DNase-I-binding loop in dynamic properties of actin filament. *Biophys J*. 82:321-334.

Kim, K., A. Yamashita, M.A. Wear, Y. Maeda, and J.A. Cooper. 2004. Capping protein binding to actin in yeast: biochemical mechanism and physiological relevance. *J Cell Biol*. 164:567-580.

Kim, T., J.A. Cooper, and D. Sept. 2010. The interaction of capping protein with the barbed end of the actin filament. *J Mol Biol*. 404:794-802.

Klejnot, M., M. Gabrielsen, J. Cameron, A. Mleczak, S.K. Talapatra, F. Kozielski, A. Pannifer, and M.F. Olson. 2013. Analysis of the human cofilin 1 structure reveals conformational changes required for actin binding. *Acta Crystallogr D Biol Crystallogr*. 69:1780-1788.

Kono, M., D. Prusty, J. Parkinson, and T.W. Gilberger. 2013. The apicomplexan inner membrane complex. *Front Biosci (Landmark Ed)*. 18:982-992.

Kovar, D.R., E.S. Harris, R. Mahaffy, H.N. Higgs, and T.D. Pollard. 2006. Control of the assembly of ATP- and ADP-actin by formins and profilin. *Cell*. 124:423-435.

Kursula, I., P. Kursula, M. Ganter, S. Panjikar, K. Matuschewski, and H. Schüler. 2008. Structural basis for parasite-specific functions of the divergent profilin of Plasmodium falciparum. *Structure*. 16:1638-1648.

Kusano, K., H. Abe, and T. Obinata. 1999. Detection of a sequence involved in actin-binding and phosphoinositide-binding in the N-terminal side of cofilin. *Mol Cell Biochem*. 190:133-141.

Lappalainen, P., E.V. Fedorov, A.A. Fedorov, S.C. Almo, and D.G. Drubin. 1997. Essential functions and actin-binding surfaces of yeast cofilin revealed by systematic mutagenesis. *EMBO J*. 16:5520-5530.

Lappalainen, P., M.M. Kessels, M.J. Cope, and D.G. Drubin. 1998. The ADF homology (ADF-H) domain: a highly exploited actin-binding module. *Mol Biol Cell*. 9:1951-1959.

Leonard, S.A., A.G. Gittis, E.C. Petrella, T.D. Pollard, and E.E. Lattman. 1997. Crystal structure of the actin-binding protein actophorin from Acanthamoeba. *Nat Struct Biol*. 4:369-373.

Lin, K.M., E. Wenegieme, P.J. Lu, C.S. Chen, and H.L. Yin. 1997. Gelsolin binding to phosphatidylinositol 4,5-bisphosphate is modulated by calcium and pH. *J Biol Chem*. 272:20443-20450.

Lobley, A., L. Whitmore, and B.A. Wallace. 2002. DICHROWEB: an interactive website for the analysis of protein secondary structure from circular dichroism spectra. *Bioinformatics*. 18:211-212.

Maekawa, S., E. Nishida, Y. Ohta, and H. Sakai. 1984. Isolation of low molecular weight actin-binding proteins from porcine brain. *J Biochem*. 95:377-385.

Magis, C., J.F. Taly, G. Bussotti, J.M. Chang, P. Di Tommaso, I. Erb, J. Espinosa-Carrasco, and C. Notredame. 2014. T-Coffee: Tree-based consistency objective function for alignment evaluation. *Methods Mol Biol*. 1079:117-129.

Marchesi, V.T., and E. Steers, Jr. 1968. Selective solubilization of a protein component of the red cell membrane. *Science*. 159:203-204.

Mattila, P.K., O. Quintero-Monzon, J. Kugler, J.B. Moseley, S.C. Almo, P. Lappalainen, and B.L.

Goode. 2004. A high-affinity interaction with ADP-actin monomers underlies the mechanism and in vivo function of Srv2/cyclase-associated protein. *Mol Biol Cell*. 15:5158-5171.

Matuschewski, K., J. Ross, S.M. Brown, K. Kaiser, V. Nussenzweig, and S.H. Kappe. 2002. Infectivity-associated changes in the transcriptional repertoire of the malaria parasite sporozoite stage. *J Biol Chem*. 277:41948-41953.

McLaughlin, S., J. Wang, A. Gambhir, and D. Murray. 2002. PIP(2) and proteins: interactions, organization, and information flow. *Annu Rev Biophys Biomol Struct*. 31:151-175.

Mehta, S., and L.D. Sibley. 2011. Actin depolymerizing factor controls actin turnover and gliding motility in Toxoplasma gondii. *Mol Biol Cell*. 22:1290-1299.

Meissner, M., D.J. Ferguson, and F. Frischknecht. 2013. Invasion factors of apicomplexan parasites: essential or redundant? *Curr Opin Microbiol*. 16:438-444.

Meszoely, C.A., E.F. Erbe, R.L. Steere, N.D. Pacheco, and R.L. Beaudoin. 1982. Plasmodium berghei: architectural analysis by freeze-fracturing of the intraoocyst sporozoite's pellicular system. *Exp Parasitol*. 53:229-241.

Misra, S., G.J. Miller, and J.H. Hurley. 2001. Recognizing phosphatidylinositol 3-phosphate. *Cell*. 107:559-562.

Mital, J., and G.E. Ward. 2008. Current and emerging approaches to studying invasion in apicomplexan parasites. *Subcell Biochem*. 47:1-32.

Moraczewska, J., H. Strzelecka-Golaszewska, P.D. Moens, and C.G. dos Remedios. 1996. Structural changes in subdomain 2 of G-actin observed by fluorescence spectroscopy. *Biochem J*. 317 (Pt 2):605-611.

Moraczewska, J., B. Wawro, K. Seguro, and H. Strzelecka-Golaszewska. 1999. Divalent cation-, nucleotide-, and polymerization-dependent changes in the conformation of subdomain 2 of actin. *Biophys J*. 77:373-385.

Moriyama, K., E. Nishida, N. Yonezawa, H. Sakai, S. Matsumoto, K. Iida, and I. Yahara. 1990. Destrin, a mammalian actin-depolymerizing protein, is closely related to cofilin. Cloning and expression of porcine brain destrin cDNA. *J Biol Chem*. 265:5768-5773.

Morrissette, N.S., and L.D. Sibley. 2002. Cytoskeleton of apicomplexan parasites. *Microbiol Mol Biol Rev*. 66:21-38; table of contents.

Muller, J., Y. Oma, L. Vallar, E. Friederich, O. Poch, and B. Winsor. 2005. Sequence and comparative genomic analysis of actin-related proteins. *Mol Biol Cell*. 16:5736-5748.

Murakami, K., T. Yasunaga, T.Q. Noguchi, Y. Gomibuchi, K.X. Ngo, T.Q. Uyeda, and T. Wakabayashi. 2010. Structural basis for actin assembly, activation of ATP hydrolysis, and delayed phosphate release. *Cell*. 143:275-287.

Narita, A., and Y. Maeda. 2007. Molecular determination by electron microscopy of the actin filament end structure. *J Mol Biol*. 365:480-501.

Narita, A., S. Takeda, A. Yamashita, and Y. Maeda. 2006. Structural basis of actin filament capping at the barbed-end: a cryo-electron microscopy study. *EMBO J*. 25:5626-5633.

Nichols, B.A., and M.L. Chiappino. 1987. Cytoskeleton of Toxoplasma gondii. *J Protozool*. 34:217-226.

Nishida, E. 1985. Opposite effects of cofilin and profilin from porcine brain on rate of exchange of actin-bound adenosine 5'-triphosphate. *Biochemistry*. 24:1160-1164.

Oda, T., M. Iwasa, T. Aihara, Y. Maeda, and A. Narita. 2009. The nature of the globular- to fibrous-actin transition. *Nature*. 457:441-445.

Oda, T., and Y. Maeda. 2010. Multiple Conformations of F-actin. *Structure*. 18:761-767.

Ojala, P.J., V. Paavilainen, and P. Lappalainen. 2001. Identification of yeast cofilin residues specific for actin monomer and PIP2 binding. *Biochemistry*. 40:15562-15569.

Ono, S., A. McGough, B.J. Pope, V.T. Tolbert, A. Bui, J. Pohl, G.M. Benian, K.M. Gernert, and A.G. Weeds. 2001. The C-terminal tail of UNC-60B (actin depolymerizing factor/cofilin) is critical for maintaining its stable association with F-actin and is implicated in the second actin-binding site. *J Biol Chem*. 276:5952-5958.

Opitz, C., and D. Soldati. 2002. 'The glideosome': a dynamic complex powering gliding motion and host cell invasion by Toxoplasma gondii. *Mol Microbiol*. 45:597-604.

Orlova, A., A. Shvetsov, V.E. Galkin, D.S. Kudryashov, P.A. Rubenstein, E.H. Egelman, and E. Reisler. 2004. Actin-destabilizing factors disrupt filaments by means of a time reversal of polymerization. *Proc Natl Acad Sci U S A*. 101:17664-17668.

Otterbein, L.R., C. Cosio, P. Graceffa, and R. Dominguez. 2002. Crystal structures of the vitamin D-binding protein and its complex with actin: structural basis of the actin-scavenger system. *Proc Natl Acad Sci U S A*. 99:8003-8008.

Otterbein, L.R., P. Graceffa, and R. Dominguez. 2001. The crystal structure of uncomplexed actin in the ADP state. *Science*. 293:708-711.

Paavilainen, V.O., E. Bertling, S. Falck, and P. Lappalainen. 2004. Regulation of cytoskeletal dynamics by actin-monomer-binding proteins. *Trends Cell Biol*. 14:386-394.

Paavilainen, V.O., E. Oksanen, A. Goldman, and P. Lappalainen. 2008. Structure of the actin-depolymerizing factor homology domain in complex with actin. *J Cell Biol*. 182:51-59.

Pavlov, D., A. Muhlrad, J. Cooper, M. Wear, and E. Reisler. 2007. Actin filament severing by cofilin. *J Mol Biol*. 365:1350-1358.

Perelroizen, I., M.F. Carlier, and D. Pantaloni. 1995. Binding of divalent cation and nucleotide to G-actin in the presence of profilin. *J Biol Chem*. 270:1501-1508.

Petoukhov, M.V., and D.I. Svergun. 2013. Applications of small-angle X-ray scattering to biomacromolecular solutions. *Int J Biochem Cell Biol*. 45:429-437.

Pfannstiel, J., M. Cyrklaff, A. Habermann, S. Stoeva, G. Griffiths, R. Shoeman, and H. Faulstich. 2001. Human cofilin forms oligomers exhibiting actin bundling activity. *J Biol Chem*. 276:49476-49484.

Pollard, T.D. 1986. Rate constants for the reactions of ATP- and ADP-actin with the ends of actin filaments. *J Cell Biol*. 103:2747-2754.

Pollard, T.D., L. Blanchoin, and R.D. Mullins. 2001. Actin dynamics. *J Cell Sci*. 114:3-4.

Pollard, T.D., and J.A. Cooper. 2009. Actin, a central player in cell shape and movement. *Science*. 326:1208-1212.

Pope, B.J., K.M. Zierler-Gould, R. Kuhne, A.G. Weeds, and L.J. Ball. 2004. Solution structure of human cofilin: actin binding, pH sensitivity, and relationship to actin-depolymerizing factor. *J Biol Chem*. 279:4840-4848.

Prakash, O., H.K. Chellani, A. Wadhwa, M. Mohan, and N.K. Anand. 1990. Autoimmune thrombocytopenia in newborn. *Indian Pediatr*. 27:397-400.

Raghunathan, V., P. Mowery, M. Rozycki, U. Lindberg, and C. Schutt. 1992. Structural changes in profilin accompany its binding to phosphatidylinositol, 4,5-bisphosphate. *FEBS Lett*. 297:46-50.

Razinia, Z., T. Makela, J. Ylanne, and D.A. Calderwood. 2012. Filamins in mechanosensing and signaling. *Annu Rev Biophys*. 41:227-246.

Rohatgi, R., P. Nollau, H.Y. Ho, M.W. Kirschner, and B.J. Mayer. 2001. Nck and phosphatidylinositol 4,5-bisphosphate synergistically activate actin polymerization through the N-WASP-Arp2/3 pathway. *J Biol Chem*. 276:26448-26452.

Russell, D.G., and R.G. Burns. 1984. The polar ring of coccidian sporozoites: a unique microtubule-organizing centre. *J Cell Sci*. 65:193-207.

Ryning, F.W., and J.S. Remington. 1978. Effect of cytochalasin D on Toxoplasma gondii cell entry. *Infect Immun*. 20:739-743.

Sahoo, N., W. Beatty, J. Heuser, D. Sept, and L.D. Sibley. 2006. Unusual kinetic and structural properties control rapid assembly and turnover of actin in the parasite Toxoplasma gondii. *Mol Biol Cell*. 17:895-906.

Salamun, J., J.P. Kallio, W. Daher, D. Soldati-Favre, and I. Kursula. 2014. Structure of Toxoplasma gondii coronin, an actin-binding protein that relocalizes to the posterior pole of invasive parasites and contributes to invasion and egress. *FASEB J*. 28:4729-4747.

Schmitz, S., M. Grainger, S. Howell, L.J. Calder, M. Gaeb, J.C. Pinder, A.A. Holder, and C. Veigel. 2005. Malaria parasite actin filaments are very short. *Journal of molecular biology*. 349:113-125.

Schmitz, S., I.A. Schaap, J. Kleinjung, S. Harder, M. Grainger, L. Calder, P.B. Rosenthal, A.A. Holder, and C. Veigel. 2010. Malaria parasite actin polymerization and filament structure. *J Biol Chem*. 285:36577-36585.

Scholtyseck, E., and H. Mehlhorn. 1970. Ultrastructural study of characteristic organelles (paired organelles, micronemes, micropores) of sporozoa and related organisms. *Z Parasitenkd*. 34:97-127.

Schüler, H., and K. Matuschewski. 2006. Regulation of apicomplexan microfilament dynamics by a minimal set of actin-binding proteins. *Traffic*. 7:1433-1439.

Schüler, H., A.K. Mueller, and K. Matuschewski. 2005a. A Plasmodium actin-depolymerizing factor that binds exclusively to actin monomers. *Mol Biol Cell*. 16:4013-4023.

Schüler, H., A.K. Mueller, and K. Matuschewski. 2005b. Unusual properties of Plasmodium falciparum actin: new insights into microfilament dynamics of apicomplexan parasites. *FEBS letters*. 579:655-660.

Schutt, C.E., J.C. Myslik, M.D. Rozycki, N.C. Goonesekere, and U. Lindberg. 1993. The structure of crystalline profilin-beta-actin. *Nature*. 365:810-816.

Seidel, S.A., P.M. Dijkman, W.A. Lea, G. van den Bogaart, M. Jerabek-Willemsen, A. Lazic, J.S. Joseph, P. Srinivasan, P. Baaske, A. Simeonov, I. Katritch, F.A. Melo, J.E. Ladbury, G. Schreiber, A. Watts, D. Braun, and S. Duhr. 2013. Microscale thermophoresis quantifies biomolecular interactions under previously challenging conditions. *Methods*. 59:301-315.

Sibley, L.D. 2010. How apicomplexan parasites move in and out of cells. *Curr Opin Biotechnol*. 21:592-598.

Sibley, L.D. 2011. Invasion and intracellular survival by protozoan parasites. *Immunol Rev*. 240:72-91.

Singh, B.K., J.M. Sattler, M. Chatterjee, J. Huttu, H. Schüler, and I. Kursula. 2011. Crystal

structures explain functional differences in the two actin depolymerization factors of the malaria parasite. *J Biol Chem*. 286:28256-28264.

Skillman, K.M., K. Diraviyam, A. Khan, K. Tang, D. Sept, and L.D. Sibley. 2011. Evolutionarily divergent, unstable filamentous actin is essential for gliding motility in apicomplexan parasites. *PLoS pathogens*. 7:e1002280.

Skou, S., R.E. Gillilan, and N. Ando. 2014. Synchrotron-based small-angle X-ray scattering of proteins in solution. *Nat Protoc*. 9:1727-1739.

Sreerama, N., and R.W. Woody. 1994. Protein secondary structure from circular dichroism spectroscopy. Combining variable selection principle and cluster analysis with neural network, ridge regression and self-consistent methods. *J Mol Biol*. 242:497-507.

Steimle, P.A., J.D. Hoffert, N.B. Adey, and S.W. Craig. 1999. Polyphosphoinositides inhibit the interaction of vinculin with actin filaments. *J Biol Chem*. 274:18414-18420.

Studier, F.W. 2014. Stable expression clones and auto-induction for protein production in E. coli. *Methods Mol Biol*. 1091:17-32.

Sultan, A.A., V. Thathy, U. Frevert, K.J. Robson, A. Crisanti, V. Nussenzweig, R.S. Nussenzweig, and R. Menard. 1997. TRAP is necessary for gliding motility and infectivity of plasmodium sporozoites. *Cell*. 90:511-522.

Svergun, D.I. 1999. Restoring low resolution structure of biological macromolecules from solution scattering using simulated annealing. *Biophys J*. 76:2879-2886.

Tardieux, I., X. Liu, O. Poupel, D. Parzy, P. Dehoux, and G. Langsley. 1998. A Plasmodium falciparum novel gene encoding a coronin-like protein which associates with actin filaments. *FEBS Lett*. 441:251-256.

Tobacman, L.S., and E.D. Korn. 1983. The kinetics of actin nucleation and polymerization. *J Biol Chem*. 258:3207-3214.

Trukhanov, V.A. 1991. [The first experiments which related DNA to genetics]. *Tsitol Genet*. 25:68-72.

Vahokoski, J., S.P. Bhargav, A. Desfosses, M. Andreadaki, E.P. Kumpula, S.M. Martinez, A. Ignatev, S. Lepper, F. Frischknecht, I. Siden-Kiamos, C. Sachse, and I. Kursula. 2014. Structural differences explain diverse functions of Plasmodium actins. *PLoS Pathog*. 10:e1004091.

Vitagliano, L., A. Ruggiero, M. Masullo, P. Cantiello, P. Arcari, and A. Zagari. 2004. The crystal structure of Sulfolobus solfataricus elongation factor 1alpha in complex with magnesium and GDP. *Biochemistry*. 43:6630-6636.

Vivier, E., and A. Petitprez. 1969. [The outer membrane complex and its development at the time of the formation of daughter cells in Toxoplasma gondii]. *J Cell Biol*. 43:329-342.

Volkmann, N., D. DeRosier, P. Matsudaira, and D. Hanein. 2001. An atomic model of actin filaments cross-linked by fimbrin and its implications for bundle assembly and function. *J Cell Biol*. 153:947-956.

Walsh, G. 2009. The global food crisis: an Australian dairy industry perspective. *Asia Pac J Clin Nutr*. 18:664-668.

Wang, H., R.C. Robinson, and L.D. Burtnick. 2010. The structure of native G-actin. *Cytoskeleton (Hoboken)*. 67:456-465.

Wear, M.A., and J.A. Cooper. 2004. Capping protein: new insights into mechanism and regulation. *Trends Biochem Sci*. 29:418-428.

Wear, M.A., A. Yamashita, K. Kim, Y. Maeda, and J.A. Cooper. 2003. How capping protein binds the barbed end of the actin filament. *Curr Biol*. 13:1531-1537.

Wesseling, J.G., M.A. Smits, and J.G. Schoenmakers. 1988. Extremely diverged actin proteins in Plasmodium falciparum. *Molecular and biochemical parasitology*. 30:143-153.

Wesseling, J.G., P.J. Snijders, P. van Someren, J. Jansen, M.A. Smits, and J.G. Schoenmakers. 1989. Stage-specific expression and genomic organization of the actin genes of the malaria parasite Plasmodium falciparum. *Mol Biochem Parasitol*. 35:167-176.

Wetzel, D.M., S. Hakansson, K. Hu, D. Roos, and L.D. Sibley. 2003. Actin filament polymerization regulates gliding motility by apicomplexan parasites. *Mol Biol Cell*. 14:396-406.

Winder, S.J., and K.R. Ayscough. 2005. Actin-binding proteins. *J Cell Sci*. 118:651-654.

Wirth, V.F., F. List, G. Diez, and W.H. Goldmann. 2010. Vinculin's C-terminal region facilitates phospholipid membrane insertion. *Biochem Biophys Res Commun*. 398:433-437.

Wong, W., C.T. Skau, D.S. Marapana, E. Hanssen, N.L. Taylor, D.T. Riglar, E.S. Zuccala, F. Angrisano, H. Lewis, B. Catimel, O.B. Clarke, N.J. Kershaw, M.A. Perugini, D.R. Kovar, J.M. Gulbis, and J. Baum. 2011. Minimal requirements for actin filament disassembly revealed by structural analysis of malaria parasite actin-depolymerizing factor 1. *Proc Natl Acad Sci U S A*. 108:9869-9874.

Xu, J., J.F. Casella, and T.D. Pollard. 1999. Effect of capping protein, CapZ, on the length of actin filaments and mechanical properties of actin filament networks. *Cell Motil Cytoskeleton*. 42:73-81.

Xu, Y., J.B. Moseley, I. Sagot, F. Poy, D. Pellman, B.L. Goode, and M.J. Eck. 2004. Crystal structures of a Formin Homology-2 domain reveal a tethered dimer architecture. *Cell*. 116:711-723.

Yadav, R., P.P. Pathak, V.K. Shukla, A. Jain, S. Srivastava, S. Tripathi, S.V. Krishna Pulavarti, S. Mehta, L.D. Sibley, and A. Arora. 2011. Solution structure and dynamics of ADF from

Toxoplasma gondii. *J Struct Biol*. 176:97-111.

Yamashiro, S., D.S. Gokhin, S. Kimura, R.B. Nowak, and V.M. Fowler. 2012. Tropomodulins: pointed-end capping proteins that regulate actin filament architecture in diverse cell types. *Cytoskeleton (Hoboken)*. 69:337-370.

Yamashita, A., K. Maeda, and Y. Maeda. 2003. Crystal structure of CapZ: structural basis for actin filament barbed end capping. *EMBO J*. 22:1529-1538.

Yarmola, E.G., S. Parikh, and M.R. Bubb. 2001. Formation and implications of a ternary complex of profilin, thymosin beta 4, and actin. *J Biol Chem*. 276:45555-45563.

Yin, H.L., and P.A. Janmey. 2003. Phosphoinositide regulation of the actin cytoskeleton. *Annu Rev Physiol*. 65:761-789.

Zhao, H., M. Hakala, and P. Lappalainen. 2010. ADF/cofilin binds phosphoinositides in a multivalent manner to act as a PIP(2)-density sensor. *Biophys J*. 98:2327-2336.

9   Curriculum Vitae

Name: **Moon Chatterjee**

Gender: Female

Personal Details

Date of Birth: 21-02-1982

Nationality: Indian

Residence: Windmuhlenweg 27, Hamburg, Germany

Telephone: +49-176-32056732

Email Address: chatterjee4665@gmail.com

Education

Sept 2009 – April 2015

> Ph.D. in Biochemistry, University of Hamburg, Germany
>
> Thesis: "Apicomplexan actin depolymerizing factors and capping proteins in the regulation of actin filament dynamics."
>
> Advisor: Dr. Inari Kursula

July 2007- August 2009

> Research assistant, Indian Institute of Technology, Kanpur, India
>
> Topic: "Cloning, purification and crystallization of EngA (bacterial GTPase) and nitrate reductase of *Escherichia coli*"
>
> Advisor: Prof. S. Sarkar

June 2005 - June 2007

> M.Sc. in Biotechnology, University of Mysore, Mysore, India (Full Scholarships from Department of Biotechnology, Government of India)
>
> Thesis: "Purification and crystallization of mutant EngA (bacterial GTPase)"
>
> Advisor: Dr. Balaji Prakash

June 2000 - June 2005

> B.Sc. Chemistry and Botany as main subjects, Deen Dayal Upadhyaya University, Gorakhpur, India

Language Skills

> Bengali, (native)
>
> Hindi, (fluent)
>
> English, (fluent)

Teaching Experience

Co-supervision of M.Sc. thesis

> Benjamin Götte (University of Lübeck, 2013)

Supervised a number of project students from biological technical assistant schools and universities

Talks and posters/ presentation

> Poster Presentation: 7th Annual BioMalPar Symposium, Heildelberg 2011
>
> Talk: Actin Summer School on Actin Dynamics, Regensburg 2012

Publications

> Singh BK, Sattler JM, Chatterjee M, Huttu J, Schüler H & Kursula I (2011) Crystal structures explain functional differences in the two actin depolymerization factors of the malaria parasite. J Biol Chem, 286: 28256-28264. (Equal contributions from 1st three authors)

> Tomar SK, Dhimole N, Chatterjee M & Prakash B (2009) Distinct GDP/GTP bound states of the tandem G-domains of EngA regulate ribosome binding. Nucleic Acids Res, 37: 2359-3270

10 Acknowledgements

It gives me great pleasure and satisfaction to place on record my gratitude for a number of people who have brought joy, courage and inspiration in my life.

It will not be an exaggeration to say that possibly the only reason I am writing this Thesis, and this acknowledgement, today is because of my thesis advisor, Dr. Inari Kursula. She has been not only a mentor and an advisor, but also a friend and, often, a confidante. I would like to place on record my debt to her for my training in turbulence and for allowing me to work with others and independently. Apart from being an example of how an academician should approach her work, Inari has shown me what it means to have infinite patience, propriety and encouragement for all and always with a smile. These are virtues I can only admire and, hard as I try, never imbibe. It has been a pleasure to know her and I am sure we will stay in touch in the years to come. And in true sense I could have never wished to have better guide than her.

I am thankful to Dr. Petri Kursula for his valuable inputs into my projects which helped to shape them. I was fortunate to work in a wonderful group. I undoubtedly owe gratitude to Dr. Gopinath Muruganandam, for lending me support whenever I required. I believe I was extremely fortunate to share office with Dr. Huijong Han, Nele Vervat, Esa Pekka Kumpula, Benjamin Gotte, Manuela Mirow and the newest addition Atta Samoo, who all made the office environment extremely friendly. A special mention to Dr. Huijong Han for answering all my naïve questions and the support I had from her over the years. Esa-Pekka, who joined as a PhD student 2 yrs later to me, is undoubtedly one of the finest undergraduate students I have known. His gentleness and kindnesses are the virtues which I really envy. Certainly, over the last one year Atta and I have developed a special bond and I am confident that I will miss our coffee breaks and discussions. I am obliged and thankful to Dr. Juha Kallio for all the efforts and patience he showed in teaching me crystallography. Also, his reassuring presence at any point of time made me confident while trying new things. A special mention for Susanne Meier for her constant source of support during my tenure. I will always remember Saara with great fondness and cherish the moments we have spent together.

I appreciate the support and inputs from my group members in Oulu, Finland. I thank Dr. Alexander Ignatev, Dr. Juha Vahokoski, Dr. Saligram Prabhakar Bhargav, Markku Soronen, Dr.

Salla Ruskamo, Dr. Matti Myllykoski, Arne Raasakka and Maryna Chucklieb for insightful advices and fruitful conversations.

I wish to thank my NMR collaborators, Dr. Bernd Simon and Dr. Teresa Carlomagno from EMBL Heidelberg.

Outside my group, in the same building my interactions with Dr. Yang Ge, Kun Yu and Daniel Worms were always motivating, refreshing and fun filled.

There are then a number of people who shared their knowledge, experiences and most importantly friendship. I would like to thank Koushik da, Jhunu, Sovan, Purbasha, Pinki, Sahoo Sir and Jayshree Mam for your support and love. Koushik da, Sovan and Purbasha, certainly our long discussions have helped me to discover several facets of many issues and undoubtedly you have helped to grow as an individual.

Then my travel group, Karthick, Raj Kiran, Bala, and Sumit I should accept that travelling is my passion and you people helped me to bring my dreams come true. I enjoyed thoroughly each and every trip we did together. Karthick, you have always inspired and amused me with your enthusiasm for outdoor activities. Raj Kiran, I should admit I always enjoyed your presence, as it made me more confident about myself.

I thank my dida and mamma for all the love, affection and support I had from them over the years.

Then a few words for my family: Ma and baba, I know how you feel not seeing me for more than 2 years. I am grieved about not being there when you needed me. I feel miserable that I make you wait for my phone calls, but I know irrespective of all this I am your beloved daughter. Whatever I am, it is because of you both.

Mithu, as times passed by phone calls became more and more infrequent, but truly you are and will be the strongest pillar of my life.

I would like to thank the management of Centre for Structural Systems Biology (CSSB) - Helmholtz Centre for Infection Research (HZI) for state-of-the-art laboratory resources. The administrative support from the Personal Department of HZI (Braunschweig) is gratefully acknowledged.

I also appreciate the efforts of International office at DESY who have been considerate of helping me with any administrative need I have had over the years.

And above all I thank my country for providing me the resources and giving me the platform that has enabled me to live a life full of new experiences and adventures.

11 Erklärung

Erklärung über frühere Promotionsversuche

Hiermit erkläre ich, Moon Chatterjee, dass vorher keine weiteren Promotionsversuche unternommen worden sind, oder an einer anderen Stelle vorgelegt wurden.

Hamburg, 29.4.2015

<div align="right">Moon Chatterjee</div>

Eidesstattliche Versicherung

Hiermit erkläre ich an Eides Statt, dass die vorliegende Dissertationsschrift selbstständig und allein von mir unter den angegebenen Hilfsmitteln angefertigt wurde.

Hamburg, 29.4.2015

<div align="right">Moon Chatterjee</div>